1. Introduction

1.1 Background and Overview

In the mid-nineteenth century, scientists began to notice that some materials showed time dependence in their elastic response. In shear or extension loading, materials like glass, rubber, silk etc. showed an instantaneous deformation followed by a continuous deformation. The instantaneous deformation was expected for a Hookean solid, but the continuous deformation 'creep' was not. This time dependent response is called viscoelasticity. Viscoelasticity is a material property. Viscoelastic materials behave as viscous fluids and elastic solids at the same time, hence the term viscoelastic.

Most polymers are viscoelastic in nature. Some known viscoelastic phenomena such as rod climbing, extrudate swell, and elastic recoil are well documented in the literature [Eggen *et al.* 1996, Bushko *et al.* 1996 and Bird *et al.* 1987]. In rod climbing, when a viscoelastic solution is stirred by rotating a rod in a beaker of viscoelastic fluid, the solution moves toward the centre of the beaker and climbs the rod. Newtonian fluid moves in the opposite direction, creating a vortex as it is pushed outward by centrifugal force. A common household example of material demonstrating rod climbing is dough for bread making. In extrudate swell, if a polymer solution and a Newtonian fluid are pushed through a capillary, the diameter of the polymer extrudate is much larger than the capillary diameter, whilst the diameter of the Newtonian fluid extrudate is almost equal to the capillary diameter. A common household example of extrudate swell is seen in shampoo, which, when squeezed on cold days, shows the diameter of the shampoo stream to be much larger than the nozzle diameter.

1.2 Problem Description

Realistic numerical simulations of viscoelastic fluids have practical relevance for the development and optimisation of polymer processing techniques such as injection

moulding, where molten polymers are injected into complex cavities to form fabricated parts. Injection moulding is a non-isothermal process and strongly affected by viscoelastic fluid flow phenomena i.e. extensional flow, stress relaxation, extrudate swell, secondary flow, residual stress, jetting etc. [Coyle *et al.* 1987,Eggen *et al.* 1996, Bushko *et al.* 1996 and Baaijens *et al.* 1990]. Commercial injection moulding software does not always predict realistic flow behaviour of polymer melt inside the mould, because the viscoelastic nature of polymer melts is not taken into account.

Most commercial polymer processing simulation software has been dominated by assuming Newtonian, Power Law and other Generalised Newtonian constitutive equations for fluid flow. For more realistic results, it may be necessary to use a suitable viscoelastic constitutive equation to predict polymer flow behaviour inside the mould.

However, application of viscoelastic constitutive equations in commercial polymer processing has not been successful so far. The main reasons for this are explained below.

Selection of suitable viscoelastic constitutive equations has been ellusive. This is largely because a particular viscoelastic constitutive equation is generally only suitable for a particular simple flow. However, polymer processing involves complex flows. Also the material data for most commercial polymers are not available and, when it is available, the processes for obtaining this data are complex and expensive. Furthermore, almost all viscoelastic constitutive equations do not characterise polymers well enough to emulate realistic flow behaviour. In addition, because of their non-linearity, numerical simulations of viscoelastic constitutive equations in fluid flow require much more sophisticated numerical techniques and extended computer facilities than do Newtonian or Generalised Newtonian constitutive equations. Concomitantly, the “memory effect” of viscoelastic constitutive equations contributes to chronic numerical instability when conventional numerical schemes are applied.

It is anticipated that flows in complex geometries can be assembled from flows in simple geometries. A successful flow simulation in a simple geometry, such as contraction geometry, will ultimately lead to improvement of simulations of polymer flow in such processes as extrusion and injection moulding, where the complex flows can involve much simple-geometry, such as contractions and expansions. However, most polymers are viscoelastic in nature and it is necessary to simulate viscoelastic constitutive equation in three-dimensional space and time to observe the viscoelastic effect or phenomena. So a three-dimensional code was developed in this research work to simulate viscoelastic constitutive equation for steady and time dependent fluid flow.

1.3 Contribution of Dissertation

The aim of this research project was to characterise a commercial polymer for viscoelastic simulations, and to develop a suitable numerical technique to accurately and successfully simulate viscoelastic fluid flow in simple geometry using the characterised material properties.

One of the objectives of this research program was to assess the current state of research in the application of viscoelastic constitutive equations to fluid flow. This was used to ascertain whether any of the currently proposed viscoelastic models, material characterisation methods and numerical techniques could be applied to simulate complex flows of commercially known polymers in three dimensions. Investigating and comparing all the possible techniques in applications of viscoelastic constitutive equations in fluid flow, the research program has provided the following specific contributions to new knowledge:

1. A comprehensive review of most viscoelastic constitutive equations with the emphasis being placed on the advantages and disadvantages of such equations for a particular flow. The review also includes some Newtonian and generalised

Newtonian constitutive equations. This is because some of the viscoelastic constitutive equations are extensions of Newtonian constitutive equations.

2. Selection of suitable viscoelastic constitutive equations for arbitrary flows. A number of considerations were taken into account in choosing a well suited viscoelastic constitutive equation.
3. Characterisation process using commercial polymer for viscoelastic constitutive equations. For the first time the equation and material parameters of a multi-mode differential type viscoelastic constitutive equation in shear flow for commercial polymer were presented.
4. Extension of a three-dimensional Generalised Newtonian flow simulation to steady state and time dependent viscoelastic flow simulation using differential type single mode viscoelastic constitutive equations.
5. Development of a three-dimensional segregated finite element algorithm with an equal order interpolation scheme based on the work of Rice and Schnipke [1986] proposed by them for two-dimensional Newtonian steady flow. Extension of Rice and Schnipke algorithm to three dimensional time dependent Generalised Newtonian flow and three dimensional time dependent viscoelastic flow
6. A successful comparison of experimental pressure drops in 4:1 axisymmetric contraction using commercial polymer with numerical simulation of viscoelastic flow at a maximum Weissenberg number of 5.44.

Moreover, various preliminary simulations are done to test some of the previous studies reported in the literature.

1.4 Thesis Structure

This dissertation is organised in the following structure:

Chapter two contains a review of known viscoelastic phenomena and constitutive equations, including the advantages and disadvantages of each equation. Chapter two also describes the considerations for selection of a well-suited viscoelastic constitutive equation, and the process for viscoelastic characterisation of a polymer melt.

Chapter three discusses the numerical techniques and numerical boundary constraints used to solve the chosen viscoelastic flow equations. This chapter also discusses the extension of Newtonian simulations to three-dimensional viscoelastic steady state and time dependent simulations.

The overall solution scheme used for the fluid flow analysis is discussed in Chapter four.

Polymer processing generally involves complex geometry that comprises combinations of planar Poiseuille flow, simple shear flow, and contraction flow etc. A better understanding of viscoelastic flows in complex geometry can be gained by analysing fluid flows individually in simple shear, planar Poiseuille flow and contraction flows. Chapter five presents results of simple shear flow, planar Poiseuille flow, and four to one contraction flows along with relevant boundary conditions.

Chapter six concludes this research with some recommendations for future research.

2. Viscoelastic Phenomena and Constitutive Equations

2.1 Introduction

The earliest equations for flow of fluids were developed by experimenting with Newtonian fluid in various flow fields. These equations were so simple and so reliable that people called them laws. However these laws and equations are incapable of describing flow of non-Newtonian, viscoelastic fluids. Viscoelastic constitutive equations describe polymeric fluids that, although liquid, have some of the properties of elastic solids. Viscoelastic constitutive equations are mathematical relationships between stress and shear rate, using certain material-parameters and equation-parameters, which describe transport in materials. The material-parameters are dependent upon material, and the equation-parameters constraint the constitutive equation to be mathematically complete. Viscoelastic constitutive equations are equations of state needed to provide the material dependent relationships between state of stress and the motion. One of the major differences between viscoelastic and Newtonian equations is that viscoelastic constitutive equations are almost always non-linear and mathematically complex in form. They require special numerical treatments for flow analysis. On the other hand Newtonian fluids obey linear and simple laws.

Non-Newtonian, viscoelastic phenomena are manifest in a number of situations. Section 2.2 briefly describes a range of phenomena that viscoelastic studies aim to model.

There are a variety of viscoelastic constitutive equations that have been proposed over the last several decades. Although most of these equations are derived from molecular theory, some have also been derived from basic empirical flow equations. Section 2.3 reviews constitutive equations for fluid flow.

The selection of suitable viscoelastic equations for a particular polymer processing flow has been difficult and elusive. In Section 2.4 we have selected a constitutive equation for this project.

The equation and material parameters in viscoelastic constitutive equations are obtained by fitting simplified forms of viscoelastic constitutive equations to the material experiment data. The experimental procedures and the processes for fitting viscoelastic equations to the experimental data are given in section 2.5.

2.2 An Overview of Viscoelastic Phenomena

Polymer materials do not behave exactly like Newtonian fluid, for example water do not behave exactly like Hookean solid say steel. Polymer fluids behave in between i.e. they behave as viscous liquid and elastic solids. This behaviour of both viscous and elastic is termed as viscoelastic. The well-known viscoelastic behaviours are time dependence, rod climbing, siphon flow, die swell, vortex growth, elastic recoil, etc.

Some polymeric fluids behave as elastic solid in shot period of time and if left alone for periods of time it tends to flow like fluid. This behaviour is due to viscoelastic nature of the material; the example of it will be ‘silly putty’. If dropped it bounces like a rubber ball but if left to sit in a surface for several hours it flows like a fluid. This time dependence behaviour is similar to creep in solids.

Some other viscoelastic behaviour is shear thinning. An example is mayonnaise if put on the bread it does not flow by itself but as soon as a knife is used to spread it flows like fluid. This is because mayonnaise behaves like liquid when sheared. This termed as shear thinning.

In rod climbing if polymeric and Newtonian fluid is placed in a beaker and rotated, it can be observed that Newtonian fluid pushes away from the rotating rod while the polymeric liquid accumulates near the rotating rod and starts to climb the rod. This

happens due to the Normal stresses in the polymeric fluid, which generates a pressure towards the centre and driving the fluid up the rod. The common household example of this behaviour can be observed in bread making dough. Predicting this rod climbing or Normal stresses is important for manufacturing process.

In siphon flow when the siphon slowly removed from a Newtonian fluid it breaks closely to the surface, but in polymeric fluid it can be removed for many centimetres still maintaining fluid flow [Macosko 1994]. This behaviour is due to viscoelastic nature of polymeric liquid.

If polymeric fluid is extruded, the diameter of the extruded polymer is generally larger than the diameter of extrusion die itself. Newtonian fluids do not exhibit this kind of behaviour. Predicting this behaviour is quite important in polymer manufacturing processes as these process involves contraction in the forms of extrusion e.g. gate in injection moulding, blow moulding and extrusion etc [Eggen 1996].

Vortex growth generally happens in contraction/expansion geometry for entry flow [Bogger *et al.* 1985, 1982, Evans *et al.* 1986,1989]. Vortex growth or commonly known as 'lip vortex' generally happens in the flows of highly elastic fluids. Although vortex depends upon the type of contraction, contraction ratio, flow rate and rheological properties of polymer, a better understanding of the vortex growth will aid in predicting or simulating flows in complex manufacturing process.

Polymer liquids tend to posses some memory of its original state. If a polymeric fluid is deformed under applied force and upon withdrawal of the force the polymeric fluid tend to approach its original shape or state. This behaviour is due to viscoelastic nature of polymer. However it does not fully exhibit elastic behaviour like Hookean elastic solids. This behaviour is termed as elastic recoil. Predicting elastic recoil is important as most polymers go through many deformations during polymer manufacturing processes.

Ideally a viscoelastic constitutive equations should describe the above complex phenomena i.e. time dependence, shear thinning/thickening, Normal stresses and extensional thickening. Next section provides a review of well-known viscoelastic constitutive equations.

2.3 An Overview Of Constitutive Equations

This section discusses some well known viscoelastic constitutive equations used in commercial and educational fields and classifies them into linear viscoelastic, differential and integral constitutive equations. This section also contains Newtonian laws. Although it seems irrelevant to discuss Newtonian equations, they are fundamental constitutive equations. Without them viscoelastic constitutive equations would not exist, as some of them are also empirical models. The limitations and properties of each constitutive equation are listed along with its mathematical form.

2.3.1 Newtonian Model

In the Newtonian model the viscosity is constant. The mathematical form of this is:

$$\boldsymbol{\tau}=\mu\dot{\boldsymbol{\gamma}} \tag{2.3-1}$$

where μ, the viscosity, is constant for a given temperature, pressure and composition, and $\boldsymbol{\tau}$ is the stress tensor.

The shear rate tensor $\dot{\boldsymbol{\gamma}}$ is defined as:

$$\dot{\boldsymbol{\gamma}} = \nabla \boldsymbol{v} + (\nabla \boldsymbol{v})^T \tag{2.3-2}$$

where $\boldsymbol{v}$ is the velocity vector and superscript T is transpose of matrix.

A fluid is said to be Newtonian if the viscosity does not depend upon shear rate $\dot{\boldsymbol{\gamma}}$, which implies μ is independent of $\dot{\boldsymbol{\gamma}}$.

2.3.2 Generalised Newtonian Constitutive equations

A Generalised Newtonian fluid is a minor modification of the Newtonian fluid. The mathematical form of a Generalised Newtonian fluid is given below:

$$\tau=\eta\left(|\dot{\boldsymbol{\gamma}}|\right)\dot{\boldsymbol{\gamma}} \tag{2.3-3}$$

where η is viscosity and a function of the scalar invariant of the deformation rate tensor $|\dot{\boldsymbol{\gamma}}|$ which is defined as:

$$|\dot{\boldsymbol{\gamma}}|=\sqrt{\frac{1}{2}(\dot{\gamma}:\dot{\gamma})} \tag{2.3-4}$$

There are other forms of the Generalised Newtonian model which include the Power law and Carreau-Yassuda model, which are discussed subsequently.

2.3.2.1 Power Law Model

The Power Law model is an empirical curve fit of viscosity as a function of shear rate. If one plots log η vs log $\dot{\gamma}$, the linear region is called the Power Law region. The straight line can be described by a Power Law expression:

$$\eta=m|\dot{\boldsymbol{\gamma}}|^{n-1} \tag{2.3-5}$$

where m is a Power law constant with units Pa.s^n, and superscript n is the Power Law index, which is dimensionless.

In general the Power Law can be written as

$$\boldsymbol{\tau} = m\dot{\boldsymbol{\gamma}}^{n} \tag{2.3-6}$$

In three dimensional form:

$$\tau_{ij} = m\left|II_{2D}\right|^{\frac{n-1}{2}}(2D_{ij}) \tag{2.3-7}$$

where $2\boldsymbol{D}$ is the same as $\dot{\boldsymbol{\gamma}}$, which is called rate of deformation tensor or shear rate tensor, I_{2D} is first invariant and defined as trace of $2\boldsymbol{D}$ and II_{2D} is the second invariant of the rate of deformation tensor, and II_{2D} is defined as:

$$II_{2D} = \frac{1}{2}\left[\mathrm{I}_{2D}^{2} - tr\left(2\boldsymbol{D}^{2}\right)\right] \tag{2.3-8}$$

The variants of the Power Law can be obtained by changing the Power Law index n, and Power Law constant m. When $n = 1$ and $m = \mu$ the Power Law becomes the Newtonian fluid model.

If $n < 1$ the fluid is said to be pseudoplastic or shear thinning, and if $n > 1$ the fluid is called dilatant or shear thickening.

The Power Law model is generally used in engineering work. This model cannot describe viscosity over a broad range of shear rates and in some problems it can lead to large errors [Bird 1987]. For real polymer melts it has been observed that at low and very high shear rates, melt viscosity can reach a Newtonian plateau. The Power Law

model cannot describe this behaviour [Macosko 1993]. Also the Power Law can not be used in pursuing dimensionless analysis. This is because a characteristic time and a characteristic viscosity can not be constructed from the parameters *m*, and *n* alone [Bird *et al.* 1987]. There is no way to relate the parameters *m* and *n* of the Power Law model to molecular weight and concentration, since the standard corrections are in terms of η_0 and $\eta^*(\omega)$, where η_0 is the zero shear viscosity and η^* is the complex viscosity [Bird 1987].

For narrow molecular weight distribution material the transition zone from η_0 to the Power Law region is narrow. A broad molecular weight distribution material gives a broader transition zone. For the Power Law a change of temperature does not affect the functional dependence of η or $\dot{\gamma}$. This change merely alters the zero shear rate viscosity and shear rate at which the transition from constant viscosity to power law behaviour occurs. Generally, an increase in temperature causes a decrease in zero shear rate viscosity and increases the transition of $\dot{\gamma}$ to the Power Law region [Bird *et al.* 1987]

2.3.2.2 The Carreau - Yassuda Constitutive equation

This constitutive equation was originally developed by Carreau [Carreau 1968] and modified by Yassuda [Yasuda *et al.* 1981]. This constitutive equation is useful in numerical calculations of Generalised Newtonian models. It has five parameters which enable it to fit a wide variety of experimental viscosity $\eta(\dot{\gamma})$ curves. The mathematical form of the constitutive equation is:

$$\frac{\eta-\eta_\infty}{\eta_0-\eta_\infty}=\left[1+(\lambda\dot{\gamma})^a\right]^{\frac{n-1}{a}} \tag{2.3-9}$$

where η_0 is the zero shear rate viscosity, η_∞ is the infinite shear rate viscosity, a is a dimensionless parameter describing the transition region between the zero shear rate and power law region, and $\frac{\eta-\eta_\infty}{\eta_0-\eta_\infty}$ is the slope of the power law region.

When $a = 2$ it is usually referred to as the Carreau equation. The parameter a, was added by Yassuda [Yasuda *et al.* 1981].

Strictly speaking, all the constitutive equations above apply only to shear-dominated flow, in which the viscous force dominates the material response.

2.3.3 Linear Viscoelastic Constitutive Equations

For sufficiently small regions of strain the stress relaxation modulus is considered constant. This linear dependence of stress on a small strain is called linear viscoelasticity. When larger strains are considered, the relaxation modulus is dependent on strain [Macosko 1993].

2.3.3.1 Maxwell Constitutive equation

The Maxwell constitutive equation was the first constitutive equation to consider both elastic and viscous effects in fluid flow. Maxwell [1867] first developed this model thinking that gasses are viscoelastic. Mathematically the constitutive equation can be written as:

$$\boldsymbol{\tau}+\lambda_1 \frac{\partial \boldsymbol{\tau}}{\partial t}=\eta_0 \dot{\boldsymbol{\gamma}} \tag{2.3-10}$$

where $\boldsymbol{\tau}$ is the stress tensor, λ_1 is the relaxation time, t is time, and the remaining terms carry the same meaning as in the models presented earlier.

The Maxwell constitutive equation can also be written in the form:

$$\boldsymbol{\tau}(t)=-\int_{-\infty}^{t}\left\{\frac{\eta_0}{\lambda_1}e^{\frac{-(t-t')}{\lambda_1}}\right\}\dot{\boldsymbol{\gamma}}(t')dt' \tag{2.3-11}$$

where the term in brackets is the Relaxation Modulus [Bird *et al.* 1987]

The Maxwell constitutive equation can also be written as:

$$\boldsymbol{\tau}(t)=\int_{-\infty}^{t}\left\{\frac{\eta_0}{\lambda_1^2}e^{\frac{-(t-t')}{\lambda_1}}\right\}\gamma(t,t')dt' \tag{2.3-12}$$

where the term in brackets is called the Memory Function [Bird *et al.* 1987].

Derivation of the relaxation modulus can be obtained from the simple Maxwell constitutive equation and by assuming a Hookean solid as shown in Macosko [1993].

The Maxwell constitutive equation can be generalised using the Superposition Principle to establish the *Generalised Maxwell Constitutive equation* [Bird *et al.* 1987]. For this it is assumed that stress is defined as:

$$\boldsymbol{\tau}(t)=\sum_{k=1}^{\infty}\boldsymbol{\tau}_k(t) \tag{2.3-13}$$

where k denotes the number of modes. The three forms of the Generalised Maxwell constitutive equation can then be written as respectively:

$$\boldsymbol{\tau}_k + \lambda_k \frac{\partial}{\partial t}\boldsymbol{\tau}_k = \eta_k \dot{\boldsymbol{\gamma}} \tag{2.3-14}$$

$$\boldsymbol{\tau}(t) = -\int_{-\infty}^{t} \left\{ \sum_{k=1}^{\infty} \frac{\eta_k}{\lambda_k} e^{\frac{-(t-t')}{\lambda_k}} \right\} \dot{\boldsymbol{\gamma}}(t')dt' \tag{2.3-15}$$

$$\boldsymbol{\tau}(t) = \int_{-\infty}^{t} \left\{ \sum_{k=1}^{\infty} \frac{\eta_k}{\lambda_k^2} e^{\frac{-(t-t')}{\lambda_k}} \right\} \gamma(t,t')dt' \tag{2.3-16}$$

With $\lambda_1 > \lambda_2 > \lambda_3$ …. (without any loss of generality)

$$\eta_k = \eta_0 \frac{\lambda_k}{\sum_k \lambda_k} \tag{2.3-17}$$

$$\lambda_k = \frac{\lambda}{k^{\alpha}} \tag{2.3-18}$$

where α is a dimensionless quantity. Note that η_k and λ_k relations are empirical.

Maxwell model is the first equation that included viscosity and elasticity and described viscoelastic behaviour of material. However, in steady state the Maxwell model simplifies to Newtonian fluid with constant viscosity. For sudden changes in stress, the time derivative terms dominate the left-hand side of the equation, and the integration with respect to time gives Hookean solid [Bird *et al.* 1987].

2.3.3.2 Jeffreys Constitutive equation

Jeffreys constitutive equation has two constants and an extra term added to the Maxwell Constitutive equation. This constitutive equation in mathematical form is stated as:

$$\boldsymbol{\tau}+\lambda_1 \frac{\partial}{\partial t}\boldsymbol{\tau}=\eta_0\left(\dot{\boldsymbol{\gamma}}+\lambda_2 \frac{\partial}{\partial t}\dot{\boldsymbol{\gamma}}\right) \tag{2.3-19}$$

where the constants λ_1 and λ_2 are relaxation and retardation time constants respectively, and η_0 is the zero shear rate viscosity.

Jeffreys model first included the retardation time, which was originally proposed for wave propagation in the earth's mantle [Bird *et al.* 1987]. This model also used to derive other non-linear viscoelastic models.

2.3.3.3 General Linear Viscoelastic constitutive equation

This constitutive equation is the integral form of the Maxwell constitutive equation with relaxation modulus or memory function included. Mathematically, this is written in the form:

$$\boldsymbol{\tau}=-\int_{-\infty}^{t} G(t-t')\dot{\boldsymbol{\gamma}}(t')dt' \tag{2.3-20}$$

$$\boldsymbol{\tau}=\int_{-\infty}^{t} M(t-t')\gamma(t,t')dt' \tag{2.3-21}$$

where $G(t-t')$ is the relaxation modulus, and $M(t-t')$ is the memory function. The memory function is defined as:

$$M(t-t') = \frac{\partial}{\partial t'} G(t-t') \tag{2.3-22}$$

The functional form above makes the Maxwell equation easy to understand. The first term depends upon the nature of the fluid and the second depends upon the nature of the flow.

Linear viscoelastic constitutive equations are used in fluid motions that involve infinitesimal displacement gradients. The General Linear Viscoelastic constitutive equation has many limitations [Larson 1988a]. These include:

- It cannot describe the shear rate dependence of viscosity inasmuch that its effect occurs for flows with $\lambda_{max}\dot{\gamma} \geq 1$.
- It cannot describe normal stress phenomena.
- It cannot describe small-strain phenomena if these involve large displacement gradients due to superposed rigid rotation ($2D_{ij} = 0$) [Bird 1987].
- It is valid only if $\dot{\gamma}(-\infty)$ is finite [Larson 1988a].

2.3.4 Retarded Motion Expansion

Retarded motion expansion [Bird *et al.* 1987] is the expansion of the rate of the strain tensor in order of increasing powers as well as powers of the first, second, and higher order partial derivatives. It is designed for systematic investigation of slowly varying velocity gradient departure from Newtonian behaviour. In mathematical form up to third order in series expansion this constitutive equation is described as:

$$\tau = -[b_1\boldsymbol{\gamma}_{(1)} + b_2\boldsymbol{\gamma}_{(2)} + b_{11}\{\boldsymbol{\gamma}_{(1)}\boldsymbol{\gamma}_{(1)}\} + b_3\boldsymbol{\gamma}_{(3)} + b_{12}\{\boldsymbol{\gamma}_{(1)}\boldsymbol{\gamma}_{(2)} + \boldsymbol{\gamma}_{(2)}\boldsymbol{\gamma}_{(1)}\} + b_{1:11}(\boldsymbol{\gamma}_{(1)}:\boldsymbol{\gamma}_{(1)})\,\boldsymbol{\gamma}_{(1)} + \ldots] \tag{2.3-23}$$

where constants b_1, b_2, b_{11}, b_{12}, etc. are material parameters which are called retarded motion constants. Note that $\boldsymbol{\gamma}_{(n)}$ is the kinetic rate of strain tensor [Bird 1987] defined as:

$$\boldsymbol{\gamma}_{(n+1)} = \frac{D}{Dt}\boldsymbol{\gamma}_{(n)} - \left\{(\nabla \boldsymbol{v})^T \cdot \boldsymbol{\gamma}_{(n)} + \boldsymbol{\gamma}_{(n)} \cdot (\nabla \boldsymbol{v})\right\} \tag{2.3-24}$$

where the derivative, D, is the material derivative. If every retarded motion constant becomes zero except b_1, then the expression is that of Newtonian fluid $\boldsymbol{\tau} = -b_1 \boldsymbol{\gamma}_{(1)}$.

If all of the second order terms are included and the retarded motion constants associated with the third or higher orders are zero, we obtain a Second Order fluid. The mathematical form of the Second Order fluid is described as:

$$\boldsymbol{\tau} = -[b_1\boldsymbol{\gamma}_{(1)} + b_2\boldsymbol{\gamma}_{(2)} + b_{11}\{\boldsymbol{\gamma}_{(1)}.\boldsymbol{\gamma}_1\}] \tag{2.3-25}$$

Mathematically, it can be shown that for a second order fluid [Example 6.2 -1, Bird 1987] the viscosity η is constant and so is the first and second normal stress coefficients.

Another way of writing the second order fluid equation is given in Macosko [1993], which is more helpful for physical interpretation.

$$\boldsymbol{T} = -P\boldsymbol{I} + 2\eta_0\boldsymbol{D} - \boldsymbol{\Psi}_{1,,0}\boldsymbol{D}_{(1)} + 4\boldsymbol{\Psi}_{2,0}\boldsymbol{D}\cdot\boldsymbol{D} \tag{2.3-26}$$

where the total shear stress $\boldsymbol{T} = -P\boldsymbol{I} + \boldsymbol{\tau}$, $\boldsymbol{\tau}$ is stress tensor or extra viscous stress tensor, and $\boldsymbol{D}_{(1)}$ is the upper convected derivative of deformation rate tensor. The fluid at rest $\boldsymbol{T} = -P\boldsymbol{I}$, and fluid with motion $\boldsymbol{T} = -P\boldsymbol{I} + \boldsymbol{\tau}$ [Macosko 1993, Eq^n-4.3.2].

There are many disadvantages and advantages of using the second order fluid in real flow analysis. Its application entirely depends upon the type of flow and analysis. The property of the Second Order fluid is given below.

- Second Order fluid will hold only if the shear rate is low enough to prevent the viscosity and first and second normal stress coefficients departing from their low shear rate values η_0, $\psi_{1,0}$, and $\psi_{2,0}$.
- Second Order fluids only occur for small Deborah number (De = λ/t) where λ is the characteristic relaxation time and t is the characteristic flow time.
- With a Second Order fluid, one may predict a shear stress vs. shear rate curve with a maximum, even negative viscosity, or elongation viscosity [Bird 1987].
- It can be predicted that the Second Order fluid is unstable in the rest-state unless one chooses some unrealistic values for the Retarded Motion constants [Bird 1987].
- One cannot describe qualitatively the stress relaxation experiments [Bird 1987].

The Retarded Motion Expansion constitutive equation deals with small deformation rates. The ordered fluids can not describe the relation between η and $\dot{\gamma}$ faithfully and neither can they describe the full range of the time dependent behaviour. Retarded Motion Expansion is used to investigate qualitative behaviours of polymer flow phenomena such as the direction of secondary flow [Bird 1987]. The Retarded Motion Expansion constitutive equation is used to compare with numerical (or approximate) solution of more realistic constitutive equations in limited situations. It is used to compare with experimental data in order to characterise polymeric fluids by their values η_0, $\psi_{1,0}$ and $\psi_{2,0}$. It is also used to explore the nature of the motion of orientable or deformable particles in suspension with polymeric suspending flow.

2.3.5 Linear Differential Constitutive Equation

From the previous section we know that the generalised Newtonian fluid model is applicable only to steady state shear flow in which material information is contained in

the viscosity parameter, $\eta(\dot{\gamma})$. The Linear Viscoelastic constitutive equation is restricted to small displacement gradient flows and the material information is given by the relaxation modulus, $G(t-t')$. The Retarded Motion Expansion model is restricted to slow and slowly varying deformation flows and the material information in this model is contained in the material constants, b_1, b_2, b_{11}, b_3, etc.

Differential equation models are more general constitutive equations that are used for arbitrary flows, including all the flow models discussed above.

2.3.5.1 Oldroyd Fluid B (Convected Jeffrey Model)

This model is a modification of the Jeffreys Linear model and is obtained by replacing the partial time derivative with the convected time derivative. Mathematically, the model is described as:

$$\boldsymbol{\tau} + \lambda_1 \boldsymbol{\tau}_{(1)} = -\eta_0 (\boldsymbol{\gamma}_{(1)} + \lambda_2 \boldsymbol{\gamma}_{(2)}) \tag{2.3-27}$$

This model is also called the Oldroyd Fluid B [Bird *et al.* 1987]. This model is not a non-linear model but a quasi-linear model and λ_1 and λ_2 are the same constants as in the Jeffreys Linear model [Bird 1987].

If relaxation time equals retardation time, the model is reduced to a Newtonian model. If the retardation time, λ_2, is zero, the model derives the convected Maxwell model. If the relaxation time, λ_1, is zero, this gives the following Retardation Expansion model.

$$\boldsymbol{\tau} = -\eta_0 (\boldsymbol{\gamma}_{(1)} + \lambda_2 \boldsymbol{\gamma}_{(2)}) \tag{2.3-28}$$

where $b_1 = \eta_0$, and $b_2 = \lambda_2 \eta_0$.

The convected Jeffreys model gives a constant viscosity and a first normal stress coefficient. The second normal stress coefficient is zero in steady shear flow.

2.3.6 Non-linear Differential Models

Non-Linear viscoelasticity includes the independent linear region of Relaxation modulus at small strains as well as the region which is dependent upon larger strains. This section discusses the viscoelastic constitutive equations that can predict normal stresses or normal stress coefficients and other non-linear viscoelastic phenomena in viscoelastic fluid flow. For example, in a Newtonian fluid, first and second Normal Stress coefficients (ψ_1, ψ_2) are zero which is not true for polymer materials [Bird 1987], and [Macosko 1993]. Non-linear models describe normal stress differences, shear thinning and extensional thickening behaviour well, while other models discussed so far fail to do so.

2.3.6.1 White-Metzner Model

This model is a modification of the convected Maxwell model. As previously stated, viscosity in Generalised Newtonian fluid is dependent on the second invariant of the rate of strain tensor. So substituting $\dot{\gamma}=\sqrt{\frac{1}{2}\left(\boldsymbol{\gamma}_{(1)}:\boldsymbol{\gamma}_{(1)}\right)}$ in the convected Maxwell model we obtain:

$$\boldsymbol{\tau}+\frac{\eta(\dot{\gamma})}{G}\boldsymbol{\tau}_{(1)}=-\eta(\dot{\gamma})\dot{\boldsymbol{\gamma}}_{(1)} \tag{2.3-29}$$

where $\boldsymbol{\gamma}_{(1)}$ is the first rate of strain-tensor.

This is the White-Metzner [White *et al.* 1963] model, and is classified under Maxwell differential equation as follows:

$$\boldsymbol{\tau}_{(1)}+F_c(\boldsymbol{\tau},\boldsymbol{D})+\frac{1}{\lambda}\boldsymbol{\tau}+F_d(\boldsymbol{\tau})=2G\boldsymbol{D} \qquad (2.3\text{-}30)$$

For the White-Metzner model $F_d = 0$ and $F_c = a(2\boldsymbol{D}:\boldsymbol{D})^{1/2}$

The function $F_c(\boldsymbol{\tau}, \boldsymbol{D})$ depends on both the stress tensor, $\boldsymbol{\tau}$, and strain rate tensor, $2\boldsymbol{D}$, and modifies the rate at which stress tends to build up. The function $F_d(\boldsymbol{\tau})$, which only depends upon the stress tensor, $\boldsymbol{\tau}$, modifies the rate at which the stress tends to decay. Shear thinning or strain softening can be introduced to the Maxwell equation through either F_c or F_d. In principle, non-linear effects introduced through F_d affect the time dependence of the stresses in transient flows somewhat differently from Non-Linearity introduced through F_c. But, the above equation is generalised to allow distribution of relaxation times typical of commercial material [Macosko 1993].

The White Metzner model has the advantage of being relatively simple, and gives a reasonable fit for the shear rate dependent viscosity, and first normal stress coefficients. This model can be used in fast time dependent motions. However, its predictions are not completely realistic in such problems. This is due to its lack of a linear viscoelastic limit for small displacement gradients.

In steady shear free flow the model gives infinite elongational viscosity similar to the Convected Maxwell model at finite extension rates. This model also gives second normal stress coefficient $\psi_2 = 0$ in steady shear rate.

Small amplitude oscillatory shearing η'(dynamic viscosity), and η''(imaginary part of complex viscosity) are not defined in this model [Bird 1987]. Above all, this model behaves poorly in step shear, predicts that second normal stress difference is zero, and gives singularities in extensional flow [Macosko 1993].

2.3.6.2 Oldroyd Constant Model

Oldroyd suggested that a possible generalisation of the Convected model could be obtained by adding to the latter all possible quadratic terms involving products of $\boldsymbol{\tau}$ with $\boldsymbol{\gamma}_{(1)}$ and $\boldsymbol{\gamma}_{(1)}$ with itself. This model includes all possible quadratic terms. The mathematical form of the model is:

$$\boldsymbol{\tau}+\lambda_1\boldsymbol{\tau}_{(1)}+\frac{1}{2}\lambda_3\{\boldsymbol{\gamma}_{(1)}\boldsymbol{\tau}+\boldsymbol{\tau}\boldsymbol{\gamma}_{(1)}\}+\frac{1}{2}\lambda_5(\mathrm{tr}\boldsymbol{\tau})\boldsymbol{\gamma}_{(1)}+\frac{1}{2}\lambda_6(\boldsymbol{\tau}\boldsymbol{\gamma}_{(1)})\boldsymbol{\delta}=$$

$$\eta_0[\boldsymbol{\gamma}_{(1)}+\lambda_{(2)}\boldsymbol{\gamma}_{(2)}+\lambda_4\{\boldsymbol{\gamma}_{(1)}\boldsymbol{\gamma}_{(1)}\}+\frac{1}{2}\lambda_7(\boldsymbol{\gamma}_{(1)}:\boldsymbol{\gamma}_{(1)})\boldsymbol{\delta}] \qquad (2.3\text{-}31)$$

where $\boldsymbol{\delta}$ - unit dyad, the symbol (**:**) double dot product, and λ_1-λ_7 and η_0 are constants.

It is easy to see, that if every constant is zero, except λ_1 and η_0, the model is the same as the Convected Maxwell model. If every constant is zero, except λ_1, λ_2 and η_0 the model is the same as the Convected Jeffreys model. If every constant is zero, except λ_2, λ_4 and η_0, then the fluid is same as the Second Order fluid model with b_1, b_2 and b_{11} being η_0, $\eta_0\lambda_2$ and $\eta_0\lambda_4$ respectively.

As the Oldroyd model is a polynomial quadratic expansion, in order to agree with experimental results, constraints need to be applied to the constants. This are explained below.

Since η' is known to decrease with increasing (ω), we must impose the requirement that $0 < \lambda_2 < \lambda_1$ [Bird 1987]. For the viscosity to be generally a monotone decreasing function of $\dot{\boldsymbol{\gamma}}$, we must require that $0 < \sigma_2 < \sigma_1$, where $\sigma_i = \lambda_i\,(\lambda_3 + \lambda_5\,) + \lambda_{i+2}\,(\lambda_1 - \lambda_3 - \lambda_5) + \lambda_{i+5}\,(\,\lambda_1 - \lambda_3 - 1.5\lambda_5)$ with i = 1,2 [Bird 1987]. For $|\tau_{yx}|$ to be a monotone

increasing function of $\dot{\gamma}$ for steady shear flow, it is required that $\sigma_2 \geq \frac{1}{9}\sigma_1$ [Bird 1987]. When $\eta(\dot{\gamma})$ and $\eta'(\omega)$ are plotted on the same graph with $\dot{\gamma} = \omega$ the η curve generally lies above the η' curve. For this to be true, in the region of moderate $\dot{\gamma}$ and ω, it is required that $\sigma_1 - \sigma_2 < \lambda_1(\lambda_1 - \lambda_2)$. For the elongational viscosity to be bounded by positive and negative $\dot{\varepsilon}$ it is necessary that $\lambda_1 - \lambda_3$ is between $\frac{2}{3}(\lambda_5 + \lambda_6) \pm \frac{1}{3}\left[4\lambda_6^2 - 11\lambda_5\lambda_6 + 4\lambda_5^2\right]^{\frac{1}{2}}$ [Bird 1987]

Because of the polynomial quadratic expansion and the eight constants involved, the Oldroyd constant model has more flexibility to explain the variety of rheological response than the Convected Jeffreys model. The Oldroyd 8 constant model does not fit the data quantitatively when compared with White-Metzner model. However, a wide range of properties can be correctly described qualitatively. For example, with suitable constants, stress overshoot in start up of steady shear flow, and bounded elongational viscosity can be obtained. The algebraic form in which non-linear terms have been included makes it generally easier to obtain better analytical solutions than with the White Metzner model, which has been found to be a useful and relatively simple constitutive equation for making exploratory fluid calculations [Bird 1987].

The Oldroyd 8 Constant model (with all 8 constants) is numerically limited, because dealing with all the terms is tedious and difficult. The behaviour of the equation in elongation is unrealistic, showing singularities at finite elongation rate, except when special values of the parameters are considered [Larson 1988a].

2.3.6.3 Giesekus Model

This Giesekus constitutive equation [Giesekus 1982, 1983] is based on anisotropic drag. The Oldroyd Constant model only contains linear stress terms, while the Giesekus model contains non-linear stress terms. By assuming the extra stress tensor as a sum of solvent and polymer stresses:

$$\boldsymbol{\tau} = \boldsymbol{\tau}_s + \boldsymbol{\tau}_p \tag{2.3-32}$$

where $\boldsymbol{\tau}_s$ is defined as:

$$\boldsymbol{\tau}_s = -\eta_s \dot{\boldsymbol{\gamma}} \tag{2.3-33}$$

then Giesekus constitutive equation is defined as:

$$\boldsymbol{\tau}_P + \lambda_1 \boldsymbol{\tau}_{P(1)} - \alpha \frac{\lambda_1}{\eta_P} \{\boldsymbol{\tau}_P \cdot \boldsymbol{\tau}_P\} = -\eta_P \dot{\boldsymbol{\gamma}} \tag{2.3-34}$$

where subscript *s* and *p* stands for solvent and polymer contribution respectively and α is the dimensionless mobility factor.

Substituting $\boldsymbol{\tau}_p = \boldsymbol{\tau} - \boldsymbol{\tau}_s = \boldsymbol{\tau} + \eta_s \dot{\boldsymbol{\gamma}}$, and arranging the terms according to the Oldroyd Constant model, the Giesekus model can be written as:

$$\boldsymbol{\tau} + \lambda_1 \boldsymbol{\tau}_{(1)} - a \frac{\lambda_1}{\eta_0} \{\boldsymbol{\tau} . \boldsymbol{\tau}\} - a\lambda_2 \{\boldsymbol{\gamma}_{(1)} \boldsymbol{\tau} + \boldsymbol{\tau} \boldsymbol{\gamma}_{(1)}\} = -\eta_0 [\boldsymbol{\gamma}_{(1)} + \lambda_2 \boldsymbol{\gamma}_{(2)} - a \frac{\lambda_2^2}{\lambda_1} \{\boldsymbol{\gamma}_{(1)} \cdot \boldsymbol{\gamma}_{(1)}\}] \tag{2.3-35}$$

where η_0 is zero shear rate viscosity, *a* is modified mobility factor, and λ_2 is retardation time.

If $a = 0$, the mobility factor = 0 and $\lambda_2 > 0$, the Giesekus model turns to Convected Jeffreys model.

The Giesekus model can be converted to other differential type constitutive equations by changing the material and equation parameters. If a = 0, and λ_2 = 0, the Giesekus model turns to the Convected Maxwell model. If α = 0, and $\lambda_1 = \lambda_2$, the Giesekus model turns to the Newtonian model. If λ_2 = 0 and α = ½, the model is called the Leonov model [Bird *et al.* 1987, Leonov *et al.* 1976] (shear free flow). If λ_2 = 0 and α = 1, the model is called Corotational Maxwell model [DeWitt 1955, Froman *et al.* 1947] for shear free flow. The Giesekus model is algebraically similar to the Oldroyd-8 constant model where an extra non linear term - $a \frac{\lambda_1}{\eta_0} \{\boldsymbol{\tau} . \boldsymbol{\tau}\}$ is added.

By including $\boldsymbol{\tau}.\boldsymbol{\tau}$, the Giesekus model gives material functions that are more realistic than those obtained for the Oldroyd 8 Constant model. For example large decreases in viscosity and normal stress coefficients with increasing shear rates are possible. For all $\alpha \neq 0$ or 1 (note that α varies in the closed set between 0 and 1), the power law slope of the viscosity is -1 when λ_2 = 0; this is unrealistically steep. The second normal stress coefficient is non zero and can be varied in size relative to the first normal stress coefficients. For example, $\psi_{2,0} = (\alpha/2)\psi_{1,0}$ provided that $\alpha \neq 0$. The elongational viscosity in Giesekus model is banded and reaches a constant value at large strain rates.

Although α is in a closed set between 0 and 1 in general, to get realistic properties, α should lie within the open interval of 0 and 1/2 [Bird 1987]. The Giesekus model can also be written in the differential type Maxwell model form, which is given below with $F_c = 0$ and $F_d = (\alpha/\lambda G)(\boldsymbol{\tau}.\boldsymbol{\tau})$ [Macosko 1993].

$$\boldsymbol{\tau}_{(1)} + F_c(\boldsymbol{\tau}, \boldsymbol{D}) + \frac{1}{\lambda}\boldsymbol{\tau} + F_d(\boldsymbol{\tau}) = 2G\boldsymbol{D} \qquad (2.3\text{-}36)$$

Above all the Giesekus model provides an excellent fit in shearing flows, but not the best for extensional flows.

2.3.6.4 Phan-Thien and Tanner Model

This model is classified under the Maxwell type differential equation with

F_c equal to:

$$F_c = \xi (\boldsymbol{D}.\boldsymbol{\tau} + \boldsymbol{\tau}\boldsymbol{D}) \tag{2.3-37}$$

and F_d equal to:

$$F_d = \frac{1}{\lambda}\exp(\frac{\beta}{G}\,\mathrm{tr}\ \boldsymbol{\tau}(\boldsymbol{\tau}\text{-}\boldsymbol{I})) \tag{2.3-38}$$

where G and λ are linear viscoelastic parameters, and ξ, and β are non-linear parameters. This implies that they must be obtained from non-linear rheological experiments.

The Phan-Thien and Tanner model fits data reasonably well for a variety of different types of deformation. However there are spurious oscillations in start up steady shearing, when $\xi \neq 0$, which gives the second normal stress difference (N_2) as zero [Macosko 1993]. More information on this model is available in reference [Phan-Thien *et al.* 1977, Phan-Thien 1978].

2.3.6.5 Johnson and Segalman Model

Johnson and Segalman model [Johson *et al.* 1980] also can be classified as a Maxwell type differential equation and Oldroyd Constant model [Oldroyd 1961]. In the Maxwell type differential model the value of $F_c = \xi (\boldsymbol{D}.\boldsymbol{\tau} + \boldsymbol{\tau}\boldsymbol{D})$ and $F_d = 0$. In the Oldroyd

constant model it has three constants $\lambda_1 = \eta_s\lambda_1/\eta_0$, $\lambda_2 = \xi\lambda_1$, and $\lambda_3 = \xi\eta_s\lambda_1/\eta_0$ with all other constants being zero.

This model predicts negative shear stress in step shear, spurious oscillation in start up of steady shearing, singularities in steady extensional flows, and infinite viscosity at finite elongational strain.

2.3.6.6 Larson Model

In Maxwell type differential equations the Larson model [Larson 1984] represents with

$F_d = 0$, and F_c equals to:

$$F_c = \frac{2\alpha}{3G}\boldsymbol{D}:\boldsymbol{\tau}(\boldsymbol{\tau} + G\boldsymbol{I}) \tag{2.3-39}$$

The model fits data reasonably well for a variety of deformations, it also predicts second normal stress difference as zero. This model is generally applied to steady shear and shear free flows.

2.3.6.7 Leonov Model

In Maxwell type differential equation the Leonov model is represented by

$F_c = 0$, and F_d equals to

$$F_d = \frac{\boldsymbol{\tau}\cdot\boldsymbol{\tau}}{2G\lambda} - \frac{\boldsymbol{\tau}+\boldsymbol{I}}{6G\lambda}tr(\boldsymbol{\tau}+\boldsymbol{I}) + \frac{G(\boldsymbol{\tau}+\boldsymbol{I})}{6\lambda}tr(\boldsymbol{\tau}+\boldsymbol{I})^{-1} \tag{2.3-40}$$

Notice that the Leonov model has no non-linear parameter and the only linear parameters are G and λ. This model provides an excellent fit in shearing flows, but not the best fit in extensional flows. The Leonov equation is similar to the Giesekus equation but it derives from a thermodynamic rather than a molecular approach [Larson 1988a] and [Leonov 1992].

2.3.6.8 Gordon - Schowalter Model

In the Oldroyd Constant model form, the representation the Gordon-Schowalter model [Gordon *et al.* 1972] includes three constants λ_1, λ_2 and λ_3, with the rest of them equal to zero. The constants are $\lambda_1 = \eta_s\lambda_1/\eta_0$, $\lambda_2 = \xi\lambda_1$ and $\lambda_3 = \xi\eta_s\lambda_1/\eta_0$. It has almost the same properties as the Johnson-Segalman model except that, $\eta_0 = (1\text{-}\xi)\eta_p + \eta_s$. In the Johnson-Segalman, $\eta_0 = \eta_s + \eta_p$ is the same as in the Giesekus model.

None of the differential type equations fit time dependent experiment data well unless a spectrum of relaxation models is introduced in a way analogous to that described earlier in the Generalised Maxwell model [Macosko 1993].

2.3.7 Integral Constitutive Models

Integral constitutive equations tend to be more accurate than differential constitutive equations, with the exception of linear viscoelastic integral equations. Integral type equations are also comparatively tedious to implement numerically as compared with the differential constitutive equation. Integral constitutive equations describe linear viscoelastic fluids accurately because of their inclusion of relaxation times, and because they keep track of time history of the deformation (integration from infinite past to present).

2.3.7.1 Lodge Integral Equation

The Lodge Integral equation is a quasi-linear equation [Macosko 1993]. It is the integral representation of the Upper Convected Maxwell model, and is defined as:

$$\boldsymbol{\tau}=\int_{-\infty}^{t}\frac{\eta_0}{\lambda^2}e^{-(t-t')/\lambda}\boldsymbol{B}((t,t')-\boldsymbol{I})dt' \tag{2.3-41}$$

where $\boldsymbol{B}$ is the finger tensor, time is t, and t' is past time.

In incompressible liquids, the stress tensor $\boldsymbol{\tau}$ is determined only to within an isotropic constant. So the unit tensor, $\boldsymbol{I}$, in the above equation can be left out [Macosko 1993]. The simplified Lodge Integral equation is defined as:

$$\boldsymbol{\tau}=\int_{-\infty}^{t}\frac{\eta_0}{\lambda^2}e^{-(t-t')/\lambda}\boldsymbol{B}(t,t')dt' \tag{2.3-42}$$

This integral equation has serious drawbacks. The elastic part of the equation is of the Hookean type and similar to the Upper Convected Maxwell model. The Lodge Integral type equation does not adequately describe all the material properties [Macosko 1993].

2.3.7.2 K - BKZ Type Constitutive Equations

The Lodge Integral equation and upper Convected Maxwell model's elasticity are of a simple Hookean solid. A more general version has been developed by K-BKZ (Initials of four Persons Kaye A., Bernstein B., Kearsley E., and Zapas L.) [Kearsley *et al.* 1976, Zapas *et al.* 1981]. The K-BKZ equation arose from an *ad hoc* transformation of a general non-linear expression for the stress tensor of an ideal elastic solid undergoing large deformations to a constitutive equation for a fluid that combines elastic and viscous material states [Bird 1987]. This equation originally came from the idea of a rubber elastic theory. Mathematically the model is defined as:

$$\boldsymbol{\tau}=\int_{-\infty}^{t}2\frac{\partial u(I_B,II_B,t-t')}{\partial I_B}\boldsymbol{B}(t,t')-2\frac{\partial u(I_B,II_B,t-t')}{\partial II_B}\boldsymbol{B}^{-1}(t,t')dt' \tag{2.3-43}$$

where $u(I_B, II_B, t-t')$ is a time dependent elastic energy kernel function. The K - BKZ model can be written in terms of the relative strain tensor, which is given below.

$$\boldsymbol{\tau}=\int_{-\infty}^{t} 2\frac{\partial u(I_B,II_B,t-t')}{\partial I_B}\boldsymbol{\gamma}_{[0]}\frac{\partial u(I_B,II_B,t-t')}{\partial II_B}\boldsymbol{\gamma}^{[0]}dt' \tag{2.3-44}$$

Very little work has been done describing material functions or solving flow problems using the K - BKZ equation in its general form. Instead, it has been customary to introduce the additional assumptions that the scalar function u may be written as a product of time dependent and strain dependent factors [Bird 1987].

$$u(I_B, II_B, t-t') = M(t-t')U(I_B, II_B) \tag{2.3-45}$$

where $M(t-t')$ is the linear viscoelastic memory function and $U(I_B, II_B)$ is the strain dependent function called *potential function*. So, only non-linear experiments are required to obtain the strain dependent function, $U(I_B, II_B)$. Using the memory function and potential functions the K - BKZ can be simplified as:

$$\boldsymbol{\tau}(t)=\int_{-\infty}^{t} M(t-t')\left[\frac{\partial U(I_B,II_B)}{\partial I_B}\boldsymbol{\gamma}_{[0]}+\frac{\partial U(I_B,II_B)}{\partial II_B}\boldsymbol{\gamma}^{[0]}\right]dt' \tag{2.3-46}$$

By changing the relative finite strain tensor to finite tensor or finger tensor the above equations gives:

$$\boldsymbol{\tau}(t)=\int_{-\infty}^{t} 2M(t-t')\left[\frac{\partial U(I_B,II_B)}{\partial I_B}\boldsymbol{B}(t,t')-\frac{\partial U(I_B,II_B)}{\partial II_B}\boldsymbol{B}^{-1}(t,t')\right]dt' \tag{2.3-47}$$

The above two simplified K-BKZ equations constitute the factorised K-BKZ equation.

In step strain the, K-BKZ equation closely predicts the stress, if the two strains are in the same direction. However, the prediction is sometimes poor if the strains are in opposite direction to each other [Larson 1988a].

The weakness of the K-BKZ equation is that its generality demands that an almost impossible suite of experimental data to be taken, if one wishes to predict the response to an arbitrary deformation history. As in the Oldroyd differential equations, continuum mechanic principles, such as frame invariance, are not in themselves strong enough to restrict the range of possible constitutive equations into manageable proportions [Larson 1988a].

There are many other constitutive equations that have similar form to that of the factorised K-BKZ, which can be found in the reference [Bird *et al.*1987, Table 8.3 –2].

2.3.7.3 Rivlin - Sawyer Equation

The Rivlin-Sawyer model [Rivilin *et al.* 1971] includes the K-BKZ model mathematically, but it is simpler than the K-BKZ equation. Mathematically it is described as:

$$\boldsymbol{\tau}(t)=\int_{-\infty}^{t}\left[\Psi_1(I_B,II_B,t-t')\boldsymbol{B}(t,t')+\Psi_2(I_B,II_B,t-t')\boldsymbol{B}^{-1}(t,t')\right]dt' \qquad (2.3\text{-}48)$$

where Ψ_1 is a scalar function.

and $\Psi_i\,(I_B,\ II_B,\ t-t') = M(t-t')\Phi_i(I_B,\ II_B)$. So, the factorised Rivlin-Sawyer equation is described as:

$$\boldsymbol{\tau}(t)=\int_{-\infty}^{t} M(t-t')\left[\Phi_1(I_B,II_B)\boldsymbol{\gamma}_{[0]}+\Phi_2(I_B,II_B)\boldsymbol{\gamma}^{[0]}\right]dt' \tag{2.3-49}$$

In terms of the finger tensor, the factorised Rivilin-Sawyer equation is:

$$\boldsymbol{\tau}(t)=\int_{-\infty}^{t} M(t-t')\left[\Phi_1(I_B,II_B)\boldsymbol{B}(t,t')+\Phi_2(I_B,II_B)\boldsymbol{B}^{-1}(t,t')\right]dt' \tag{2.3-50}$$

The Rivlin-Sawyer equation is based on the physical assumption that the effects on the stress at time, *t,* of the deformations and at different past times, *t',* are independent of each other. So, the pure form of the Rivlin-Sawyer equation is the most general constitutive equation for isotropic fluids [Bird 1987].

There are other constitutive equations in the form of Rivlin-Sawyer equation, which are given below.

2.3.7.4 Phillips Model

The potential functions of the Phillips model [Phillips 1977a,b,c] are described as:

$$\Phi_1 = (1-q)\exp(-\beta|\gamma_{yx}|) \tag{2.3-51}$$

and

$$\Phi_2 = q\exp(-\beta|\gamma_{yx}|) \tag{2.3-52}$$

where q and β are adjustable parameters, and $q = -\Phi_2/\Phi_1$.

This model has no retarded motion expansion and is generally used in simple shear flow.

2.3.7.5 Wagner Model

The Wagner model's [Wagner 1979] potential functions are:

$$\Phi_1 = \exp(-\beta\sqrt{\alpha I_B + (1-\alpha) II_B - 3}) \tag{2.3-53}$$

and the second potential function $\Phi_2 = 0$.

This model has no retarded expansion and gives second normal stress coefficient as zero.

2.3.7.6 Papanastasiou, Scriven and Macosko

The mathematical form of Papanastasiou, Scriven and Macosko [Papanastasiou *et al.* 1983] potential function in general flow is described as:

$$\Phi_1 = \frac{\alpha}{(\alpha-3)+\beta I_B + (1-\beta) II_B} \tag{2.3-54}$$

and the second potential function $\Phi_2 = 0$.

In simple shear flow the potential functions are:

$$\Phi_1 = \frac{\alpha}{\alpha + \gamma_{yx}^2} \tag{2.3-55}$$

and the second potential function is $\Phi_2 = 0$.

This model gives a second normal stress coefficient = 0.

More information on the Papanastasiou, Scriven and Macosko model could be found in reference [Papanastasiou *et al.* 1987].

The positive features of both the factorised K-BKZ and factorised Rivlin-Sawyer model are that they include the general linear viscoelastic fluid completely [Bird 1987]. The finite strain tensor approaches γ in infinitesimal displacement gradient. This is because of the inclusion of relative finite strain tensor. These equations provide a framework that includes a rather large number of non-linear constitutive equations both of molecular and empirical origin. It is possible to choose simple empirical functions for $M(s)$ and $U(I_B, II_B)$ or $\Phi_i\ (I_B, II_B)$ using up to five constants [Bird 1987]. These constants usually have simple physical meaning and are easy to determine from rheological data. These equations also provide the basis for the characterisation of polymers, and it is possible to use these constitutive equations to interrelate material functions.

One of the limitations for these types of equations is the prediction of extra recoiling in elastic recoil experiments. There is one more extra limitation that applies to the Rivlin-Sawyer model; this being that in certain fast strain experiments the Rivlin-Sawyer model may form the basis for a work producing a perpetual motion machine which is physically unreasonable [Bird 1987].

Because of this last limitation, most scientists prefer the K-BKZ equation than the Rivlin–Sawyer equation. However, several considerations should be taken into account while using a specific K-BKZ equation. Some of these considerations are associated with the limit of small displacement gradients in that I_B and II_B both approach three and both of the non-linear strain tensors simplify to $\dot{\gamma}$. So, the potential function should be analytic at $(I_B, II_B) = (3,3)$, which implies that the model simplifies properly the retarded motion expression. Also, the potential and memory functions should be chosen so that the shear stress vs. shear rate curve monotonically increases. [Bird 1987]

2.4 Constitutive Equation Selection

The foregoing list of constitutive equations is not exhaustive. However, it covers most of the well-known viscoelastic constitutive equations. There is no particular viscoelastic constitutive equation that is best suited for all complex flows [Larson 1988a]. Most constitutive equations are very good at predicting a particular flow. For example, the Giesekus model [Giesekus 1982, and Bird 1987] provides a good prediction in shear flow but not so good in elongational flow. The Leonov model [Leonov *et al.* 1976, Leonov 1992, and Bird 1987] fits the shear data accurately but not the elongational data [Bird 1987, and Baaijens 1994]. Larson [1988a] has described certain considerations regarding selecting viscoelastic constitutive equations. The considerations are outlined below.

The fundamental factors considered when selecting viscoelastic constitutive equations include the type of flow, material, prediction phenomena, and numerical or analytical scheme that is to be used to solve the flow problems.

The type of flow is a very important consideration. Is the flow predominantly shear or extensional or are both equally important? The material is important in the sense that certain viscoelastic constitutive equations are good for solutions and some are good for polymer melts. The numerical scheme to be used to solve the flow problem is of paramount importance. Differential type constitutive equations force different

constraints on the numerical scheme as compared to the integral type constitutive equations. The number of relaxation parameters that the scheme can handle is also an important consideration. The more the relaxation parameters, the more computationally intensive the scheme. With integral type constitutive equations one has to keep track of the past time history (one has to integrate from negative infinity to present time), which is computationally intensive. Prediction phenomena such as extrudate swell, vortex formation or secondary flow, and transition to time dependent are hard to predict. So, one should always consider what are the simple flows the constitutive equation can describe.

Many polymer-processing techniques involve complex flow dominated by viscoelasticity. For example, in the injection moulding process a mixture of flows exists. It comprises shear flow (cavity), extensional flow (gate), steady flow (runner) and transient flow (travelling flow front and unsteady mode of operation). In studying prediction phenomena, viscoelasticity becomes important at the gate where the time scale of flow is extremely small. It would be ideal to find the viscoelastic constitutive equations that can predict all such complex flows. However, it is not presently possible to find a single equation which can describe all the complex flow phenomena existing to date.

It is not obvious *a priori* which viscoelastic constitutive equations are best suited for a particular polymer process. Considering the above for the selection of constitutive equations and keeping in mind the computational intensity and feasibility of this research, it was decided that this research would focus on a differential type viscoelastic constitutive equation. In particular the Giesekus and Oldroyd-B models were chosen.

Since Giesekus model contains non-linear stress terms it gives more realistic material behaviour. For example, large decreases in viscosity and normal stress coefficients with increasing shear rate are possible. The Giesekus model was also selected because by suitably choosing the parameters (relaxation, retardation time, and mobility factor) it is possible to get other models such as Newtonian, Second-order Fluid, Convected

Maxwell, Convected Jeffreys, Leonov and Corotational Maxwell models. Giesekus model was chosen to fit experimental material data to obtain material parameters.

Oldroyd-B was selected for its good flow description with the least number of parameters. The Oldroyd-B model can provide good prediction when Boger fluids are considered [Larson 1988a]. Therefore, it was also selected to test the robustness of the numerical simulation and benchmark the flow problems when Boger fluids are used. In the 'Working groups on constitutive equations modelling' [Larson 1988b], it was agreed that Oldroyd-B and Maxwell equation have been the most often used in numerical simulations of the viscoelastic flow. There are many choices of constitutive equations that go beyond these simple Oldroyd models, in the sense of being better founded in molecular theory, or being better able to fit experimental data for polymeric fluids, or in avoiding infinite stresses [Larson 1988b]. Although the general agreement was lacking as to which 'improvements' to the simple Oldroyd models are most needed, there was a consensus that finite extensibility is a phenomenon that surely plays a role in real polymeric fluids. The Oldroyd model can be at least qualitatively modelled and has measurable consequences for the rheology of the fluid, particularly in alleviating the stress singularity in extensional flow [Larson 1988b].

Since it is assumed that a complex flow problem consists of a variety of simple flows, it was anticipated that the Oldroyd-B model could predict these flows fairly well with proper material parameters. Furthermore, because of computational cost and time constraints it was decided to simulate flows using single mode viscoelastic constitutive equations rather than the multi-mode varieties.

The selection of Oldroyd-B and Giesekus did not imply that these are the best-suited models for arbitrary complex flows.

2.5 Model Fit

Appropriate material and equation parameters for Giesekus and Oldroyd-B are necessary to test the viscoelastic constitutive equations. Material parameters such as relaxation time, retardation time etc. come from a simple shear testing. The equation parameter, mobility factor, α, in the Giesekus model is more or less an empirical fit. In general, the value of the mobility factor lies in between 0 and ½ [Bird 1987].

This section describes the experimental methods, equipment and the data fitting which were carried out to obtain the equation and material parameters for viscoelastic constitutive equations for polypropylene melts.

2.5.1 Equipment and Experimental Methods

The equipment used for experimental testing was a Rheometrics® Dynamic Spectrometer Model II (RDS-II). The RDS-II was calibrated in strict accordance with the manual before the start of the experiments. The instrument was stabilised by heating it to a particular temperature for at least half an hour. Tool geometry was zero gapped at every temperature.

Tool geometry for the experiment was cone and plate with 25mm plate-diameter and 0.1 radian cone angle. The Cone and Plate tool was chosen because it was considered appropriate for stress measurements. It has a homogenous strain or deformation field and proved to be more useful for high and low viscosity materials than the parallel plate tool geometry [Macosko 1993].

Polypropylene [Montell®, KMT6100] discs of 25mm diameter and approximately 1.2 mm thick were used. Samples with this initial size were chosen because upon squeezing the heated 1.2mm sample, the edge produced was uniform and of spherical curvature. The sample gap was 0.0457mm as required for cone and plate. Most of these discs were cut from compression moulded polypropylene plate. Discs cut from

injection-moulded plate buckled when heated and gave markedly different results than compression moulded discs. It was assumed that the injection-moulded discs gave different results because of their inherent strain history. So it was decided not to use the injection-moulded discs for any further investigations. The discs used in this experiment were cut from compression moulded polypropylene plates.

The material parameters, relaxation and retardation time were obtained from linear viscoelastic shear testing data. It was felt possible to obtain these material parameters from a single experiment on polymer melt. However, in order to obtain better accuracy and reliability, it was necessary to perform a series of different experiments at different temperatures. The experiments were repeated to check the repeatability of the experiment. The repeatability was checked by determining the percentage change in each data point for particular temperatures and was found that the percentage change was between 0.0001 to 0.001%. Overlaying the graphs also gave no discrepancy.

The first step of the procedure was to determine the linear viscoelastic strain range of the polymer. This was accomplished by conducting dynamic strain sweep experiments at various temperatures. The second step was to obtain the relaxation modulus data inside the linear viscoelastic strain range, from which relaxation times were obtained. This was achieved by performing stress relaxation experiments at various temperatures on the polymer melt. The dynamic frequency sweep experiment was performed to obtain complex viscosity within the linear viscoelastic range at various temperatures, from which retardation times were obtained. Finally steady state rate sweep experiments were performed to obtain viscosity data, and normal stress differences at various temperatures. This viscosity and normal stress differences provided the equation parameter mobility factor, α.

Experimental data obtained from Rheometrics® were exported to Excel [Microsoft® Office 97]. Data fitting was performed by writing various Macros in Excel and using the in-house Solver functionality [Microsoft® Office 97 Reference Manual]. The solver used central derivative, quadratic tangent and conjugate gradient searching method with

a precision of 10^{-10}, tolerance of 5% and the convergence measure of 0.0000001 to solve data fitting equations [Microsoft® Office 97 Reference Manual].

The equation and material parameters were obtained by fitting simplified viscoelastic constitutive equations for particular flow to the experimental data using Excel [Microsoft® Office 97] as explained previously. Since single mode models are inadequate to capture the full effect of the flow, multi-mode models were used to characterise the flow. Although our numerical simulation only involved single mode models, we have presented the result of multi-mode model for comparison. Generally, the more the modes the more computationally intensive the simulations are [Bird 1987]. In multi-mode model simulation, the number of unknowns in a problem increases approximately with the number of modes; with current computers, using more than two or possibly three modes is not reasonable.

2.5.1.1 Dynamic Strain Sweep

Since material parameters were to be obtained from linear viscoelastic experiments, it was necessary to find the linear viscoelastic range of the polypropylene melt at various temperatures. To accomplish this a dynamic strain sweep experiments was carried out on polypropylene melt at 180°C, 200°C, 220°C, and 240°C. Dynamic strain sweep applies a range of sinusoidal strains, each at a constant frequency. The peak amplitude of each strain was determined by the 'commanded strain' or input strain. Successive measurements were taken at each of the commanded strains. The strain amplitude was either incremented or decremented. This experiment was used to determine the limits of linear viscoelasticity and characterise polymers that exhibit extreme non-linear behaviour [Rheometrics® controlled strain test guide-9].

The input parameters for dynamic strain sweep at 180°C, 200°C, 220°C, and 240°C were frequency = 1rad/sec, initial strain = 0.1%, final strain = 100%, and point per decade = 10 with logarithmic sweep mode. The point per decade means that the number of data points measured between each decade of logarithmically incremented strain included initial strain but excluded final strain. This experiment calculated torque at constant

frequency and temperature within the limits of initial strain and final strain. The linear increase in torque with increase in strain determined the region of linear viscoelasticity. Since we were interested only in a particular value of strain for all the temperatures that lay inside the linear viscoelastic region, we chose the strain to be 10%. This strain value was used in the stress relaxation and dynamic frequency sweep experiments. The dynamic strain sweep experiments at the four temperatures noted earlier were repeated. The repeatability was determined by calculating percentage change in each data point for particular temperatures and it was found that the percentage change was between 0.0001 and 0.001%.

2.5.1.2 Stress Relaxation

Stress relaxation manifests itself most simply when a polymeric liquid is subjected to a step increase in strain, and it is observed that the stress relaxes in an exponential fashion. If a purely viscous liquid is subjected to the same deformation, the stress relaxes instantly to zero as soon as the strain becomes constant. Elastic solids exhibit no relaxation [Macosko 1993].

The stress relaxation experiment applied and maintained a single transient step strain. Data was then collected during a specified time, which was specified by the user/experimentalist. The relaxation modulus, $G(t)$, was calculated during the specified time. Four Stress relaxation experiments were performed on polypropylene melt at 180°C, 200°C, 220°C, and 240°C, with 10% strain for 180 seconds for each temperature. The repeatability was checked as explain previously and found that the percentage change in data points at different temperatures lie between 0.0001 and 0.001%. Overlaying graphs also gave reasonable good fit.

The mathematical form of relaxation modulus is:

$$G(t) = G_0 e^{-t/\lambda} \tag{2.5-1}$$

where G_0 is a constant, t is time and λ is relaxation time.

The single-mode relaxation modulus equation described above did not fit the typical data very well, as seen in Figures 2.4-1 to 2.4-4. A logical improvement on this model was to try several relaxation times. This was written as a series of relaxation times λ_k multiplied by the weighting constant G_k [Macosko 1994]. This is also called a multi-mode relaxation modulus. The equation is of the form:

$$G(t) = \sum_{k=1}^{N} G_k e^{-t/\lambda_k} \tag{2.5-2}$$

where N is the total number of modes.

The mathematical equation for relaxation modulus $G(t)$ was fitted using Excel [Microsoft®, Office 97] as explained previously to stress relaxation data obtained from the experiments to obtain the relaxation time. Since a single mode was inadequate to describe the full effect of stress relaxation, a multi-mode relaxation modulus was fitted to the experimental data. Figures 2.4-1 to 2.4-4 represent the relaxation modulus fit of one mode (N=1), three mode (N=3), and nine mode (N=9) model at 180°C, 200°C, 220°C, and 240°C respectively.

Notice that the nine modes fit more accurately than the three modes. However, viscoelastic constitutive equations using nine relaxation times were computationally much more intensive than three modes, which will be discussed in detail anon.

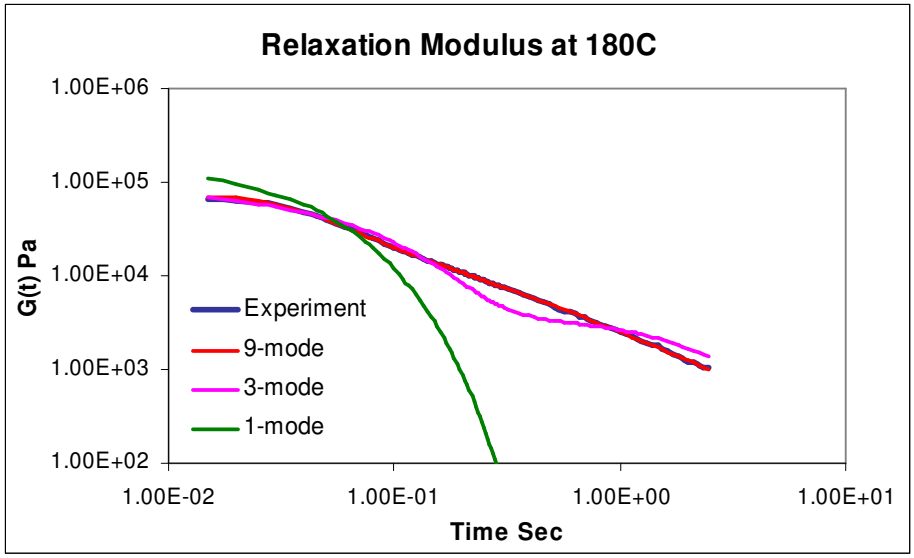

Figure 2.4-1. Multi-mode Relaxation modulus data fitting of Polypropylene melt at 180°C.

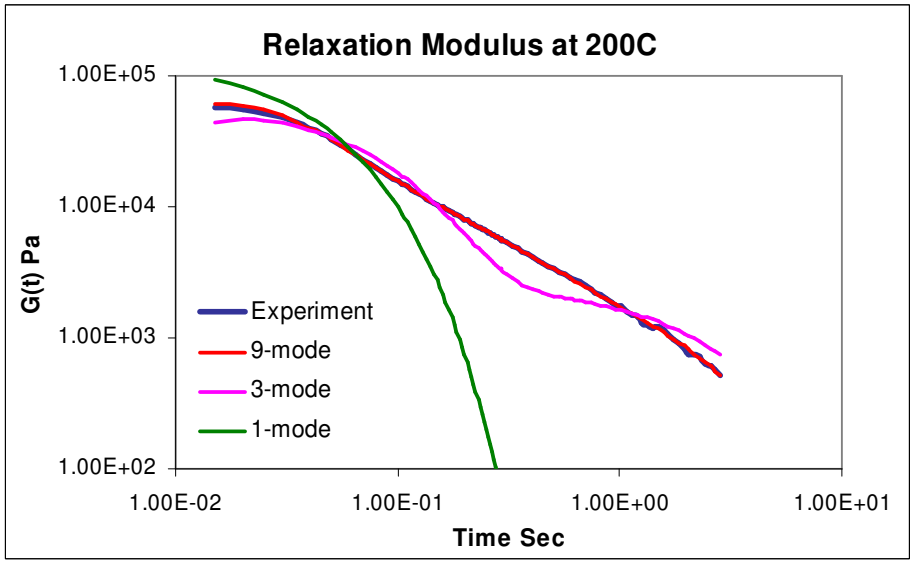

Figure 2.4-2. Multi-mode Relaxation modulus data fitting of Polypropylene melt at 200°C.

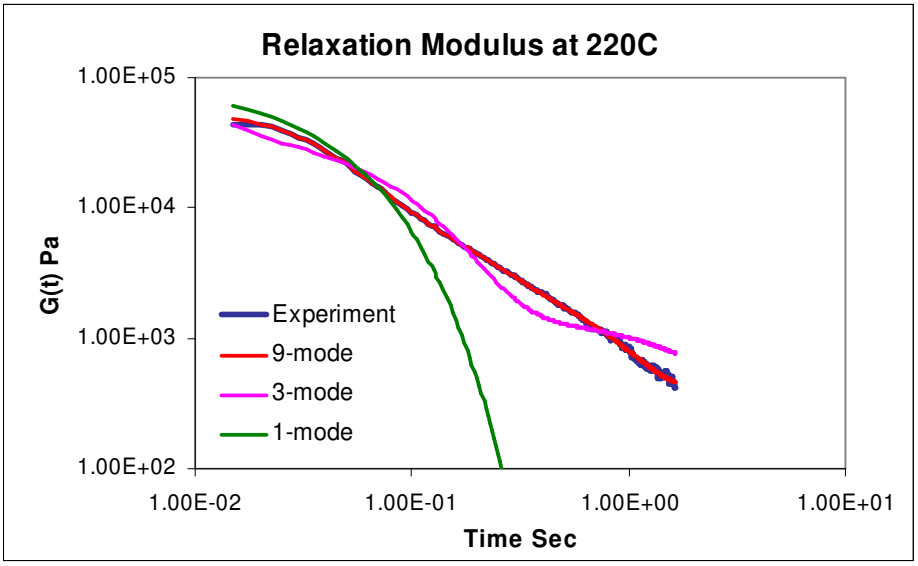

Figure 2.4-3. Multi-mode Relaxation modulus data fitting of Polypropylene melt at 220°C.

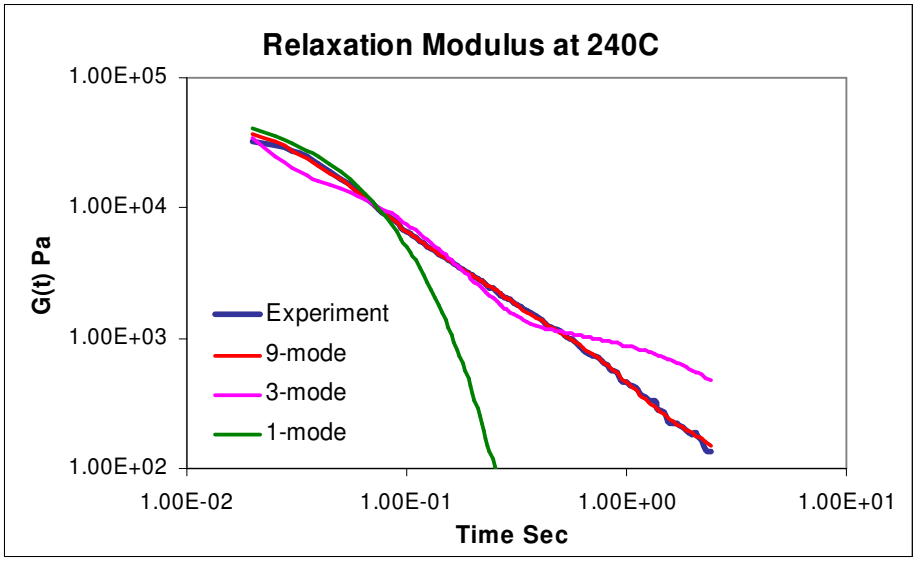

Figure 2.4-4. Multi-mode Relaxation modulus data fitting of Polypropylene melt at 240°C.

From the above figures the relaxation modulus for polypropylene melt decreases with time. A nine-mode model (consists of 9 relaxation parameters) fitted data quite accurately. As expected a three-mode model fitted the relaxation modulus data more accurately than the one-mode (one relaxation parameter) model but not as good as a nine-mode model. In the above figures, a single-mode model was fitted to relaxation modulus data at low time periods. This was to give relaxation times soon after the material relaxes.

2.5.1.3 Frequency Sweep

Relaxation modulus is a function of relaxation time. The previous section presented relaxation times from stress relaxation experimental data. Complex viscosity is a function of retardation time, the other material parameter. Dynamic frequency sweep experiments were conducted to obtain complex viscosity data.

In the dynamic frequency sweep experiments, a sinusoidal strain of constant peak amplitude was applied over a range of frequencies. The peak amplitude of strain was determined by the input strain. One measurement was taken at each of the selected frequencies. Frequencies were either incremented or decremented. Dynamic frequency sweep experiments were used to analyse the time dependent behaviour of material.

Four dynamic frequency sweep experiments were carried out at 180°C, 200°C, 220°C, and 240°C, with 10% strain. Ten points per decade mode with logarithmic sweep mode, an initial frequency of 0.1read/s, and final frequency of 500rad/s were chosen. The points per decade in these experiments meant that the number of data points measured between each decade of logarithmically incremented frequency, which included the initial frequency but excluded the final frequency.

The mathematical form of complex (dynamic) viscosity is:

$$\eta^* = \eta' - i\eta'' \tag{2.5-3}$$

where η' is the real part of the complex viscosity or dynamic viscosity, and η'' is the imaginary part of the complex viscosity.

In small amplitude oscillatory flow, the material functions (real and imaginary viscosity) of the Giesekus model are:

$$\frac{\eta'}{\eta_0} = \frac{1 + \lambda_1\lambda_2\omega^2}{1 + \lambda_1^2\omega^2} \tag{2.5-4}$$

$$\frac{\eta''}{\eta_0\omega} = \frac{\lambda_1 - \lambda_2}{1 + \lambda_1^2\omega^2} \tag{2.5-5}$$

where η_0 is the zero shear rate viscosity, λ_1 is the relaxation time, λ_2 is the retardation time, and ω is the frequency. The zero shear rate viscosity and retardation time are defined as:

$$\eta_0 = \eta_s + \eta_p \tag{2.5-6}$$

$$\lambda_2 = \lambda_1 \frac{\eta_s}{\eta_0} \tag{2.5-7}$$

where η_s and η_p are solvent and polymer contribution to viscosity.

The retardation time was obtained by fitting dynamic and imaginary viscosity equations to the experimental data using Excel [Microsoft®, Office 97] as explained previously. The single mode material function equations described above did not fit the experimental data very well as seen in Figures 2.4-5 to 2.4-12. A logical improvement on this model was to try to fit a multi-mode model. The multi-mode dynamic viscosity and imaginary part of viscosity equations are described as:

$$\eta' = \sum_{k=1}^{N} \eta_0[k] \frac{1 + \lambda_1[k]^2 \omega^2 \eta_s/\eta_0}{1 + \lambda_1[k]^2 \omega^2} \tag{2.5-8}$$

$$\eta'' = \sum_{k=1}^{N} \eta_0[k] \omega \frac{\lambda_1[k] - \lambda_2[k]}{1 + \lambda_1[k]^2 \omega^2} \tag{2.5-9}$$

where N is the number of modes.

Figures 2.4-5 to 2.4-8 present the dynamic viscosity data fitting of multi-mode Giesekus model to experimental data.

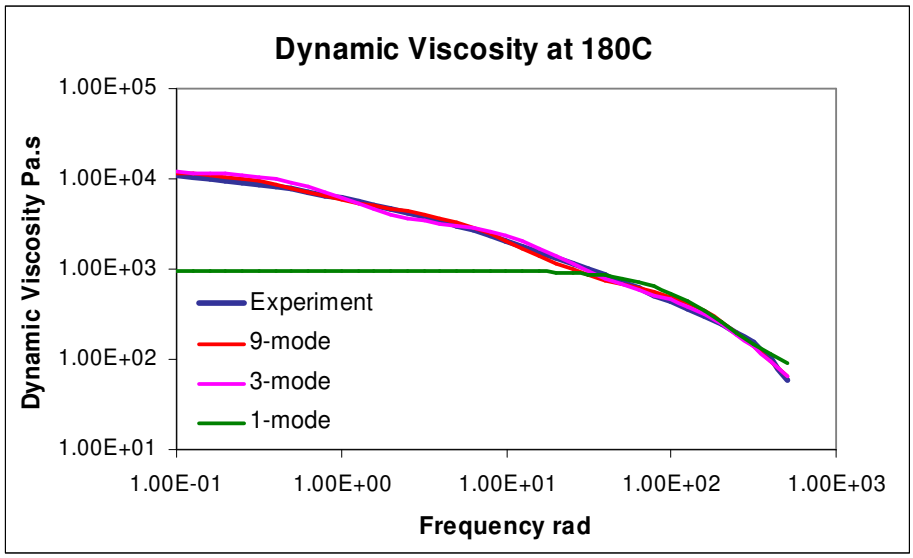

Figure 2.4-5. Multi-mode Giesekus model data fitting to dynamic viscosity of Polypropylene melt at 180°C.

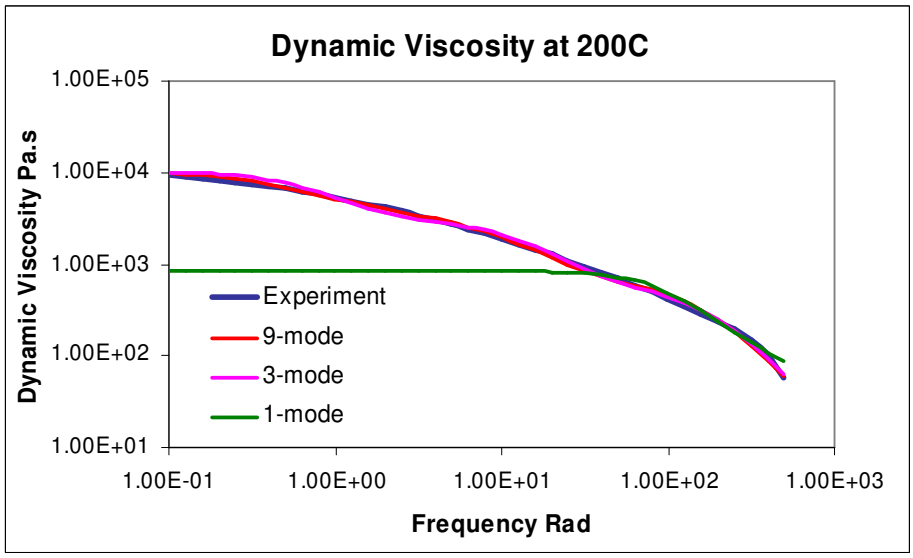

Figure 2.4-6. Multi-mode Giesekus model data fitting to dynamic viscosity of Polypropylene melt at 200°C.

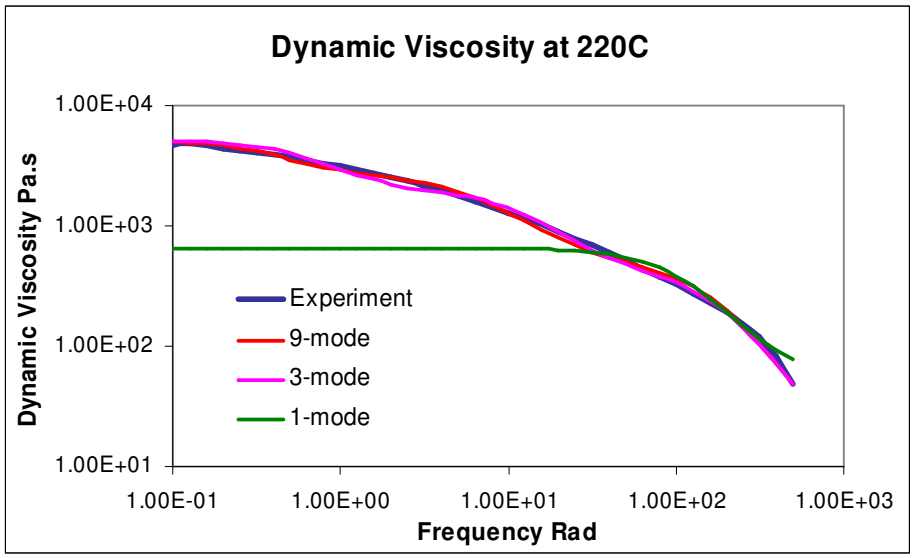

Figure 2.4-7. Multi-mode Giesekus model data fitting to dynamic viscosity of Polypropylene melt at 220°C.

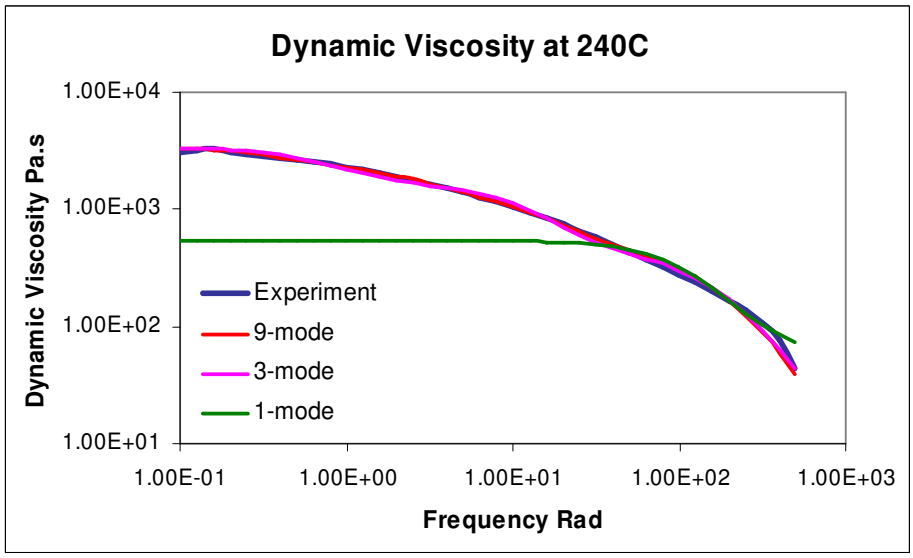

Figure 2.4-8. Multi-mode Giesekus model data fitting to dynamic viscosity of Polypropylene melt at 240°C.

In Figures 2.4-5 to 2.4-8 the dynamic viscosity (the major contributor to the complex viscosity) is seen to decrease with increasing frequency. Notice that in the above figures for the single mode model, the dynamic viscosity is constant at low frequencies. Clearly the single mode model did not predict the dynamic viscosity at low frequencies well. The three and nine mode model however did predict the dynamic viscosity very well as seen in the in the figures above.

Figures 2.4-9 to 2.4-12 present the imaginary part of complex viscosity data fitting of multi-mode Giesekus model to the experimental data using Excel [Microsoft®, Office 97]as explained previously.

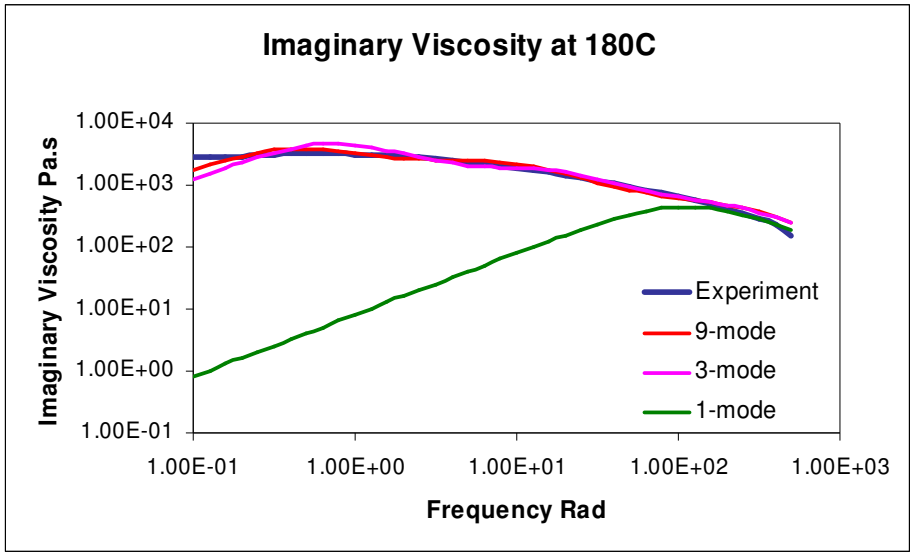

Figure 2.4-9. Multi-mode Giesekus model data fitting to imaginary part of complex viscosity of Polypropylene melt at 180°C.

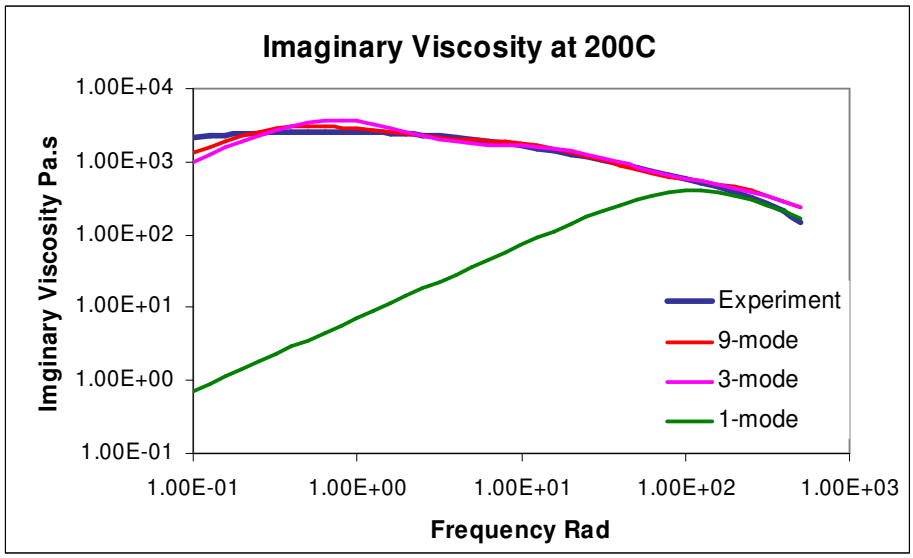

Figure 2.4-10. Multi-mode Giesekus model data fitting to imaginary part of complex viscosity of Polypropylene melt at 200°C.

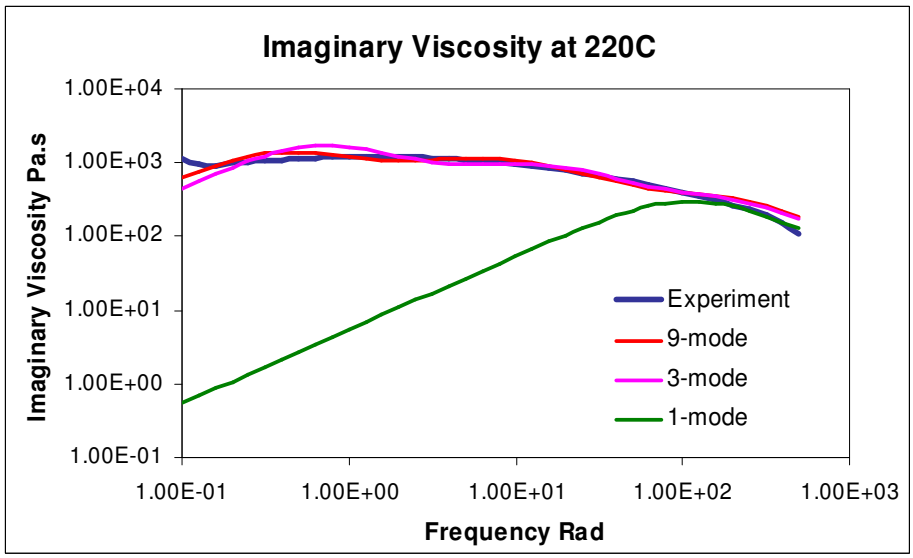

Figure 2.4-11. Multi-mode Giesekus model data fitting to imaginary part of complex viscosity of Polypropylene melt at 220°C.

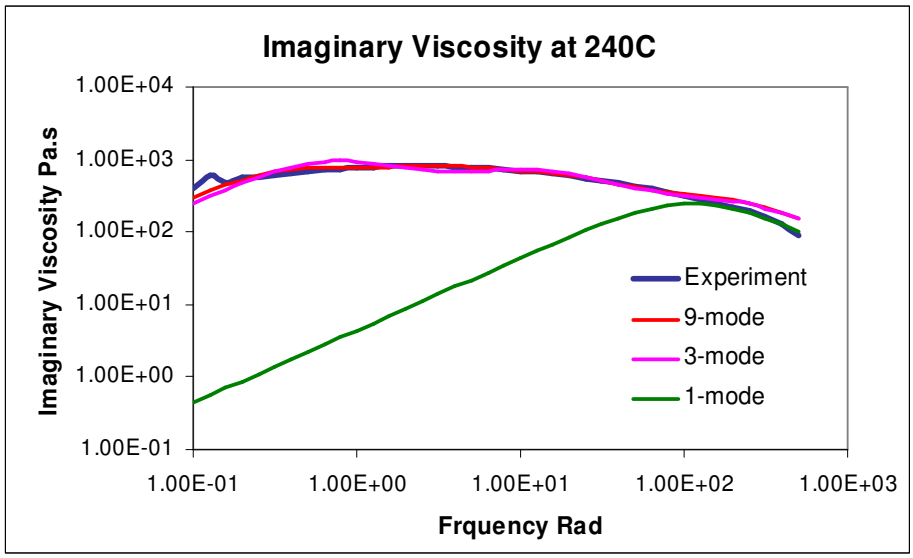

Figure 2.4-12. Multi-mode Giesekus model data fitting to imaginary part of complex viscosity of Polypropylene melt at 240°C.

In Figures 2.4-9 to 2.4-12 the experimental value of the imaginary viscosity (the minor contributor to the complex viscosity) was plotted against nine, three, and single model. Notice that in the figures above, the single-mode model prediction of the imaginary viscosity is quite poor. Given that the imaginary viscosity's contribution to complex viscosity is quite small, the nine and three mode model predictions are acceptable.

2.5.1.4 Steady Rate Sweep

The materials relaxation and retardation times parameters were obtained from stress relaxation and dynamic frequency sweep experiments respectively. The mobility factor, α, was obtained from viscosity data at various temperatures during the rate sweep experiment.

The rate sweep applies a steady shear deformation at user commanded shear rates. Data was collected in time-based mode (one measurement was taken at each rate).

Four rate sweep experiments were conducted at 180°C, 200°C, 220°C, and 240°C, with logarithmic sweep mode, ten points per decade, initial rate of $0.01s^{-1}$, and final rate of 100 s^{-1}. The point per decade in this experiment meant that the number of data points measured between each decade of logarithmically incremented shear rate, included the initial shear rate but excluded the final shear rate. The prescribed final shear rate of 100 s^{-1}, the transducer's limit in RDS II, which is very low and does not describe the material in a wider range of shear rate. However, since all the material parameters were known from the dynamic frequency sweep experiment, we were only interested in obtaining the value of the equation parameter, α, from the rate sweep experiment. It was anticipated that the number of data points from the rate sweep experiment was good enough to obtain the equation parameter. Data for first-normal stress coefficient however, were obtained. Since the data for first-normal stress coefficients was hard to get and unreliable, prediction of first-normal stress coefficient was made using the material parameters obtained from the dynamic frequency sweep experiments and the equation parameter, α, was obtained from the rate sweep viscosity.

In steady shear flow, the material function viscosity, η, and first normal stress coefficient, Ψ_1, of the Giesekus model are given respectively as:

$$\frac{\eta}{\eta_0} = \frac{\lambda_2}{\lambda_1} = \left(1 - \frac{\lambda_2}{\lambda_1}\right)\frac{(1-f)}{1+(1-2\alpha)f} \tag{2.5-10}$$

and

$$\frac{\Psi_1}{2\eta_0(\lambda_1 - \lambda_2)} = \frac{f(1-\alpha f)}{(\lambda_1\dot{\gamma})^2\alpha(1-f)} \tag{2.5-11}$$

where f is defined as:

$$f = \frac{1-\chi}{1+(1-2\alpha)\chi} \tag{2.5-12}$$

$$\chi^2 = \frac{(1+16\alpha(1-\alpha)(\lambda_1\dot{\gamma})^2)^{1/2}-1}{8\alpha(1-\alpha)(\lambda_1\dot{\gamma})^2} \tag{2.5-13}$$

The mobility factor was obtained by fitting viscosity and the first-normal-stress coefficient equations to the experimental data. The multi-mode viscosity and first-normal-stress coefficient equations are described as:

$$\eta = \sum_{k=1}^{N} \eta_0[k]\left[\frac{\eta_s}{\eta_o} + \frac{\eta_p}{\eta_0}\frac{(1-f[k])^2}{1+(1-2\alpha[k])f[k]}\right] \tag{2.5-14}$$

and

$$\psi_1 = \sum_{k=1}^{N} 2\eta_0[k](\lambda_1[k]-\lambda_2[k])\frac{f[k](1-\alpha[k]f[k])}{(\lambda_1[k]\dot{\gamma})^2\alpha[k](1-f[k])} \tag{2.5-15}$$

where

$$f = \sum_{k=1}^{N} \frac{1-\chi[k]}{1+(1-2\alpha[k])\chi[k]} \tag{2.5-16}$$

$$\chi = \sum_{k=1}^{N} \sqrt{\frac{(1+16\alpha[k](1-\alpha[k])(\lambda_1[k]\dot{\gamma})^2)^{1/2}-1}{8\alpha[k](1-\alpha[k])(\lambda_1[k]\dot{\gamma})^2}} \qquad (2.5\text{-}17)$$

Figures 2.4-13 to 2.4-16 present the viscosity data fitting of multi-mode Giesekus model using Excel [Microsoft®, Office 97].

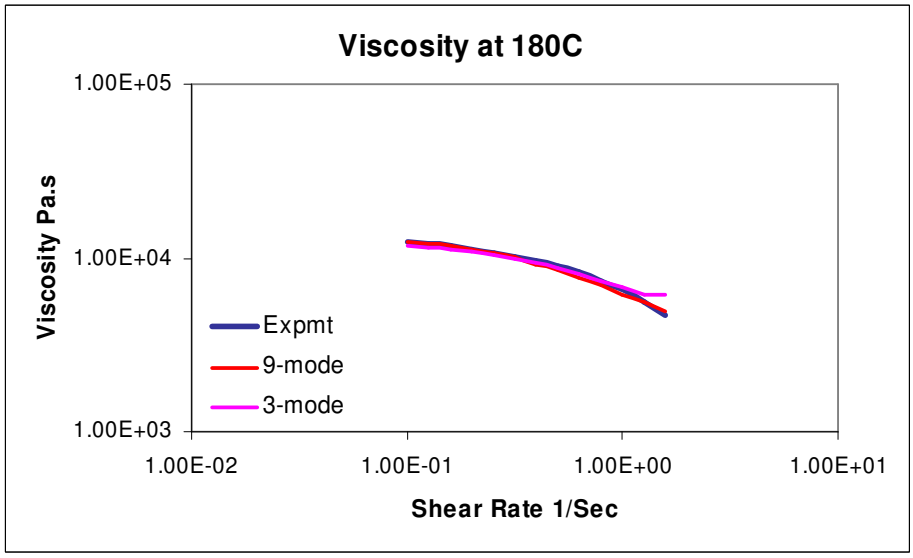

Figure 2.4-13. Multi-mode Giesekus model data fitting of viscosity for Polypropylene melt at 180°C.

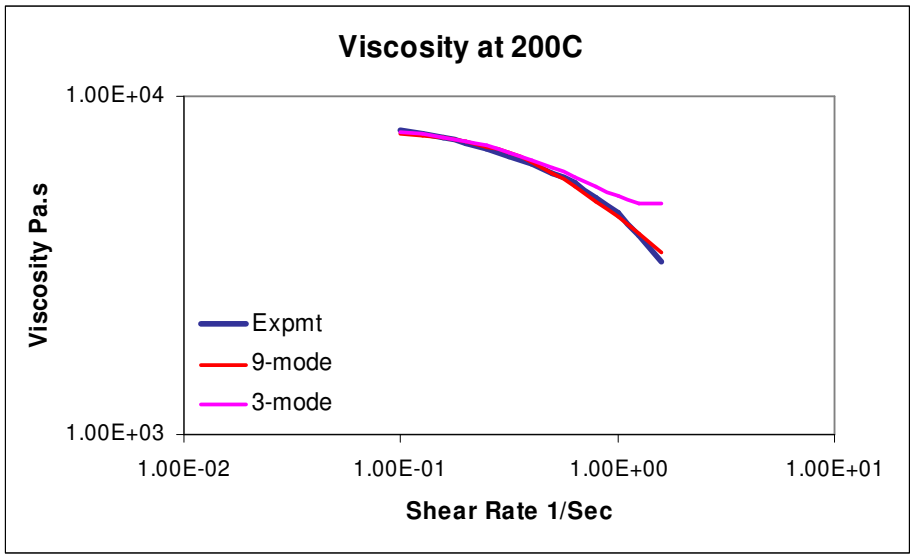

Figure 2.4-14. Multi-mode Giesekus model data fitting of viscosity for Polypropylene melt at 200°C.

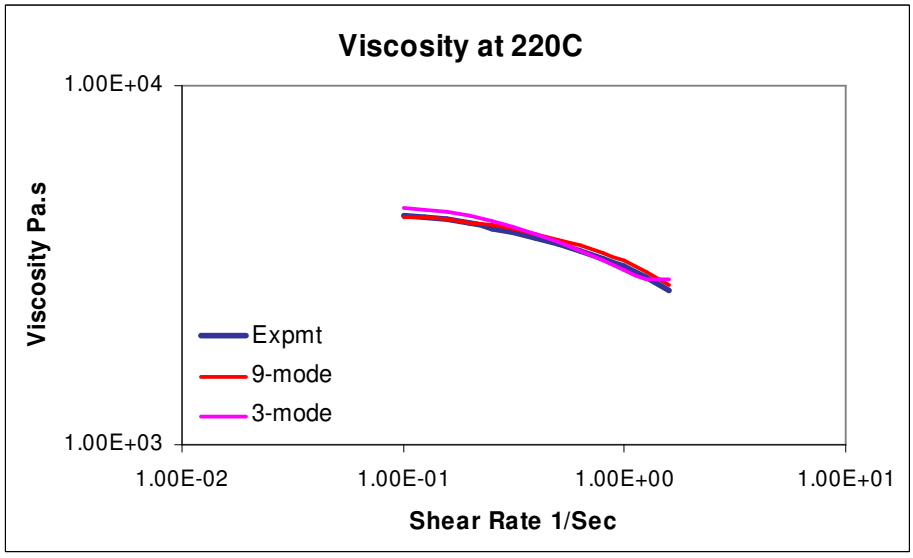

Figure 2.4-15. Multi-mode Giesekus model data fitting of viscosity for Polypropylene melt at 220°C.

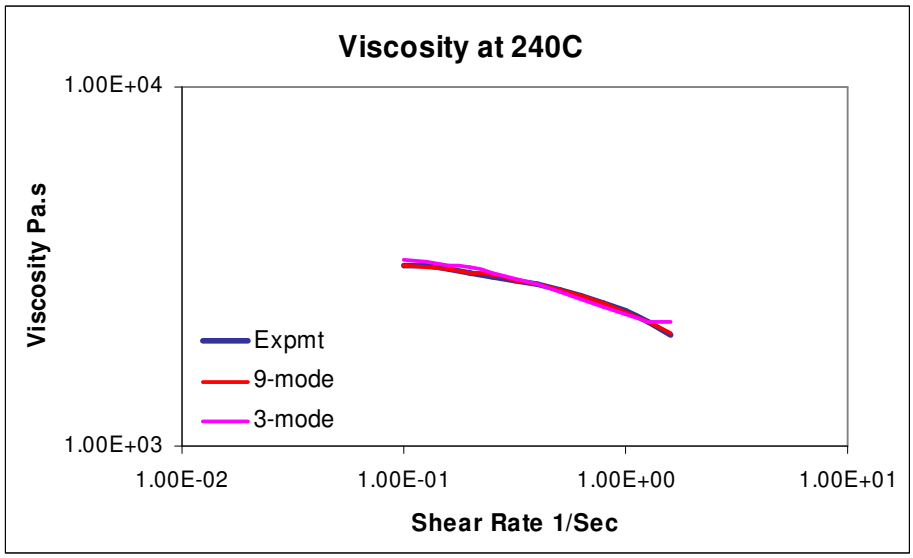

Figure 2.4-16. Multi-mode Giesekus model data fitting of viscosity for Polypropylene melt at 240°C.

Figures 2.4-13 to 2.4-16 represent data fitting of the Giesekus model to experimental viscosity data in steady shear flow. From the figures above it is clear that the experimental viscosity decreased with increasing shear rate. In this experiment, due to the limitation of the experimental apparatus, we were unable to obtain experimental data for high shear rates as normally experienced in injection molding. However, using the material parameters we have already obtained from stress relaxation and dynamic frequency sweep experiments in the previous sections, it can be seen, in the figures above, that the prediction for steady state viscosity is quite accurate.

Figures 2.4-17 to 2.4-20 present predictions of the first-normal stress coefficient. Note that the material parameter, relaxation times, were obtained by data fitting multi-mode relaxation modulus to stress relaxation experiment data. The retardation times were obtained by data fitting the multi-mode Giesekus model to dynamic frequency sweep experiment data. The equation parameter mobility factor was obtained by data fitting the multi-mode Giesekus model to rate sweep experiment viscosity data.

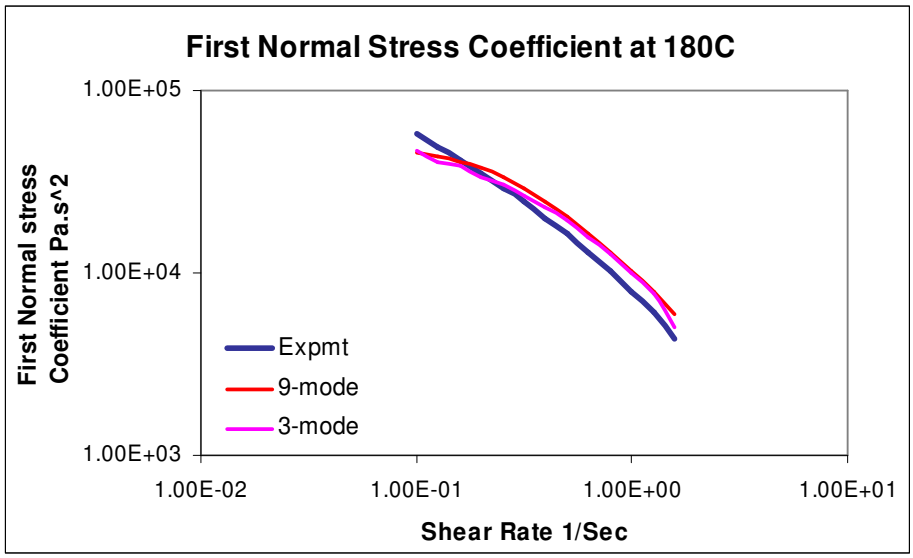

Figure 2.4-17. Prediction of first normal stress coefficient using multi-mode Giesekus model for Polypropylene melt at 180°C.

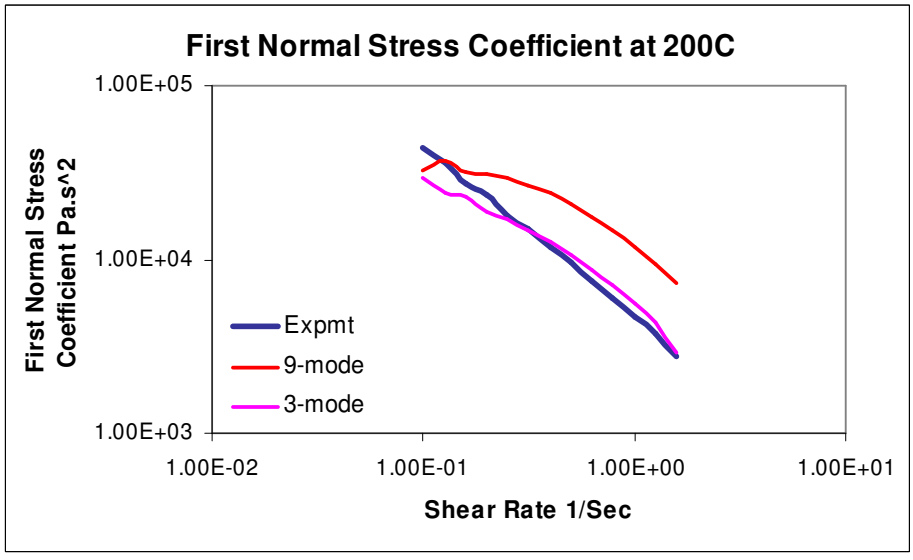

Figure 2.4-18. Prediction of first normal stress coefficient using multi-mode Giesekus model for Polypropylene melt at 200°C.

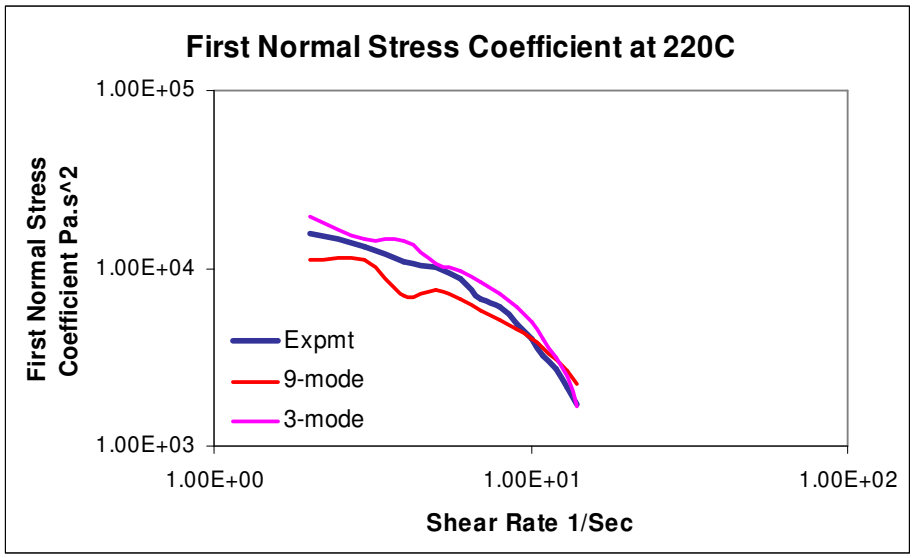

Figure 2.4-19. Prediction of first normal stress coefficient using multi-mode Giesekus model for Polypropylene melt at 220°C.

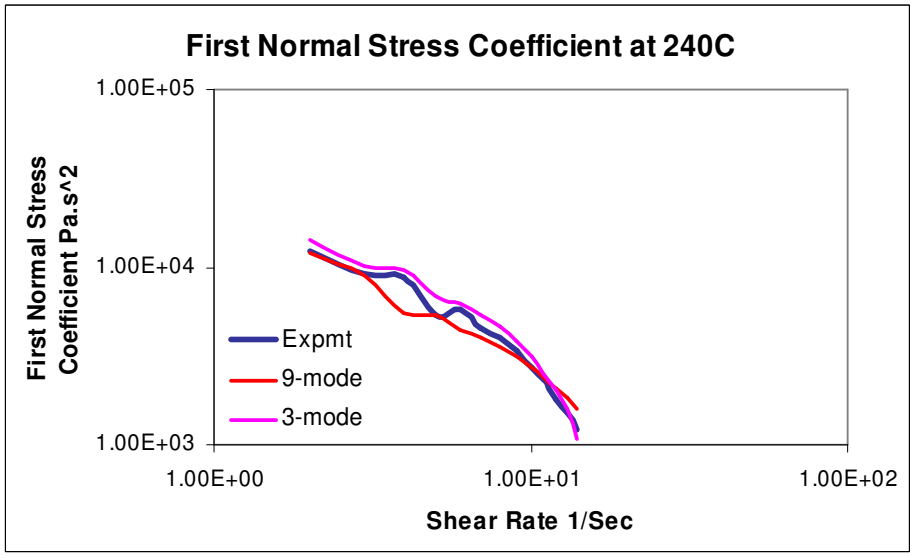

Figure 2.4-20. Predictions of first normal stress coefficient using multi-mode Giesekus model for polypropylene melt at 240°C.

Figures 2.4-17 to 2.4-20 represent data fitting of the Giesekus model to experimental first normal-stress coefficient data in steady state. From the Figures above it is clear that the experimental data decreased with increasing shear rate. Since it was difficult to measure first normal stress coefficient, the data we have obtained might not emulate the real value for the stress coefficients. So the discrepancy in prediction of first normal stress coefficient using the material parameters we have already obtained from stress relaxation and dynamic frequency sweep experiments in previous section, and the experimental data was anticipated. The reason for this discrepancy was solely due to the limitation of the experimental apparatus and the difficulty of measuring the stress coefficient.

The values of relaxation times, retardation times, mobility factors, and zero shear rate viscosity are given in Appendix - 1.

Comparing the multi-mode data fitting, it is obvious that single mode was inadequate in describing the full effect of the flow. The single mode model only describes a narrow region of the flow well. A single mode model would be useful if the flow regime was known in advance. In the 3-mode and 9-mode model, the data fitting error between them was similar. Bearing in mind that in simulations using multi-mode models the number of unknowns increases with the number of modes, it is would be preferable to use the 3-mode model where possible. For the purposes of further simulation work, it was assumed that the single-mode model would be adequate, if the flow range of interest was known. For example, if the exact shear rate was known, the one-mode model, which best describes the shear rate well, could be used. Also, since the computational cost is substantially less, it was established that simulation work would proceed with a single-mode viscoelastic constitutive equation.

2.6 Chapter Summary

Selection of viscoelastic constitutive equations for flows in complex geometries is difficult. There is no one constitutive equation that is best for describing arbitrary

viscoelastic flow in arbitrary domains. Upon considering the concerns of Larson the Giesekus and Oldroyd-B models were selected.

Certain integral type viscoelastic constitutive equations present difficulties in determining the potential function. However, the experimental procedures for polymer characterisation will be the same no matter which viscoelastic constitutive equations are being used. The relaxation times were obtained from the stress relaxation experiments (linear viscoelastic). The retardation times were obtained from dynamic frequency sweep (oscillatory shear flow) experiments. The mobility factors were obtained from steady state rate sweep experiments. Generally, the more the modes the more computationally intensive the simulations are. In the multi-mode model simulation, the number of unknowns in a problem increases approximately with the number of modes; with present computers, using more than two or possibly three modes is not practical.

In numerical computations of complex flows involving viscoelastic liquids the implicit form and the non-linear character of the constitutive equations give rise to fundamental difficulties which are discussed in Chapter 3.

3. Numerical Methods

The equation and material parameters for a viscoelastic constitutive equation are necessary to simulate flow fields. Since the methods for obtaining them have been shown in the previous chapter, this chapter will describe the numerical techniques used for flow simulation of a single-mode differential type viscoelastic constitutive equation.

3.1 Background and Overview

In the early 70s development of numerical methods for the Navier-stokes equation led to further developments in extending the viscoelastic constitutive equations. However, the viscoelastic constitutive equations are either an implicit equation of the differential type, or an integral memory equation. Many research works have been completed on different numerical techniques for flow simulation. Apart from other problems, one of the most common in simulation is the failure of the numerical schemes to provide solutions beyond some critical values of *Weissenberg* number, a dimensionless number that determines the elastic character of the flow. Failure of the numerical simulation generally contributes to the type of viscoelastic constitutive equation chosen, or to the numerical scheme chosen, or both. A negative feature of all the existing numerical techniques for calculating viscoelastic flow is their lack of robustness [Debbaut *et al.* 1986]. It is necessary to develop an entirely different method to solve viscoelastic flow accurately. Crochet [1986] outlined that, "it was initially thought that the development of appropriate non-linear algorithms would allow one to reach high values of the *Weissenberg* number; and to simulate problems of industrial interest in polymer processing, the numerical problem was found much more difficult". It is obvious there are no standard techniques available for viscoelastic flow although definite progress has been made in simulating viscoelastic constitutive equations. Crochet [1986] also states that, "the comparisons between numerical and experimental observations have not been entirely satisfactory". The main reason for this might not be numerical since the selection of an appropriate constitutive equation conditions the final-result. One of the main causes for the breakdown of the numerical solution at low value of *Weissenberg* number is due to the numerical errors which either produce inaccurate stress fields with

fluids of the differential type, or incompatible strain histories with fluids of integral type.

Several numerical techniques have been used to simulate viscoelastic constitutive equations. Some of the most popular numerical methods include the finite element method, finite volume method, boundary element method, and finite difference method. Crochet, Davies and Walters [1984] have reviewed finite difference and finite element methods used for solving Non-Newtonian flows. In their work a wealth of bibliographic references are presented.

Among these methods, the finite element method has been most popular among researchers and practitioners. In the finite element method of approximation, the continuum is divided into a finite number of elements, and the behaviour of elements is specified by a finite number of parameters. The solution of the complete system as an assembly of its elements follows precisely the same rules as those applicable to standard discrete problems [Zienkiewicz 1977].

Many sophisticated algorithms have been developed to solve fluid flow within the framework of the finite element method. The mixed finite element algorithm was first proposed by Crochet et al. [1984]. The 4X4 algorithm was developed by Marchal *et al.* [1987]. Rajgopalan *et al.* [1990] first introduced the elastic-viscous-stress-splitting (EVSS) technique. Rice and Schnipke [1986] used the equal-order-velocity-pressure algorithm. King *et al.* [1988] first proposed the Explicitly Elliptic Momentum Equation (EEME) algorithm.

Debae *et al.* [1994] evaluated some of these algorithms for the flow of a Maxwell fluid around a sphere, through a wavy tube, an abrupt contraction, and in a circular extrusion. They found that the 4X4 method is expensive in computer time, but showed coherently good behaviour in all problems. The presence of sub-elements reduces the effects of artificial diffusion with the SU method: SUPG [Brooks *et al.* 1982] fails in the presence of stress singularities. The EVSS1 method [Rajgopalan *et al.*1990], which is a variant

of EVSS method, is relatively cheap in computer time and remarkably stable. The MIX0 method is cheap but it exhibited an erratic behaviour [Debae *et al.* 1994].

Debbaut and Crochet have used the mixed finite-element method MIX1 [Crochet *et al.* 1984] for non-Newtonian flow, and simulated the Phan-Thien-Tanner model in a 4:1 abrupt contraction and showed that the loss of convergence is of purely numerical origin. Similarly Keunings [1986], using a mixed algorithms approach through a sudden contraction, also concluded the high *Weissenberg* problem is of numerical origin. Marchal and Crochet [1987] using a mixed finite element method on a 4:1 abrupt contraction, concluded that at high values of *Deborah* number the numerical instabilities are due to the numerical technique used, but not due to the intrinsic property of the viscoelastic constitutive equations. The other researchers who have reached similar conclusions in their research are given in reference [Crochet *et al.* 1985].

Rajgopalan *et al.* [1990, and 1992] used EVSS/FEM for stability and accuracy in solving viscoelastic, and free surface flows, without contact-singularities. Rao and Finlayson [1992] used the EEME and inconsistent Petrov-Galerkin streamline upwinding method (SU) for flow simulation of Maxwell and Oldroyd-B fluids in a 4:1 axisymmetric contraction. Rasmussen and Hassager [1993, and 1995] have developed a Galerkin finite element method based on a Lagaragian kinematics description for integral models. This Lagarangian integral method also converges with time increment. A viscoelastic flow in 4:1 contraction was solved, by Carew, Townsend, and Webster [1993] using the generalised Taylor-Galerkin Pressure correction scheme that incorporates consistent Petrov-Galerkin streamline upwinding within the discretization of Oldroyd-B and Phan-Thien-Tanner constitutive equations. Similarly, Baaijens [1993, and 1994] simulated Giesekus, Phan-Thien-Tanner, and Maxwell fluid through a 4:1 axisymmetric contraction. The algorithm used for this was constructed by employing discontinuous interpolants for the extra stress components and the pressure field. Baaijens [1993] also used an operator splitting methodology to extract the advective parts of the constitutive equations. The comparison of the results in Baaijens study found that a much higher *Deborah* number could be obtained than the EEME method

employed by Coates et al. [1992]. Keiller [1993] used a decoupled finite difference scheme with time stepping to simulate the entry flow in Oldroyd-B and FENE constitutive equations. Lou and Tanner simulated flow of Maxwell type fluid in extrusion using the streamline-element-scheme (S.E.S) algorithm in their finite element method. Azaiez et al. [1996] used a mixed finite element method to simulate differential type viscoelastic constitutive equations in 4:1 contraction. However, their results showed a stronger stress overshoot near the entry region than has been observed in the experiment. Guénette and Fortin [1995] used a new mixed finite element method for viscoelastic flow. This mixed formulation is based on the introduction of the deformation rate tensor as an additional unknown. Contrary to the popular EVSS method, no change of variable was performed in the constitutive equation. Hence, the described method can be used to compute solutions of rheological models where the EVSS method does not apply [Guénette *et al.* 1995].

Many researchers have used a combination of finite element and finite volume approximations to solve viscoelastic flow problems. In the finite volume method [Patankar 1980], the volume integral of the governing equations, over a finite control volume express the conservation principle just as the differential equations express it for an infinitesimal control volume.

Sato *et al.* [1994] used a combination of the finite element and finite volume methods for momentum and viscoelastic constitutive equations respectively for viscoelastic flow problems. Sasmal [1995] used the finite volume method along with the EVSS [Rajgopalan *et al.* 1990] form and a first order upwind approximation to simulate the upper convected Maxwell model in a 4:1 contraction flow to a *Deborah* number of 6.25. Yoo *et al.*[1991] used the finite volume technique to simulate Oldroyd-B fluid in a 4:1 contraction using a non-uniform staggered grid system, which incorporates the SIMPLER [Patankar 1980] algorithm in discretising momentum equations.

Various other researches have published numerical techniques on viscoelastic flow simulations. Their research can be found in many number of references [Fortin *et al.*

1987,Hadj *et al.* 1990, Laso *et al.* 1993, Lou *et al.* 1986, 1988, 1989, Lunsman *et al.* 1993, Rasmuseen *et al.* 1993, 1995, Talwar *et al.* 1995, and Wesson *et al.* 1989].

Some authors, with varying degree of success, have simulated complex viscoelastic flows. For example Coyle *et al*. [1987] specifically addressed the fountain flow in mould filling. Papathanasiou *et al*. [1993] simulated the filling stage of injection moulding using the White-Metzner model. However most of these simulations focus on particular aspects of two dimensional injection moulding rather than the overall moulding (complex) simulation, with the exception of Couniot *et al.* who have simulated a filling stage of injection moulding on a thin planar section with the Generalized Newtonian fluid in three dimensions.

Almost all of these viscoelastic constitutive equation simulations have a simple contraction flow geometry. However a better understanding of this flow problem can ultimately lead to improving the prediction of polymer melt flow in complex geometry such as polymer processing flow.

Over the past years, definite progresses have been made towards finding better numerical techniques for solving governing equations in viscoelastic flow. In this study, a finite element method to solve the governing equations in viscoelastic flow field was employed.

To predict the flow using viscoelastic constitutive equations means obtaining velocities, pressure and stresses at every point or node of the solution domain were used. Generally, the velocities were obtained by solving the momentum equation using known or estimated pressure. The pressure was obtained by solving the pressure equation that was specifically derived from continuity and velocity-pressure relationships, using known velocity fields. Polymeric stresses were also obtained by solving the viscoelastic constitutive equations using known velocity fields.

This chapter contains two major sections. Section 3.2 discusses the basic governing equations that were solved for the viscoelastic flow field. Section 3.3 discusses the discretization methods that were used to simplify the governing equations. This section discretizes momentum, viscoelastic constitutive equations, and pressure equation, which were derived from the relationship between velocity and pressure, and continuity equation.

3.2 Governing Equations

The governing equations for the viscoelastic flow field include the conservation of mass, conservation of momentum and viscoelastic constitutive equations.

The Conservation of Mass equation for incompressible fluid is defined as:

$$\nabla \cdot \boldsymbol{V} = 0 \tag{3.2-1}$$

where $\boldsymbol{V}$ is velocity vector.

The conservation of mass in three-dimensional *ij* form is described as:

$$\sum_i \frac{\partial v_i}{\partial x_i} = 0 \tag{3.2-2}$$

where x_i is the direction co-ordinate, (i.e. $x_1 = x$, $x_2 = y$, and $x_3 = z$ direction), v_i is the velocity component (i.e. $v_1 = u$, $v_2 = v$, and $v_3 = w$) of velocity vector $\boldsymbol{V}$. So the conservation of mass in simpler notation is defined as:

$$\frac{\partial u}{\partial x}+\frac{\partial v}{\partial y}+\frac{\partial w}{\partial z}=0 \tag{3.2-3}$$

where u, v, and w are velocity components in x, y, and z direction respectively.

The Conservation of Momentum equation is defined as:

$$\rho\frac{D\boldsymbol{V}}{Dt}=-\nabla P+\nabla\cdot\boldsymbol{S}+\rho g \tag{3.2-4}$$

where P is the pressure, $\boldsymbol{V}$ is the velocity vector, $\boldsymbol{S}$ is the extra stress tensor, ρ is the density and g is the acceleration due to gravity. The extra stress tensor, $\boldsymbol{S}$, can be conveniently decomposed to Newtonian and Non-Newtonian contributions to $\boldsymbol{S}$, and is expressed as follows:

$$\boldsymbol{S}=\boldsymbol{\tau}_p+\boldsymbol{\tau}_s \tag{3.2-5}$$

where $\boldsymbol{\tau}_p$ is the polymeric or non-Newtonian contribution and $\boldsymbol{\tau}_s$ is the solvent contribution to the extra stress tensor $\boldsymbol{S}$. This is called Elastic-Viscous-Stress-Spliting or EVSS [Rajgopalan 1990, 1992]. An explicitly elliptic operator was introduced into the momentum equation by splitting the deviatoric or extra stress tensor into Newtonian and polymer contribution. The resulting EVSS/FEM method technique [Rajgopalan, 1992, 1990] had good stability properties for both quasi-linear and non-linear constitutive equations [Lunsmann 1993]. The solvent contribution of the extra stress tensor can be further defined as:

$$\boldsymbol{\tau}_s=\eta_s 2\boldsymbol{D} \tag{3.2-6}$$

where η_s is the solvent contribution to zero shear rate viscosity and $2\boldsymbol{D}$ is the deformation rate tensor. The solvent viscosity and deformation rate tensor are defined as:

$$\eta_s = \eta_0 - \eta_p \tag{3.2-7}$$

$$2\boldsymbol{D} = \nabla \boldsymbol{V} + (\nabla \boldsymbol{V})^T \tag{3.2-8}$$

where η_0 is zero shear rate viscosity, η_p is polymer contribution to zero shear rate viscosity, and the superscript, *T,* is the symbol for matrix transpose. In three-dimensional *ij* form the deformation rate tensor is defined as:

$$2D_{ij} = \sum_i \sum_j \boldsymbol{\delta}_i \boldsymbol{\delta}_j \left(\frac{\partial v_j}{\partial x_i} + \frac{\partial v_i}{\partial x_j} \right) \tag{3.2-9}$$

where $\boldsymbol{\delta}$ is the unit vector.

Simplifying the equation (3.2-5) using equation (3.2-6), we obtain:

$$\boldsymbol{S} = \boldsymbol{\tau}_P + 2\eta_S \boldsymbol{D} \tag{3.2-10}$$

Substituting equation (3.2-10) in to the momentum equation (3.2-4), we obtain

$$\rho \frac{DV}{Dt} = -\nabla P + \nabla \cdot \boldsymbol{\tau}_P + \nabla \cdot \left(2\eta_s \boldsymbol{D}\right) + \rho g \tag{3.2-11}$$

In three-dimensional rectangular co-ordinate *ij* form the momentum equation is defined as:

$$\sum_i \boldsymbol{\delta}_i \rho \left(\frac{\partial v_i}{\partial t} + \sum_j v_j \frac{\partial v_i}{\partial x_j} \right) = -\sum_i \boldsymbol{\delta}_i \frac{\partial P}{\partial x_i} + \sum_i \boldsymbol{\delta}_i \sum_j \frac{\partial \tau_{pji}}{\partial x_j} + \eta_s \sum_i \boldsymbol{\delta}_i \sum_j \frac{\partial 2D_{ji}}{\partial x_j} + \rho g \tag{3.2-12}$$

Since the polymer contribution to extra stress tensor is symmetric, the above momentum equation in the *x* co-ordinate direction is simplified as:

$$\begin{aligned} \rho \left(\frac{\partial u}{\partial t} + u \frac{\partial u}{\partial x} + v \frac{\partial u}{\partial y} w \frac{\partial u}{\partial z} \right) = \frac{\partial \tau_{pxx}}{\partial x} + \frac{\partial \tau_{pxy}}{\partial y} + \frac{\partial \tau_{pxz}}{\partial z} + \\ \eta_s \left(\frac{\partial 2D_{xx}}{\partial x} + \frac{\partial 2D_{xy}}{\partial y} + \frac{\partial 2D_{xz}}{\partial z} \right) - \frac{\partial P}{\partial x} + \rho g_x \end{aligned} \tag{3.2-13}$$

Similarly, the simplified momentum equation in *y* co-ordinate direction is simplified as:

$$\begin{aligned} \rho \left(\frac{\partial v}{\partial t} + u \frac{\partial v}{\partial x} + v \frac{\partial v}{\partial y} w \frac{\partial v}{\partial z} \right) = \frac{\partial \tau_{pxy}}{\partial x} + \frac{\partial \tau_{pyy}}{\partial y} + \frac{\partial \tau_{pzy}}{\partial z} + \\ \eta_s \left(\frac{\partial 2D_{xy}}{\partial x} + \frac{\partial 2D_{yy}}{\partial y} + \frac{\partial 2D_{zy}}{\partial z} \right) - \frac{\partial P}{\partial y} + \rho g_y \end{aligned} \tag{3.2-14}$$

Again, the corresponding equation in *z* direction was simplified as:

$$\rho\left(\frac{\partial w}{\partial t}+u\frac{\partial w}{\partial x}+v\frac{\partial w}{\partial y}w\frac{\partial w}{\partial z}\right)=\frac{\partial \tau_{pxz}}{\partial x}+\frac{\partial \tau_{pyz}}{\partial y}+\frac{\partial \tau_{pzz}}{\partial z}+ \eta_s\left(\frac{\partial 2D_{xz}}{\partial x}+\frac{\partial 2D_{yz}}{\partial y}+\frac{\partial 2D_{zz}}{\partial z}\right)-\frac{\partial P}{\partial z}+\rho g_z \tag{3.2-15}$$

The momentum equations (3.2-13), (3.2-14), and (3.2-15) were further simplified by substituting the simplified deformation-rate tensor equation (3.2-9) and neglecting the body force. The simplified momentum equations in the *x* co-ordinate is then defined as follows:

$$\rho\left(\frac{\partial u}{\partial t}+u\frac{\partial u}{\partial x}+v\frac{\partial u}{\partial y}w\frac{\partial u}{\partial z}\right)=-\frac{\partial P}{\partial x}+\frac{\partial \tau_{pxx}}{\partial x}+\frac{\partial \tau_{pxy}}{\partial y}+\frac{\partial \tau_{pxz}}{\partial z}+ \eta_s\left(2\frac{\partial}{\partial x}\left(\frac{\partial u}{\partial x}\right)+\frac{\partial}{\partial y}\left(\frac{\partial u}{\partial y}+\frac{\partial v}{\partial x}\right)+\frac{\partial}{\partial z}\left(\frac{\partial u}{\partial z}+\frac{\partial w}{\partial x}\right)\right) \tag{3.2-16}$$

Similarly, in the *y* co-ordinate, it is defined as:

$$\rho\left(\frac{\partial v}{\partial t}+u\frac{\partial v}{\partial x}+v\frac{\partial v}{\partial y}w\frac{\partial v}{\partial z}\right)=-\frac{\partial P}{\partial y}+\frac{\partial \tau_{pxy}}{\partial x}+\frac{\partial \tau_{pyy}}{\partial y}+\frac{\partial \tau_{pzy}}{\partial z}+ \eta_s\left(\frac{\partial}{\partial x}\left(\frac{\partial u}{\partial y}+\frac{\partial v}{\partial x}\right)+2\frac{\partial}{\partial y}\left(\frac{\partial v}{\partial y}\right)+\frac{\partial}{\partial z}\left(\frac{\partial v}{\partial z}+\frac{\partial w}{\partial y}\right)\right) \tag{3.2-17}$$

and in the *z* co-ordinate it is simplified as:

$$\rho\left(\frac{\partial w}{\partial t}+u\frac{\partial w}{\partial x}+v\frac{\partial w}{\partial y}w\frac{\partial w}{\partial z}\right)=-\frac{\partial P}{\partial z}+\frac{\partial \tau_{pxz}}{\partial x}+\frac{\partial \tau_{pyz}}{\partial y}+\frac{\partial \tau_{pzz}}{\partial z}+ \eta_s\left(\frac{\partial}{\partial x}\left(\frac{\partial u}{\partial z}+\frac{\partial w}{\partial x}\right)+\frac{\partial}{\partial y}\left(\frac{\partial v}{\partial z}+\frac{\partial w}{\partial y}\right)+2\frac{\partial}{\partial z}\left(\frac{\partial w}{\partial z}\right)\right) \tag{3.2-18}$$

The viscoelastic constitutive equation for the Oldroyd-B [Zheng 1991] fluid can be written as:

$$\boldsymbol{S} + \lambda_1 \overset{\nabla}{\boldsymbol{S}} = 2\eta_0 (\boldsymbol{D} + \lambda_2 \overset{\nabla}{\boldsymbol{D}}) \tag{3.2-19}$$

where the convected derivative (superscripted ∇) of the extra stress tensor, and the deformation rate tensor, and retardation time are defined as:

$$\overset{\nabla}{\boldsymbol{S}} = \frac{\partial s}{\partial t} + \boldsymbol{V} \cdot \nabla \boldsymbol{S} - \boldsymbol{S} \cdot \nabla \boldsymbol{V} - (\nabla \boldsymbol{V})^T \cdot \boldsymbol{S} \tag{3.2-20}$$

and

$$\lambda_2 = \left(1 - \frac{\eta_p}{\eta_0}\right)\lambda_1 \tag{3.2-21}$$

Using equation (3.2-7), (3.2-10), and (3.2-21), the Oldroyd-B equation (3.2-19) can be simplified as:

$$\boldsymbol{\tau}_p + \lambda_1 \overset{\nabla}{\boldsymbol{\tau}}_p = 2\eta_p \boldsymbol{D} \tag{3.2-22}$$

where λ_1 is the relaxation time and η_p is the polymer viscosity, obtained from Chapter 2.

3.3 Discretization

This research project utilised the finite element approximation to solve the Navier-Stokes and viscoelastic constitutive equations for fluid flow. The solution domain was discretized using four node linear tetrahedral elements. Over each element, velocities, pressure, and the material properties were approximated using the unit co-ordinate interpolation functions. All variables, including velocity, pressure, stresses etc. were defined at four vertices of a tetrahedral element as a consequence of equal-order interpolation. All the components of the momentum and viscoelastic equations were discretized using the Galerkin weighted-residual method and assembled element by element to form a system of linear algebraic equations of the global form:

$$[A]\{V\} = \{F\} \tag{3.3-1}$$

The pressure equation derived from conservation of mass and momentum equations was also discretized to the above equation (3.3-1) form. The momentum equation, pressure equation and viscoelastic constitutive equations of the above discretized form were hence solved sequentially to obtain the velocity, pressure and polymeric contribution to total stresses in each components. The convective terms in the momentum and viscoelastic constitutive equations were discretized using the Streamline Upwind Petrov Galerkin (SUPG) method [Brooks *et al.* 1982] to provide upwinding. The resulting velocities by solving the discretized momentum equation were corrected by a pressure closure to impose the global conservation of mass.

Time dependent terms in momentum and viscoelastic constitutive equations were discretized using the classical backward time difference method, often called the method of *Kantorvich* [Burnet 1987]. To increase the accuracy of the derivatives of velocity and polymer contribution to total stress components, they have been calculated as piecewise linear rather than constant within each element.

3.3.1 SUPG Formulation

Viscoelastic constitutive equations contain hyperbolic character in the form of convective derivative terms. It is known that the hyperbolic problems are difficult to solve by means of the Galerkin finite elements. Typically, one is forced to use highly refined meshes and specific techniques generally labeled as 'upwinding' or 'artificial diffusitivity'. Brooks and Hughes [1982] introduced the first Streamline-Upwind/Petrov-Galerkin method (SUPG) for linear advection terms in the momentum equation.

There are two types of SUPG methods, the consistent and non-consistent. In the consistent method the weighting-function is applied to all the terms in the constitutive equations. However this is only satisfactory when one calculates the stresses on the basis of a given velocity field. The consistent SUPG fails once the constitutive equations are coupled with the equations of motion and the incompressibility constraints [Marchal & Crochet 1987]. Thus, we have used a non-consistent SUPG method. In this method, the weighting-function only applies to convective terms. Szady *et al.* [1995] simulated the Oldroyd-B constitutive equation using SU and SUPG for flows between eccentric rotating cylinders, flow through a wavy-walled tube and flow through a square array of cylinders. They found that discretization of the Oldroyd-B constitutive equation by SUPG gave superior accuracy at high values of *Deborah* number compared to the SU.

Since the convective terms only were discretized using the Streamline-Upwind Petrov-Galerkin method [Brooks *et al.* 1982], the weighting function for the convective terms were defined as:

$$\tilde{\Phi}_i = \Phi_i + C\boldsymbol{V}.\nabla\Phi_i \tag{3.3-2}$$

where Φ_i is the linear tetrahedral shape or trial function, $\boldsymbol{V}$ is the velocity and C is constant within the element. The constant C is defined as:

$$C = \frac{1}{\sqrt{15}} \frac{\left(\Delta \hat{U}\right)^{1/3}}{U} \tag{3.3-3}$$

where $\hat{U}$ is volume of the element, U is a constant within an element. The constant U was defined as:

$$U = \frac{1}{4}\left(\left|U_1\right| + \left|U_2\right| + \left|U_3\right| + \left|U_4\right|\right) \tag{3.3-4}$$

where $|U_i|$ is the magnitude of velocity at a node.

The magnitude of velocity at a node was defined as:

$$\left|U_i\right| = \left(u_i^2 + v_i^2 + w_i^2\right)^{\frac{1}{2}} \tag{3.3-5}$$

Since the solution domain was discretized using 4-node linear tetrahedral elements, the shape or trial functions of the linear tetrahedral elements were Φ_1, Φ_2, Φ_3, and Φ_4, with the relationships between the shape functions being:

$$\Phi_1 + \Phi_2 + \Phi_3 + \Phi_4 = 1 \tag{3.3-6}$$

The volume and area integral of the shape functions were given as:

$$\iiint \Phi_1^a \Phi_2^b \Phi_3^c \Phi_4^d d\Phi = \int_\Omega \Phi_1^a \Phi_2^b \Phi_3^c \Phi_4^d d\Omega = \frac{a!b!c!d!}{(a+b+c+d+3)!} 6V \tag{3.3-7}$$

and

$$\iint \Phi_1^a \Phi_2^b \Phi_3^c d\Phi = \int_A \Phi_1^a \Phi_2^b \Phi_3^c dA = \frac{a!b!c!}{(a+b+c+2)!} 2A \tag{3.3-8}$$

where V is the volume of the linear tetrahedral element and A is the area of the one of the facet of the linear tetrahedral element.

Using linear tetrahedral shape functions the velocity components were defined as:

$$u = \sum_{j=1}^{4} \Phi_j u_j \tag{3.3-9}$$

$$v = \sum_{j=1}^{4} \Phi_j v_j \tag{3.3-10}$$

$$w = \sum_{j=1}^{4} \Phi_j w_j \tag{3.3-11}$$

where j is the jth node. Similarly, the polymeric contribution to stress tensor or any other variables was also defined exactly the same way as described in the above equations.

The derivative of velocity, using linear tetrahedral shape functions was defined as:

$$\frac{\partial u}{\partial x_i} = \sum_{j=1}^{4} \frac{\partial \Phi_j}{\partial x_i} u_j \tag{3.3-12}$$

$$\frac{\partial v}{\partial x_i} = \sum_{j=1}^{4} \frac{\partial \Phi_j}{\partial x_i} v_j \tag{3.3-13}$$

$$\frac{\partial w}{\partial x_i} = \sum_{j=1}^{4} \frac{\partial \Phi_j}{\partial x_i} w_j \tag{3.3-14}$$

where j is the jth node, and i is the directional co-ordinate, i.e. x_1, x_2, and x_3 are x, y, and z co-ordinates respectively. The derivative of other variables was also calculated in the same way as described in the above equations.

The derivatives of the shape functions were calculated by forming a 3 by 3 Jacobian matrix and inverting the Jacobian matrix. The Jacobian matrix was defined as:

$$[J] = \begin{bmatrix} \frac{\partial x}{\partial \Phi_1} & \frac{\partial x}{\partial \Phi_2} & \frac{\partial x}{\partial \Phi_3} \\ \frac{\partial y}{\partial \Phi_1} & \frac{\partial y}{\partial \Phi_2} & \frac{\partial y}{\partial \Phi_3} \\ \frac{\partial z}{\partial \Phi_1} & \frac{\partial z}{\partial \Phi_2} & \frac{\partial z}{\partial \Phi_3} \end{bmatrix} \tag{3.3-15}$$

where x is the nodal value of the x co-ordinate in an element and was defined in a similar manner to equation (3.3-9) as:

$$x = \sum_{j=1}^{4} \Phi_j x_j \tag{3.3-16}$$

where Φ is the linear tetrahedral shape function. Similarly, the values of y and z co-ordinates followed the above equation with y, and z replacing x in turn. Using the relationship between linear tetrahedral shape functions equation (3.3-6), the derivative of the above equation with respect to shape functions were defined as:

$$\frac{\partial x}{\partial \Phi_{i=1\to 3}} = x_i - x_4 \tag{3.3-17}$$

where x_i is x co-ordinate value of node-i in an element and similarly x_4 is the x co-ordinate value of node-4 in an element. Similarly, the derivatives of y, and z with respect to Φ_i were defined as:

$$\frac{\partial y}{\partial \Phi_{i=1\to 3}} = y_i - y_4 \tag{3.3-18}$$

$$\frac{\partial z}{\partial \Phi_{i=1\to 3}} = z_i - z_4 \tag{3.3-19}$$

The inverse of the Jacobian matrix was then calculated by inverting the Jacobian matrix as follows:

$$[J]^{-1} = \begin{bmatrix} \frac{\partial \Phi_1}{\partial x} & \frac{\partial \Phi_1}{\partial y} & \frac{\partial \Phi_1}{\partial z} \\ \frac{\partial \Phi_2}{\partial x} & \frac{\partial \Phi_2}{\partial y} & \frac{\partial \Phi_2}{\partial z} \\ \frac{\partial \Phi_3}{\partial x} & \frac{\partial \Phi_3}{\partial y} & \frac{\partial \Phi_3}{\partial z} \end{bmatrix} \tag{3.3-20}$$

In the above equation only the derivatives of three shape functions appear. The derivatives of the fourth shape function Φ_4 with respect to x, y, and z were derived by using the shape function relationship equation (3.3-6). The derivative of fourth shape function with respect to x, y, and z co-ordinates can be expressed as:

$$\frac{\partial \Phi_4}{\partial x_i} = -\sum_{j=1}^{3} \frac{\partial \Phi_j}{\partial x_i} \tag{3.3-21}$$

where x_i is the direction co-ordinate, (i.e. $x_1 = x$, $x_2 = y$, and $x_3 = z$ direction).

Since shape functions, the derivative of shape functions and the SUPG formulations are now known, the next section will discretize the Navier-Stokes equation using these formulations.

3.3.2 Navier-Stokes Equation

Traditionally, there are three broadly classified methods for solving the Navier-Stokes equation using the finite element approximation. The methods include the velocity-pressure-integrated method, penalty method and the segregated method. In the velocity-pressure-integrated method the governing equations are solved simultaneously. This method needs few iteration but requires a large amount of memory and computational time. The penalty method requires less memory and computational time compared with the velocity pressure integrated method, but requires an additional post processing to obtain the pressure field. The penalty method also only approximates the continuity equation. As the computation in three-dimensional space and time requires more memory and computational time, the penalty and velocity-pressure integrated method is not effective [Rajupalem *et al.* 1997]. For this reason the Navier-Stokes equations are solved using an adapted segregated finite element algorithm with equal order interpolation scheme, similar to that of Rice and Schnipke [1986], originally proposed for the two-dimension steady state flow. In this method, velocities and corresponding pressure field were computed alternately. This is similar to the SIMPLER algorithm

[Patankar 1980], using a pressure-velocity coupling widely used in finite volume approximation. This method needs much less memory and execution time and satisfies the continuity equation completely.

The categorisation of the finite element methods can also be made according to the orders of interpolation functions for velocity and pressure. They are mixed-order interpolation and equal-order interpolation. In the mixed-order interpolation method, the velocity is interpolated linearly and pressure is treated as constant within the element to avoid checkerboard pressure distributions. Thus, the mixed-order scheme is not totally effective when resolving the pressure gradients and the equal-order scheme for velocity and pressure can perform better in that sense.

The segregated algorithm with the equal-order interpolation scheme of Rice and Schnipke [1986], which was proposed for two-dimensional steady flows, was extended to time-dependent and three-dimensional Newtonian and viscoelastic flows in this Chapter. The following sections describe in detail the segregated algorithm.

Rearranging the momentum equation (3.2-16) in the x direction with respect to its unknown u gives the following:

$$\rho\left(\frac{u^n}{\Delta t}+u^p\frac{\partial u^n}{\partial x}+v^p\frac{\partial u^n}{\partial y}+w^p\frac{\partial u^n}{\partial z}\right)-\eta_s\left(2\frac{\partial}{\partial x}\frac{\partial u^n}{\partial x}+\frac{\partial}{\partial y}\frac{\partial u^n}{\partial y}+\frac{\partial}{\partial z}\frac{\partial u^n}{\partial z}\right)= \rho\frac{u^{n-1}}{\Delta t}-\frac{\partial P}{\partial x}+\eta_s\left(\frac{\partial}{\partial y}\frac{\partial v^p}{\partial x}+\frac{\partial}{\partial z}\frac{\partial w^p}{\partial x}\right)+\frac{\partial \tau_{pxx}}{\partial x}+\frac{\partial \tau_{pxy}}{\partial y}+\frac{\partial \tau_{pxz}}{\partial z} \tag{3.3-22}$$

Similarly, rearranging the momentum equation (3.2-17) in the y direction with respect to its unknown v gives:

$$\rho\left(\frac{v^n}{\Delta t}+u^p\frac{\partial v^n}{\partial x}+v^p\frac{\partial v^n}{\partial y}+w^p\frac{\partial v^n}{\partial z}\right)-\eta_s\left(\frac{\partial}{\partial x}\frac{\partial v^n}{\partial x}+2\frac{\partial}{\partial y}\frac{\partial v^n}{\partial y}+\frac{\partial}{\partial z}\frac{\partial v^n}{\partial z}\right)= \rho\frac{v^{n-1}}{\Delta t}-\frac{\partial P}{\partial y}+\eta_s\left(\frac{\partial}{\partial x}\frac{\partial u^p}{\partial y}+\frac{\partial}{\partial z}\frac{\partial w^p}{\partial y}\right)+\frac{\partial \tau_{pxy}}{\partial x}+\frac{\partial \tau_{pyy}}{\partial y}+\frac{\partial \tau_{pyz}}{\partial z} \tag{3.3-23}$$

Finally, rearranging the momentum equation (3.2-18) in the z direction with respect to its unknown w gives:

$$\rho\left(\frac{w^n}{\Delta t}+u^p\frac{\partial w^n}{\partial x}+v^p\frac{\partial w^n}{\partial y}+w^p\frac{\partial w^n}{\partial z}\right)-\eta_s\left(\frac{\partial}{\partial x}\frac{\partial w^n}{\partial x}+\frac{\partial}{\partial y}\frac{\partial w^n}{\partial y}+2\frac{\partial}{\partial z}\frac{\partial w^n}{\partial z}\right)= \rho\frac{w^{n-1}}{\Delta t}-\frac{\partial P}{\partial z}+\eta_s\left(\frac{\partial}{\partial x}\frac{\partial u^p}{\partial z}+\frac{\partial}{\partial y}\frac{\partial v^p}{\partial z}\right)+\frac{\partial \tau_{pxz}}{\partial x}+\frac{\partial \tau_{pyz}}{\partial y}+\frac{\partial \tau_{pzz}}{\partial z} \tag{3.3-24}$$

In the above momentum equations, superscript *p,* is the previous iteration, but present time step value. The non-linear terms in the left-hand side of the equations were separated to present iteration values and previous iteration values for numerical ease. In the right-hand side, we have used previous iteration values for consistency. Notice that the time dependent term is simplified by using the backward time difference method, which is defined as:

$$\frac{\partial u}{\partial t}=\lim_{\Delta t\to 0}\frac{u^n-u^{n-1}}{\Delta t} \tag{3.3-25}$$

where n is present time step and n-1 is previous time step.

The linear tetrahedral shape functions were used as weighting-functions in the Galerkin weighted residual method [Burnet 1987] for every term except the convected terms, for which the SUPG method was applied. Substituting equation (3.3-9) and (3.3-12), and

applying the Galerkin weighted residuals to the momentum equation (3.3-22) in the x direction it was found that:

$$\left[\sum_{j=1}^{4}\rho\left(\frac{1}{\Delta t}\int_{\Omega}\Phi_j\Phi_i d\Omega+\sum_{k=1}^{4}\left(u_k^p\frac{\partial\Phi_j}{\partial x}+v_k^p\frac{\partial\Phi_j}{\partial y}+w_k^p\frac{\partial\Phi_j}{\partial z}\right)\int_{\Omega}\Phi_k\Phi_i d\Omega+\Pi_{ij}\right)+\right.$$
$$\eta_s\left(2\int_{\Omega}\frac{\partial\Phi_j}{\partial x}\frac{\partial\Phi_i}{\partial x}d\Omega+\int_{\Omega}\frac{\partial\Phi_j}{\partial y}\frac{\partial\Phi_i}{\partial y}d\Omega+\int_{\Omega}\frac{\partial\Phi_j}{\partial z}\frac{\partial\Phi_i}{\partial z}d\Omega\right)-$$
$$\left.\eta_s\left(\int_A 2\frac{\partial\Phi_j}{\partial x}\Phi_i\cdot\hat{n}_x+\frac{\partial\Phi_j}{\partial y}\Phi_i\cdot\hat{n}_y+\frac{\partial\Phi_j}{\partial z}\Phi_i\cdot\hat{n}_z\right)dA\right]u_j^n= \tag{3.3-26}$$
$$\sum_{j=1}^{4}\left\{\frac{\rho}{\Delta t}u_j^{n-1}\int_{\Omega}\Phi_j\Phi_i d\Omega-\frac{\partial\Phi_j}{\partial x}P_j\int_{\Omega}\Phi_i d\Omega-\eta_s\int_{\Omega}\frac{\partial\Phi_j}{\partial x}\frac{\partial\Phi_i}{\partial y}d\Omega v_j^p-\right.$$
$$\left.\eta_s\int_{\Omega}\frac{\partial\Phi_j}{\partial x}\frac{\partial\Phi_i}{\partial z}d\Omega w_j^p+\eta_s\left(\int_A\frac{\partial\Phi_j}{\partial x}v_j\Phi_i\cdot\hat{n}_y+\frac{\partial\Phi_j}{\partial x}w_j\Phi_i\cdot\hat{n}_z\right)dA\right\}+\left(\nabla\cdot\boldsymbol{\tau}_p\right)_x$$

Substituting equation (3.3-10) and (3.3-13), and applying the Galerkin weighted residuals to the momentum equation (3.3-23) in the y direction gives:

$$\left[\sum_{j=1}^{4}\rho\left(\frac{1}{\Delta t}\int_{\Omega}\Phi_j\Phi_i d\Omega+\sum_{k=1}^{4}\left(u_k^p\frac{\partial\Phi_j}{\partial x}+v_k^p\frac{\partial\Phi_j}{\partial y}+w_k^p\frac{\partial\Phi_j}{\partial z}\right)\int_{\Omega}\Phi_k\Phi_i d\Omega+\Pi_{ij}\right)+\right.$$
$$\eta_s\left(\int_{\Omega}\frac{\partial\Phi_j}{\partial x}\frac{\partial\Phi_i}{\partial x}d\Omega+2\int_{\Omega}\frac{\partial\Phi_j}{\partial y}\frac{\partial\Phi_i}{\partial y}d\Omega+\int_{\Omega}\frac{\partial\Phi_j}{\partial z}\frac{\partial\Phi_i}{\partial z}d\Omega\right)-$$
$$\left.\eta_s\left(\int_A\frac{\partial\Phi_j}{\partial x}\Phi_i\cdot\hat{n}_x+2\frac{\partial\Phi_j}{\partial y}\Phi_i\cdot\hat{n}_y+\frac{\partial\Phi_j}{\partial z}\Phi_i\cdot\hat{n}_z\right)dA\right]v_j^n= \tag{3.3-27}$$
$$\sum_{j=1}^{4}\left\{\frac{\rho}{\Delta t}v_j^{n-1}\int_{\Omega}\Phi_j\Phi_i d\Omega-\frac{\partial\Phi_j}{\partial y}P_j\int_{\Omega}\Phi_i d\Omega-\eta_s\int_{\Omega}\frac{\partial\Phi_j}{\partial y}\frac{\partial\Phi_i}{\partial x}d\Omega u_j^p-\right.$$
$$\left.\eta_s\int_{\Omega}\frac{\partial\Phi_j}{\partial y}\frac{\partial\Phi_i}{\partial z}d\Omega w_j^p+\eta_s\left(\int_A\frac{\partial\Phi_j}{\partial y}u_j\Phi_i\cdot\hat{n}_x+\frac{\partial\Phi_j}{\partial y}w_j\Phi_i\cdot\hat{n}_z\right)dA\right\}+\left(\nabla\cdot\boldsymbol{\tau}_p\right)_y$$

Substituting equation (3.3-11) and (3.3-14), and applying the Galerkins weighted residuals to the momentum equation (3.3-24) in the z direction gives:

$$\left[\sum_{j=1}^{4}\rho\left(\frac{1}{\Delta t}\int_{\Omega}\Phi_j\Phi_i d\Omega+\sum_{k=1}^{4}\left(u_k^p\frac{\partial\Phi_j}{\partial x}+v_k^p\frac{\partial\Phi_j}{\partial y}+w_k^p\frac{\partial\Phi_j}{\partial z}\right)\int_{\Omega}\Phi_k\Phi_i d\Omega+\Pi_{ij}\right)+\right.$$
$$\eta_s\left(\int_{\Omega}\frac{\partial\Phi_j}{\partial x}\frac{\partial\Phi_i}{\partial x}d\Omega+\int_{\Omega}\frac{\partial\Phi_j}{\partial y}\frac{\partial\Phi_i}{\partial y}d\Omega+2\int_{\Omega}\frac{\partial\Phi_j}{\partial z}\frac{\partial\Phi_i}{\partial z}d\Omega\right)-$$
$$\left.\eta_s\left(\int_A\frac{\partial\Phi_j}{\partial x}\Phi_i\cdot\hat{n}_x+\frac{\partial\Phi_j}{\partial y}\Phi_i\cdot\hat{n}_y+2\frac{\partial\Phi_j}{\partial z}\Phi_i\cdot\hat{n}_z\right)dA\right]w_j^n= \tag{3.3-28}$$
$$\sum_{j=1}^{4}\left\{\frac{\rho}{\Delta t}w_j^{n-1}\int_{\Omega}\Phi_j\Phi_i d\Omega-\frac{\partial\Phi_j}{\partial z}P_j\int_{\Omega}\Phi_i d\Omega-\eta_s\int_{\Omega}\frac{\partial\Phi_j}{\partial z}\frac{\partial\Phi_i}{\partial x}d\Omega u_j^p-\right.$$
$$\left.\eta_s\int_{\Omega}\frac{\partial\Phi_j}{\partial z}\frac{\partial\Phi_i}{\partial y}d\Omega v_j^p+\eta_s\left(\int_A\frac{\partial\Phi_j}{\partial z}u_j\Phi_i\cdot\hat{n}_x+\frac{\partial\Phi_j}{\partial z}v_j\Phi_i\cdot\hat{n}_y\right)dA\right\}+\left(\nabla\cdot\boldsymbol{\tau}_p\right)_z$$

In the three equations above the notation Π_{ij} represents the discretized convective terms obtained by discretizing part of the weighting function ($Cv\cdot\nabla\Phi_i$) in SUPG equation (3.3-2) and is defined as:

$$\Pi_{ij}=\sum_{k=1}^{4}\sum_{l=1}^{4}C\int_{\Omega}\Phi_k\Phi_l d\Omega\left(\frac{\partial\Phi_j}{\partial x}\left(u_k^pu_l^p\frac{\partial\Phi_i}{\partial x}+u_k^pv_l^p\frac{\partial\Phi_i}{\partial y}+u_k^pw_l^p\frac{\partial\Phi_i}{\partial z}\right)+\right.$$
$$\frac{\partial\Phi_j}{\partial y}\left(v_k^pu_l^p\frac{\partial\Phi_i}{\partial x}+v_k^pv_l^p\frac{\partial\Phi_i}{\partial y}+v_k^pw_l^p\frac{\partial\Phi_i}{\partial z}\right)+ \tag{3.3-29}$$
$$\left.\frac{\partial\Phi_j}{\partial z}\left(w_k^pu_l^p\frac{\partial\Phi_i}{\partial x}+w_k^pv_l^p\frac{\partial\Phi_i}{\partial y}+w_k^pw_l^p\frac{\partial\Phi_i}{\partial z}\right)\right.$$

where C is defined by equation (3.3-3).

In the discretized momentum equations, for brevity, we have given the end discretization value of $\nabla\cdot\boldsymbol{\tau}_p$. However, the detailed discretization $\nabla\cdot\boldsymbol{\tau}_p$ is given in section 3.3.6. Since the value of $\boldsymbol{\tau}_p$ was obtained by solving the viscoelastic constitutive equations, at this point it was assumed that the values of $\nabla\cdot\boldsymbol{\tau}_p$ in x, y, and z directions are

known quantities. In the global matrix form the above discretized momentum equations were defined as:

$$[A]_x\{u\} = \{F^u\} \tag{3.3-30}$$

$$[A]_y\{v\} = \{F^v\} \tag{3.3-31}$$

$$[A]_z\{w\} = \{F^w\} \tag{3.3-32}$$

The area integral terms in equation (3.3-26), (3.3-27) and (3.3-28) are discussed in boundary condition section. Neglecting the boundary integral terms *ad interim*, the matrix $[A]_x$ was defined as:

$$A[i,j]_x = \left[\rho\left(\frac{1}{\Delta t}\int_\Omega \Phi_j\Phi_i d\Omega + \sum_{k=1}^{4}\left(u_k^p\frac{\partial\Phi_j}{\partial x} + v_k^p\frac{\partial\Phi_j}{\partial y} + w_k^p\frac{\partial\Phi_j}{\partial z}\right)\int_\Omega \Phi_k\Phi_i d\Omega + \Pi_{ij}\right) + \eta_s\left(2\int_\Omega \frac{\partial\Phi_j}{\partial x}\frac{\partial\Phi_i}{\partial x}d\Omega + \int_\Omega \frac{\partial\Phi_j}{\partial y}\frac{\partial\Phi_i}{\partial y}d\Omega + \int_\Omega \frac{\partial\Phi_j}{\partial z}\frac{\partial\Phi_i}{\partial z}d\Omega + \right)\right] \tag{3.3-33}$$

The matrix $[A]_y$ was defined as:

$$A[i,j]_y = \left[\rho\left(\frac{1}{\Delta t}\int_\Omega \Phi_j\Phi_i d\Omega + \sum_{k=1}^{4}\left(u_k^p\frac{\partial\Phi_j}{\partial x} + v_k^p\frac{\partial\Phi_j}{\partial y} + w_k^p\frac{\partial\Phi_j}{\partial z}\right)\int_\Omega \Phi_k\Phi_i d\Omega + \Pi_{ij}\right) + \eta_s\left(\int_\Omega \frac{\partial\Phi_j}{\partial x}\frac{\partial\Phi_i}{\partial x}d\Omega + 2\int_\Omega \frac{\partial\Phi_j}{\partial y}\frac{\partial\Phi_i}{\partial y}d\Omega + \int_\Omega \frac{\partial\Phi_j}{\partial z}\frac{\partial\Phi_i}{\partial z}d\Omega + \right)\right] \tag{3.3-34}$$

Similarly the matrix $[A]_z$ was defined as:

$$A[i,j]_z = \left[\rho\left(\frac{1}{\Delta t}\int_\Omega \Phi_j \Phi_i d\Omega + \sum_{k=1}^{4}\left(u_k^p \frac{\partial \Phi_j}{\partial x} + v_k^p \frac{\partial \Phi_j}{\partial x} + w_k^p \frac{\partial \Phi_j}{\partial x} \right)\int_\Omega \Phi_k \Phi_i d\Omega + \Pi_{ij} \right) + \eta_s\left(\int_\Omega \frac{\partial \Phi_j}{\partial x}\frac{\partial \Phi_i}{\partial x} d\Omega + \int_\Omega \frac{\partial \Phi_j}{\partial y}\frac{\partial \Phi_i}{\partial y} d\Omega + 2\int_\Omega \frac{\partial \Phi_j}{\partial z}\frac{\partial \Phi_i}{\partial z} d\Omega + \right) \right] \tag{3.3-35}$$

Vector F^u was defined as:

$$F^u\{i\} = \sum_{j=1}^{4}\left\{ \frac{\rho}{\Delta t} u_j^{n-1}\int_\Omega \Phi_j \Phi_i d\Omega - \frac{\partial \Phi_j}{\partial x} P_j \int_\Omega \Phi_i d\Omega - \eta_s \int_\Omega \frac{\partial \Phi_j}{\partial x}\frac{\partial \Phi_i}{\partial y} d\Omega v_j^p - \eta_s \int_\Omega \frac{\partial \Phi_j}{\partial x}\frac{\partial \Phi_i}{\partial z} d\Omega w_j^p \right\} + \left(\nabla \cdot \boldsymbol{\tau}_p\right)_x \tag{3.3-36}$$

vector F^v as:

$$F^v\{i\} = \sum_{j=1}^{4}\left\{ \frac{\rho}{\Delta t} v_j^{n-1}\int_\Omega \Phi_j \Phi_i d\Omega - \frac{\partial \Phi_j}{\partial y} P_j \int_\Omega \Phi_i d\Omega - \eta_s \int_\Omega \frac{\partial \Phi_j}{\partial y}\frac{\partial \Phi_i}{\partial x} d\Omega u_j^p - \eta_s \int_\Omega \frac{\partial \Phi_j}{\partial y}\frac{\partial \Phi_i}{\partial z} d\Omega w_j^p \right\} + \left(\nabla \cdot \boldsymbol{\tau}_p\right)_y \tag{3.3 -37}$$

and vector F^w as:

$$F^w\{i\} = \sum_{j=1}^{4}\left\{ \frac{\rho}{\Delta t} w_j^{n-1}\int_\Omega \Phi_j \Phi_i d\Omega - \frac{\partial \Phi_j}{\partial z} P_j \int_\Omega \Phi_i d\Omega - \eta_s \int_\Omega \frac{\partial \Phi_j}{\partial z}\frac{\partial \Phi_i}{\partial x} d\Omega u_j^p - \eta_s \int_\Omega \frac{\partial \Phi_j}{\partial z}\frac{\partial \Phi_i}{\partial y} d\Omega v_j^p \right\} + \left(\nabla \cdot \boldsymbol{\tau}_p\right)_z \tag{3.3 -38}$$

Matrix $A[i,j]$ and vector F^u, F^v and F^w were easily evaluated using equations (3.3-7) and (3.3-8).

At this point no definite relationships between velocity and pressure are found. Since, in the segregated solution scheme, the pressure equation was solved to obtain the pressure field, a relationship between velocity and pressure is necessary to develop the pressure equation.

3.3.3 Velocity-Pressure Relation

In this section, velocity is expressed as an explicit function of pressure. The required relation between velocities and pressure was obtained from the discretized global momentum equations (3.3-30), (3.3-31) and (3.3-32). The discretized global momentum equation in the x co-ordinate can be expressed as:

$$a_{x_{ii}}u_i = -\sum_{j\neq i} a_{x_{ij}}u_j + \sum_{j=1}^{4}\left\{\frac{\rho}{\Delta t}u_j^{n-1}\int_\Omega \Phi_j\Phi_i d\Omega - \eta_s\int_\Omega \frac{\partial\Phi_j}{\partial x}\frac{\partial\Phi_i}{\partial y}d\Omega v_j^p - \eta_s\int_\Omega \frac{\partial\Phi_j}{\partial x}\frac{\partial\Phi_i}{\partial z}d\Omega w_j^p\right\} + \left(\nabla\cdot\boldsymbol{\tau}_p\right)_x - \int_\Omega \Phi_i\frac{\partial P}{\partial x}d\Omega \tag{3.3-39}$$

In the y co-ordinate the discretized momentum equation can be defined as:

$$a_{y_{ii}}v_i = -\sum_{j\neq i} a_{y_{ij}}v_j + \sum_{j=1}^{4}\left\{\frac{\rho}{\Delta t}v_j^{n-1}\int_\Omega \Phi_j\Phi_i d\Omega - \eta_s\int_\Omega \frac{\partial\Phi_j}{\partial y}\frac{\partial\Phi_i}{\partial x}d\Omega u_j^p - \eta_s\int_\Omega \frac{\partial\Phi_j}{\partial y}\frac{\partial\Phi_i}{\partial z}d\Omega w_j^p\right\} + \left(\nabla\cdot\boldsymbol{\tau}_p\right)_y - \int_\Omega \Phi_i\frac{\partial P}{\partial y}d\Omega \tag{3.3-40}$$

Similarly, in the z co-ordinate the discretized momentum equation can be defined as:

$$a_{zii}w_i = -\sum_{j\neq i} a_{zij}w_j + \sum_{j=1}^{4}\left\{\frac{\rho}{\Delta t}w_j^{n-1}\int_\Omega \Phi_j\Phi_i d\Omega - \eta_s\int_\Omega \frac{\partial\Phi_j}{\partial z}\frac{\partial\Phi_i}{\partial x}d\Omega u_j^p - \eta_s\int_\Omega \frac{\partial\Phi_j}{\partial z}\frac{\partial\Phi_i}{\partial y}d\Omega v_j^p\right\} + \left(\nabla\cdot\boldsymbol{\tau}_p\right)_z - \int_\Omega \Phi_i\frac{\partial P}{\partial z}d\Omega \tag{3.3-41}$$

Assuming the pressure gradients are known, the velocities in x, y, and z directions can be expressed as:

$$u_i = \hat{u}_i - K_x\frac{\partial P}{\partial x} \tag{3.3-42}$$

$$v_i = \hat{v}_i - K_y\frac{\partial P}{\partial y} \tag{3.3-43}$$

$$w_i = \hat{w}_i - K_z\frac{\partial P}{\partial z} \tag{3.3-44}$$

where the hat velocities $\hat{u}$, $\hat{v}$, and $\hat{w}$ are defined as follows:

$$\hat{u}_i = \frac{1}{a_{xii}}\left(-\sum_{j\neq i} a_{xij}u_j + \sum_{j=1}^{4}\left\{\frac{\rho}{\Delta t}u_j^{n-1}\int_\Omega \Phi_j\Phi_i d\Omega - \eta_s\int_\Omega \frac{\partial\Phi_j}{\partial x}\frac{\partial\Phi_i}{\partial y}d\Omega v_j^p - \eta_s\int_\Omega \frac{\partial\Phi_j}{\partial x}\frac{\partial\Phi_i}{\partial z}d\Omega w_j^p\right\} + \left(\nabla\cdot\boldsymbol{\tau}_p\right)_x\right) \tag{3.3-45}$$

$$\hat{v}_i = \frac{1}{a_{yii}}\left(-\sum_{j\neq i} a_{yij}v_j + \sum_{j=1}^{4}\left\{\frac{\rho}{\Delta t}v_j^{n-1}\int_\Omega \Phi_j\Phi_i d\Omega - \eta_s\int_\Omega \frac{\partial\Phi_j}{\partial y}\frac{\partial\Phi_i}{\partial x}d\Omega u_j^p - \eta_s\int_\Omega \frac{\partial\Phi_j}{\partial y}\frac{\partial\Phi_i}{\partial z}d\Omega w_j^p\right\} + \left(\nabla\cdot\boldsymbol{\tau}_p\right)_y\right) \tag{3.3-46}$$

$$\hat{w}_i = \frac{1}{a_{z\,ii}}\left(-\sum_{j\neq i} a_{z\,ij} w_j + \sum_{j=1}^{4}\left\{ \frac{\rho}{\Delta t} w_j^{n-1} \int_\Omega \Phi_j \Phi_i d\Omega - \eta_s \int_\Omega \frac{\partial \Phi_j}{\partial z}\frac{\partial \Phi_i}{\partial x} d\Omega u_j^p - \eta_s \int_\Omega \frac{\partial \Phi_j}{\partial z}\frac{\partial \Phi_i}{\partial y} d\Omega v_j^p \right\} + \left(\nabla \cdot \boldsymbol{\tau}_p\right)_z \right) \tag{3.3-47}$$

and $K_{k=x,y,\ and\ z}$ is the pressure coefficient defined as:

$$K_k = \frac{1}{a_{k\,ii}} \int_\Omega \Phi_i d\Omega \tag{3.3-48}$$

Hat velocities ($\hat{u}$, $\hat{v}$, and $\hat{w}$) and pressure coefficient (K) are calculated at nodes. The relationship between velocity and pressure, equations (3.3-42), (3.3-43) and (3.3-44) are only approximations and not exact. However, it is not required to establish exact relationships between velocity and pressure for the solution to converge. This approximation is comparable to the use of a secant approximation in Newton's method [Rice *et al.* 1986].

3.3.4 Pressure Equation

The pressure equation was derived from the continuity equation on an element-by-element basis. The pressure equation was derived by taking the weighted residual of the continuity equation (3.2-1). The weighting-function was the same as the linear tetrahedral shape or trial function. The element residual was then defined as:

$$\varepsilon_p = \int_\Omega \nabla \cdot \boldsymbol{V} \Phi d\Omega \tag{3.3-49}$$

where Φ is the weighted function, and is the same as the linear tetrahedral shape function.

It will be subsequently shown that the desired pressure equation is a second order equation regarding pressure. Thus, to reduce the order, the equation above was integrated-by-parts, using Green's theorem. Simplifying further, the order of the equation was reduced to a first-order equation, which was defined as:

$$\varepsilon_p = \int_A \boldsymbol{V}.\hat{\boldsymbol{n}}\Phi dA - \int_\Omega \boldsymbol{V}\cdot\nabla\Phi d\Omega \tag{3.3-50}$$

where A is the area and $\hat{\boldsymbol{n}}$ is the outward normal vector.

For the pressure equation, the area integral terms appearing in the above equation form the natural boundary condition. The area integrals are zero in the wall boundary. This is true for no-slip and slip wall boundary conditions. However, at the inlet and outlet, the area integrals had to be evaluated. The evaluation of area integral is discussed in the section concerned with numerical boundary conditions. Leaving out the boundary integrals for the moment, the above equation was simplified as:

$$\varepsilon_p = -\int_\Omega \left(\frac{\partial\Phi}{\partial x}u + \frac{\partial\Phi}{\partial y}v + \frac{\partial\Phi}{\partial z}w \right) d\Omega \tag{3.3-51}$$

This equation was evaluated over all elements. Discretization of the above equation gives:

$$\varepsilon_p = -\sum_{k=1}^{4} \int_\Omega \left(\frac{\partial\Phi_i}{\partial x}\Phi_k u_k + \frac{\partial\Phi_i}{\partial y}\Phi_k v_k + \frac{\partial\Phi_i}{\partial z}\Phi_k w_k \right) d\Omega \tag{3.3-52}$$

Now substituting *u*, *v*, and *w* from equations (3.3-42), (3.3-43) and (3.3-44) respectively into the above equation we obtain:

$$\varepsilon_p = -\sum_{k=1}^{4}\int_{\Omega}\left(\frac{\partial\Phi_i}{\partial x}\Phi_k\left(\hat{u}_k - K_{xk}\frac{\partial P}{\partial x}\right)+\frac{\partial\Phi_i}{\partial y}\Phi_k\left(\hat{v}_k - K_{y_k}\frac{\partial P}{\partial y}\right)+ \frac{\partial\Phi_i}{\partial z}\Phi_k\left(\hat{w}_k - K_{zk}\frac{\partial P}{\partial z}\right)\right)d\Omega \tag{3.3-53}$$

Further discretizing pressure terms we obtain:

$$\varepsilon_{ij} = -\sum_{k=1}^{4}\sum_{j=1}^{4}\int_{\Omega}\left(\frac{\partial\Phi_i}{\partial x}\Phi_k\left(\hat{u}_k - K_{xk}\frac{\partial\Phi_j}{\partial x}P_j\right)+\frac{\partial\Phi_i}{\partial y}\Phi_k\left(\hat{v}_k - K_{y_k}\frac{\partial\Phi_j}{\partial y}P_j\right)+ \frac{\partial\Phi_i}{\partial z}\Phi_k\left(\hat{w}_k - K_{zk}\frac{\partial\Phi_j}{\partial z}P_j\right)\right)d\Omega \tag{3.3-54}$$

The equation above was then defined as:

$$\sum_{k=1}^{4}\sum_{j=1}^{4}\left(K_{xk}\frac{\partial\Phi_i}{\partial x}\frac{\partial\Phi_j}{\partial x}+K_{y_k}\frac{\partial\Phi_i}{\partial y}\frac{\partial\Phi_j}{\partial y}+K_{zk}\frac{\partial\Phi_i}{\partial z}\frac{\partial\Phi_j}{\partial z}\right)\int_{\Omega}\Phi_k d\Omega P_j = \sum_{k=1}^{4}\int_{\Omega}\left(\frac{\partial\Phi_i}{\partial x}\Phi_k\hat{u}_k+\frac{\partial\Phi_i}{\partial y}\Phi_k\hat{v}_k+\frac{\partial\Phi_i}{\partial z}\Phi_k\hat{w}_k\right)d\Omega \tag{3.3-55}$$

In the global matrix form the above discretized equation was defined as:

$$[B]\{P\} = \{F^p\} \tag{3.3-56}$$

where Matrix *B*, and vector F^p are defined as:

$$B[i.j] = \sum_{i=1}^{4} \left(K_{xk} \frac{\partial \Phi_i}{\partial x} \frac{\partial \Phi_j}{\partial x} + K_{yk} \frac{\partial \Phi_i}{\partial y} \frac{\partial \Phi_j}{\partial y} + K_{zk} \frac{\partial \Phi_i}{\partial z} \frac{\partial \Phi_j}{\partial z} \right) \int_{\Omega} \Phi_k d\Omega \qquad (3.3\text{-}57)$$

and

$$F^p\{i\} = \sum_{k=1}^{4} \int_{\Omega} \left(\frac{\partial \Phi_i}{\partial x} \Phi_k \hat{u}_k + \frac{\partial \Phi_i}{\partial y} \Phi_k \hat{v}_k + \frac{\partial \Phi_i}{\partial z} \Phi_k \hat{w}_k \right) d\Omega \qquad (3.3\text{-}58)$$

Note that the values of pressure coefficient, *K,* were obtained by assembling element-by-element the contributions in the conventional manner. Matrix $B[i,j]$, and vector F^p were evaluated using equations (3.3-7) and (3.3-8).

It is interesting to note that the element pressure matrices were identical to those obtained in classical diffusion type problems with the term *K* replacing the diffusion coefficient. This fact is indicative of the stability and robust nature of the resulting pressure field. The resulting pressure equation also is similar to that obtained from a Poisson pressure equation with one important distinction. The Poisson pressure equation imparts no direct constraint on satisfying continuity whereas the above pressure equation does [Rice and Schnipke 1986].

Assembling element-by-element the contributions in the conventional manner, the global pressure equation was established which has all the features of a classical diffusion problem. The resultant matrix was positive-definite and symmetric.

3.3.5 Numerical Boundary Conditions

The boundary conditions are mathematical or physical constraints in the constitutive equations. A boundary-value problem of the order of 2*m* requires *m* boundary conditions to be specified at every point on the boundary. A boundary condition is an equation relating the values of unknown and/or some of its derivatives from order 1 up

to order $2m$-1, at points on the boundary [Burnet 1987]. There are two types of boundary conditions, namely *essential* boundary conditions and *natural* boundary conditions. Sometimes the essential and natural boundary conditions are called *Dirichlet* and *Neumann* boundary conditions respectively. The Dirichlet boundary conditions are equations relating the values of unknown and/or any of its derivatives up to order m-1. The Neumann boundary conditions are equations relating the values of any of the derivatives of the unknown from order m to $2m$-1, at points on boundary.

Since the velocities were obtained by solving the discretized momentum equations (3.3-30), (3.3-31) and (3.3-32), the pressure was obtained by solving global pressure equation (3.3-56). This Chapter outlines the mathematical constraints or boundary conditions required for solving such equations.

Since the pressure equation was derived from the velocity-pressure relationship, the boundary conditions for the pressure equations were straightforward. The velocity boundary conditions were applied to the pressure equation and thus implicitly constrained the pressure solution. This section primarily deals with wall, inlet, and outlet boundary conditions.

For a wall boundary, the area integral in equation (3.3-50) or natural boundary conditions for the pressure equation is zero. Thus, no special treatment was required for this area integral term. However, the pressure equation was further constrained by the known velocity at the wall. If no-slip wall-boundary conditions exist, the known velocity at the wall is:

$$u_i = v_i = w_i = 0 \tag{3.3-59}$$

To incorporate the above constraint the hat velocities $\hat{u}$, $\hat{v}$, and $\hat{w}$ at the wall were defined from equations (3.3-45), (3.3-46) and (3.3-47) respectively. The hat velocities at wall were considered to be:

$$\hat{u}_i = \hat{v}_i = \hat{w}_i = 0 \tag{3.3-60}$$

Since the hat velocities and the velocity components are zero at the wall, the pressure coefficient at the wall was derived from equations (3.3-42), (3.3-43) and (3.3-44). The pressure coefficient at wall was found to be:

$$K = 0 \tag{3.3-61}$$

So at the wall, boundary velocities, hat velocities, and pressure coefficient were all zero.

At the inlet boundary, the velocities are prescribed. So the velocities at the inlet were:

$$u_i = u_{inlet} \tag{3.3-62}$$

$$v_i = v_{inlet} \tag{3.3-63}$$

$$w_i = w_{inlet} \tag{3.3-64}$$

As with the wall boundary condition, the pressure coefficient at the inlet must be zero to decouple hat velocity components from pressure equation [Rice and Schnipke 1986]. From equations (3.3-42), (3.3-43) and (3.3-44), the hat velocities $\hat{u}$, $\hat{v}$, and $\hat{w}$ were derived as:

$$u_i = u_{inlet} = \hat{u}_i \tag{3.3-65}$$

$$v_i = v_{inlet} = \hat{v}_i \tag{3.3-66}$$

$$w_i = w_{inlet} = \hat{w}_i \tag{3.3-67}$$

For the outlet/exit boundary, the pressure was prescribed, so no special treatment was required for the boundary integral terms in pressure equation (3.3-50). However, for momentum equation (3.3-26), (3.3-27) and (3.3-28) the area integral at the outlet has to be evaluated.

Since velocity boundary condition is prescribed at the inlet the area integrals in pressure equation (3.3-50) were evaluated for the inlet and for momentum equation (3.3-26), (3.3-27) and (3.3-28) no special treatment was required.

The area integral term in equation (3.3-50) for inlet and outlet were evaluated by discretizing the area integral term and applying the area integration of the linear tetrahedral shape function equation (3.3-8).

The boundary conditions mentioned here apply to any flow regardless of geometry. Specific geometrical boundary conditions are discussed in the results section.

3.3.6 Viscoelastic Constitutive Equations

Since the Navier-Stokes equation was discussed in the last section, in this section we discretize the viscoelastic constitutive equations. The viscoelastic constitutive equations, namely Giesekus and Oldroyd-B were discretized using the Galerkin-weighted residual. The convective terms in the viscoelastic constitutive equations were discretized using non-consistent SUPG as described earlier.

The mathematical forms of the Giesekus and Oldroyd-B viscoelastic constitutive equations were written as:

$$\boldsymbol{\tau}_p + \lambda_1 \overset{\nabla}{\boldsymbol{\tau}}_p - \alpha \frac{\lambda_1}{\eta_p} \{\boldsymbol{\tau}_p \cdot \boldsymbol{\tau}_p\} = 2\eta_p \boldsymbol{D} \tag{3.3-68}$$

This equation is the same form as the Giesekus constitutive equation. The Oldroyd-B constitutive equation (3.2-22) was obtained from the above equation by making the mobility factor, α, equal to zero. In three-dimensional *ij,* form the above viscoelastic constitutive equation was written as:

$$\sum_i \sum_j \boldsymbol{\delta}_i \boldsymbol{\delta}_j \left(\tau_{pij} + \lambda_1 \left(\frac{\partial \tau_{pij}}{\partial t} + \sum_{k=1}^{3} v_k \frac{\partial \tau_{pij}}{\partial x_k} - \sum_{k=1}^{3} \left(\tau_{pik} \frac{\partial v_j}{\partial x_k} + \frac{\partial v_i}{\partial x_k} \tau_{pkj} \right) \right) - \alpha \frac{\lambda_1}{\eta_p} \sum_{k=1}^{3} \tau_{pik} \tau_{pkj} \right) = \sum_i \sum_i \boldsymbol{\delta}_i \boldsymbol{\delta}_j \eta_p \left(\frac{\partial v_j}{\partial x_i} + \frac{\partial v_i}{\partial x_j} \right) \tag{3.3-69}$$

where $\boldsymbol{\delta}$ is the unit vector.

The second order non-linear term $\tau_{pik}\tau_{pik}$ was too complicated to simplify using the Galerkin-weighted residual. So this second order term was reduced to a first order term by multiplying the previous iteration value of τ_{pik} to the present iteration value of τ_{pik}. Simplifying and rearranging the above viscoelastic constitutive equation (3.3-69) in *xx* component with respect to its unknown τ_{pxx} we obtain:

$$\tau_{pxx}^{n}+\lambda_1\left(\frac{\tau_{pxx}^{n}}{\Delta t}+u\cdot\frac{\partial\tau_{pxx}^{n}}{\partial x}+v\cdot\frac{\partial\tau_{pxx}^{n}}{\partial y}+w\cdot\frac{\partial\tau_{pxx}^{n}}{\partial z}-2\tau_{pxx}^{n}\frac{\partial u}{\partial x}\right)$$
$$-\alpha\frac{\lambda_1}{\eta_p}\tau_{pxx}^{p}\tau_{pxx}^{n}=\lambda_1\frac{\tau_{pxx}^{n-1}}{\Delta t}+2\eta_p\frac{\partial u}{\partial x}+\alpha\frac{\lambda_1}{\eta_p}\left(\tau_{pxy}^{p}\tau_{pxy}^{p}+\tau_{pxz}^{p}\tau_{pxz}^{p}\right)+ \qquad (3.3\text{-}70)$$
$$2\lambda_1\left(\tau_{pxy}^{p}\frac{\partial u}{\partial y}+\tau_{pxz}^{p}\frac{\partial u}{\partial z}\right)$$

where subscript, *p,* stands for polymer contribution and superscript, *p,* is previous iteration, but present time step value, *n* is present time step and *n*-1 is the previous time step. The time dependent term was simplified using the backward time difference method which was defined previously in equation (3.3-25). In the above equation, the non-linear term was separated to present iteration value and previous iteration value. In the right-hand side, we used previous iteration value for consistency.

Similarly simplifying and rearranging the viscoelastic constitutive equation (3.3-69) in the *xy* component with respect to its unknown τ_{pxy} gives:

$$\tau_{pxy}^{n}+\lambda_1\left(\frac{\tau_{pxy}^{n}}{\Delta t}+u\cdot\frac{\partial\tau_{pxy}^{n}}{\partial x}+v\cdot\frac{\partial\tau_{pxy}^{n}}{\partial y}+w\cdot\frac{\partial\tau_{pxy}^{n}}{\partial z}-\tau_{pxy}^{n}\left(\frac{\partial u}{\partial x}+\frac{\partial v}{\partial y}\right)\right)-$$
$$\alpha\frac{\lambda_1}{\eta_p}\tau_{pxy}^{n}\left(\tau_{pxx}^{p}+\tau_{pyy}^{p}\right)=\lambda_1\frac{\tau_{pxy}^{n-1}}{\Delta t}+\eta_p\left(\frac{\partial v}{\partial x}+\frac{\partial u}{\partial y}\right)+\alpha\frac{\lambda_1}{\eta_p}\tau_{pxz}^{p}\tau_{pyz}^{p}+ \qquad (3.3\text{-}71)$$
$$\lambda_1\left(\tau_{pxx}^{p}\frac{\partial v}{\partial x}+\tau_{pxz}^{p}\frac{\partial v}{\partial z}+\tau_{pyy}^{p}\frac{\partial u}{\partial y}+\tau_{pyz}^{p}\frac{\partial u}{\partial z}\right)$$

Simplifying and rearranging the above viscoelastic constitutive equation (3.3-69) in the *xz* component with respect to its unknown τ_{pxz} gives:

$$\tau_{pxz}^{n}+\lambda_1\left(\frac{\tau_{pxz}^{n}}{\Delta t}+u\cdot\frac{\partial\tau_{pxz}^{n}}{\partial x}+v\cdot\frac{\partial\tau_{pxz}^{n}}{\partial y}+w\cdot\frac{\partial\tau_{pxz}^{n}}{\partial z}-\tau_{pxz}^{n}\left(\frac{\partial u}{\partial x}+\frac{\partial w}{\partial z}\right)\right)-$$
$$\alpha\frac{\lambda_1}{\eta_p}\tau_{pxz}^{n}\left(\tau_{pxx}^{p}+\tau_{pzz}^{p}\right)=\lambda_1\frac{\tau_{pxz}^{n-1}}{\Delta t}+\eta_p\left(\frac{\partial w}{\partial x}+\frac{\partial u}{\partial z}\right)+\alpha\frac{\lambda_1}{\eta_p}\tau_{pxy}^{p}\tau_{pyz}^{p}+ \tag{3.3-72}$$
$$\lambda_1\left(\tau_{pxx}^{p}\frac{\partial w}{\partial x}+\tau_{pxy}^{p}\frac{\partial w}{\partial y}+\tau_{pyz}^{p}\frac{\partial u}{\partial y}+\tau_{pzz}^{p}\frac{\partial u}{\partial z}\right)$$

Simplifying and rearranging the above viscoelastic constitutive equation (3.3-69) in the *yy* component with respect to its unknown τ_{pyy} gives:

$$\tau_{pyy}^{n}+\lambda_1\left(\frac{\tau_{pyy}^{n}}{\Delta t}+u\cdot\frac{\partial\tau_{pyy}^{n}}{\partial x}+v\cdot\frac{\partial\tau_{pyy}^{n}}{\partial y}+w\cdot\frac{\partial\tau_{pyy}^{n}}{\partial z}-2\tau_{pyy}^{n}\frac{\partial v}{\partial y}\right)$$
$$-\alpha\frac{\lambda_1}{\eta_p}\tau_{pyy}^{p}\tau_{pyy}^{n}=\lambda_1\frac{\tau_{pyy}^{n-1}}{\Delta t}+2\eta_p\frac{\partial v}{\partial y}+\alpha\frac{\lambda_1}{\eta_p}\left(\tau_{pxy}^{p}\tau_{pxy}^{p}+\tau_{pyz}^{p}\tau_{pyz}^{p}\right)+ \tag{3.3-73}$$
$$2\lambda_1\left(\tau_{pxy}^{p}\frac{\partial v}{\partial x}+\tau_{pyz}^{p}\frac{\partial v}{\partial z}\right)$$

Simplifying and rearranging the above viscoelastic constitutive equation (3.3-69) in the *yz* component with respect to its unknown τ_{pyz} gives:

$$\tau_{pyz}^{n}+\lambda_1\left(\frac{\tau_{pyz}^{n}}{\Delta t}+u\cdot\frac{\partial\tau_{pyz}^{n}}{\partial x}+v\cdot\frac{\partial\tau_{pyz}^{n}}{\partial y}+w\cdot\frac{\partial\tau_{pyz}^{n}}{\partial z}-\tau_{pyz}^{n}\left(\frac{\partial v}{\partial y}+\frac{\partial w}{\partial z}\right)\right)-$$
$$\alpha\frac{\lambda_1}{\eta_p}\tau_{pyz}^{n}\left(\tau_{pyy}^{p}+\tau_{pzz}^{p}\right)=\lambda_1\frac{\tau_{pyz}^{n-1}}{\Delta t}+\eta_p\left(\frac{\partial v}{\partial z}+\frac{\partial w}{\partial y}\right)+\alpha\frac{\lambda_1}{\eta_p}\tau_{pxy}^{p}\tau_{pxz}^{p}+ \tag{3.3-74}$$
$$\lambda_1\left(\tau_{pxy}^{p}\frac{\partial w}{\partial x}+\tau_{pxz}^{p}\frac{\partial v}{\partial x}+\tau_{pyy}^{p}\frac{\partial w}{\partial y}+\tau_{pzz}^{p}\frac{\partial v}{\partial z}\right)$$

Finally, simplifying and rearranging the above viscoelastic constitutive equation (3.3-69) in the *zz* component with respect to its unknown τ_{pzz} gives:

$$\tau_{pzz}^{n}+\lambda_1\left(\frac{\tau_{pzz}^{n}}{\Delta t}+u\cdot\frac{\partial\tau_{pzz}^{n}}{\partial x}+v\cdot\frac{\partial\tau_{pzz}^{n}}{\partial y}+w\cdot\frac{\partial\tau_{pzz}^{n}}{\partial z}-2\tau_{pzz}^{n}\frac{\partial w}{\partial z}\right)$$
$$-\alpha\frac{\lambda_1}{\eta_p}\tau_{pzz}^{p}\tau_{pzz}^{n}=\lambda_1\frac{\tau_{pzz}^{n-1}}{\Delta t}+2\eta_p\frac{\partial w}{\partial z}+\alpha\frac{\lambda_1}{\eta_p}\left(\tau_{pxz}^{p}\tau_{pxz}^{p}+\tau_{pyz}^{p}\tau_{pyz}^{p}\right)+ \tag{3.3-75}$$
$$2\lambda_1\left(\tau_{pxz}^{p}\frac{\partial w}{\partial x}+\tau_{pyz}^{p}\frac{\partial w}{\partial y}\right)$$

Linear tetrahedral shape functions were used as weighting functions in the Galerkin weighted residual method [Burnet 1987] to every term except the convective terms, for which the SUPG method was applied. Substituting equation (3.3-9) to equation (3.3-14) and applying Galerkin weighted residuals to the viscoelastic constitutive equation in the *xx* component gives:

$$\sum_{j=1}^{4}\left(\Gamma_{ij}+\Pi_{ij}-2\lambda_1\sum_{k=1}^{4}u'_{x_k}\int_\Omega\Phi_j\Phi_k\Phi_i d\Omega-\alpha\frac{\lambda_1}{\eta_p}\sum_{k=1}^{4}\tau_{pxx_k}^{p}\int_\Omega\Phi_j\Phi_k\Phi_i d\Omega\right)\tau_{pxx_j}^{n}=$$
$$\sum_{j=1}^{4}\left(\left(\frac{\lambda_1}{\Delta t}\tau_{pxx_j}^{n-1}+2\eta_p u'_{x_j}\right)\int_\Omega\Phi_j\Phi_i d\Omega+\right. \tag{3.3-76}$$
$$\left.\sum_{k=1}^{4}\left(\alpha\frac{\lambda_1}{\eta_p}\left(\tau_{pxy_j}^{p}\tau_{pxy_k}^{p}+\tau_{pxz_j}^{p}\tau_{pxz_k}^{p}\right)+2\lambda_1\left(u'_{y_k}\tau_{pxy_j}^{p}+u'_{z_k}\tau_{pxz_j}^{p}\right)\right)\right)\int_\Omega\Phi_j\Phi_k\Phi_i d\Omega$$

Notice that in the above equation breaking the second order non-linear term to present iteration and previous iteration makes the equation more compliant. The SUPG term Π_{ij} is the same as in the Navier-Stokes equation, which was defined previously in equation (3.3-29). In the above equation the term Γ_{ij} is defined as:

$$\Gamma_{ij}=\int_\Omega\Phi_j\Phi_i d\Omega\left(1+\frac{\lambda_1}{\Delta t}\right)+\lambda_1\sum_{k=1}^{4}\int_\Omega\Phi_k\Phi_i d\Omega\left(u_k\frac{\partial\Phi_j}{\partial x}+v_k\frac{\partial\Phi_j}{\partial y}+w_k\frac{\partial\Phi_j}{\partial z}\right) \tag{3.3-77}$$

Similarly, for the *xy* component the discretized viscoelastic constitutive equation gives:

$$\begin{aligned}
&\sum_{j=1}^{4}\Bigg(\Gamma_{ij}+\Pi_{ij}-\alpha\frac{\lambda_1}{\eta_p}\sum_{k=1}^{4}\int_\Omega \Phi_j\Phi_k\Phi_i d\Omega\left(\tau^p_{pxx_k}+\tau^p_{pyy_k}\right)\\
&\qquad\qquad -\lambda_1\sum_{k=1}^{4}\int_\Omega \Phi_j\Phi_k\Phi_i d\Omega\left(u'_{x_k}+v'_{y_k}\right)\Bigg)\tau^n_{pxy_j}=\\
&\sum_{j=1}^{4}\Bigg(\left(\frac{\lambda_1}{\Delta t}\tau^{n-1}_{pxy_j}+\eta_p\left(v'_{x_j}+u'_{y_j}\right)\right)\int_\Omega \Phi_j\Phi_i d\Omega+\\
&\sum_{k=1}^{4}\left(\alpha\frac{\lambda_1}{\eta_p}\tau^p_{pxz_j}\tau^p_{pyz_k}+\lambda_1\left(v'_{x_k}\tau^p_{pxx_j}+v'_{z_k}\tau^p_{pxz_j}+u'_{y_k}\tau^p_{pyy_j}+u'_{z_k}\tau^p_{pyz_j}\right)\right)\Bigg)\int_\Omega \Phi_j\Phi_k\Phi_i d\Omega
\end{aligned}\tag{3.3-78}$$

where Γ_{ij} is same as in the discretized equation in the *xx* component, which was defined in equation (3.3-77). Similarly, for the *xz* component the discretized equation is given by:

$$\begin{aligned}
&\sum_{j=1}^{4}\Bigg(\Gamma_{ij}+\Pi_{ij}-\alpha\frac{\lambda_1}{\eta_p}\sum_{k=1}^{4}\int_\Omega \Phi_j\Phi_k\Phi_i d\Omega\left(\tau^p_{pxx_k}+\tau^p_{pzz_k}\right)\\
&\qquad\qquad -\lambda_1\sum_{k=1}^{4}\int_\Omega \Phi_j\Phi_k\Phi_i d\Omega\left(u'_{x_k}+w'_{z_k}\right)\Bigg)\tau^n_{pxz_j}=\\
&\sum_{j=1}^{4}\Bigg(\left(\frac{\lambda_1}{\Delta t}\tau^{n-1}_{pxz_j}+\eta_p\left(u'_{z_j}+w'_{x_j}\right)\right)\int_\Omega \Phi_j\Phi_i d\Omega+\\
&\sum_{k=1}^{4}\left(\alpha\frac{\lambda_1}{\eta_p}\tau^p_{pxy_j}\tau^p_{pyz_k}+\lambda_1\left(w'_{x_k}\tau^p_{pxx_j}+w'_{y_k}\tau^p_{pxy_j}+u'_{y_k}\tau^p_{pyz_j}+u'_{z_k}\tau^p_{pzz_j}\right)\right)\Bigg)\int_\Omega \Phi_j\Phi_k\Phi_i d\Omega
\end{aligned}\tag{3.3-79}$$

where Γ_{ij} is same as in the discretized equation in the *xx* component, which was defined in equation (3.3-77). Similarly, for the the *yy* component the discretized equation is given by:

$$\sum_{j=1}^{4}\left(\Gamma_{ij}+\Pi_{ij}-2\lambda_1\sum_{k=1}^{4}v'_{y_k}\int_\Omega\Phi_j\Phi_k\Phi_i d\Omega-\alpha\frac{\lambda_1}{\eta_p}\sum_{k=1}^{4}\tau^p_{pyy_k}\int_\Omega\Phi_j\Phi_k\Phi_i d\Omega\right)\tau^n_{pyy_j}=$$
$$\sum_{j=1}^{4}\left(\left(\frac{\lambda_1}{\Delta t}\tau^{n-1}_{pyy_j}+2\eta_p v'_{y_j}\right)\int_\Omega\Phi_j\Phi_i d\Omega+\right. \tag{3.3-80}$$
$$\left.\sum_{k=1}^{4}\left(\alpha\frac{\lambda_1}{\eta_p}\left(\tau^p_{pxy_j}\tau^p_{pxy_k}+\tau^p_{pyz_j}\tau^p_{pyz_k}\right)+2\lambda_1\left(v'_{x_k}\tau^p_{pxy_j}+v'_{z_k}\tau^p_{pyz_j}\right)\right)\right)\int_\Omega\Phi_j\Phi_k\Phi_i d\Omega$$

where Γ_{ij} is the same as in the discretized equation in the *xx* component, which was defined in equation (3.3-77). Similarly, for the *yz* component the discretized equation is given by:

$$\sum_{j=1}^{4}\left(\Gamma_{ij}+\Pi_{ij}-\alpha\frac{\lambda_1}{\eta_p}\sum_{k=1}^{4}\int_\Omega\Phi_j\Phi_k\Phi_i d\Omega\left(\tau^p_{pyy_k}+\tau^p_{pzz_k}\right)\right.$$
$$\left.-\lambda_1\sum_{k=1}^{4}\int_\Omega\Phi_j\Phi_k\Phi_i d\Omega\left(v'_{y_k}+w'_{z_k}\right)\right)\tau^n_{pyz_j}= \tag{3.3-81}$$
$$\sum_{j=1}^{4}\left(\left(\frac{\lambda_1}{\Delta t}\tau^{n-1}_{pyz_j}+\eta_p\left(v'_{z_j}+w'_{y_j}\right)\right)\int_\Omega\Phi_j\Phi_i d\Omega+\right.$$
$$\left.\sum_{k=1}^{4}\left(\alpha\frac{\lambda_1}{\eta_p}\tau^p_{pxy_j}\tau^p_{pxz_k}+\lambda_1\left(w'_{x_k}\tau^p_{pxy_j}+v'_{x_k}\tau^p_{pxz_j}+w'_{y_k}\tau^p_{pyy_j}+v'_{z_k}\tau^p_{pzz_j}\right)\right)\right)\int_\Omega\Phi_j\Phi_k\Phi_i d\Omega$$

where Γ_{ij} is the same as in the discretized equation in the *xx* component, which was defined in equation (3.3-77). Similarly, for the *zz* component the discretized equation is given by:

$$\sum_{j=1}^{4}\left(\Gamma_{ij}+\Pi_{ij}-2\lambda_1\sum_{k=1}^{4}w'_{z_k}\int_\Omega\Phi_j\Phi_k\Phi_i d\Omega-\alpha\frac{\lambda_1}{\eta_p}\sum_{k=1}^{4}\tau^p_{pzz_k}\int_\Omega\Phi_j\Phi_k\Phi_i d\Omega\right)\tau^n_{pzz_j}=$$
$$\sum_{j=1}^{4}\left(\left(\frac{\lambda_1}{\Delta t}\tau^{n-1}_{pzz_j}+2\eta_p w'_{z_j}\right)\int_\Omega\Phi_j\Phi_i d\Omega+\right. \tag{3.3-82}$$
$$\left.\sum_{k=1}^{4}\left(\alpha\frac{\lambda_1}{\eta_p}\left(\tau^p_{pxz_j}\tau^p_{pxz_k}+\tau^p_{pyz_j}\tau^p_{pyz_k}\right)+2\lambda_1\left(w'_{x_k}\tau^p_{pxz_j}+w'_{y_k}\tau^p_{pyz_j}\right)\right)\right)\int_\Omega\Phi_j\Phi_k\Phi_i d\Omega$$

where Γ_{ij} is same as in the discretized equation in the *xx* component, which was defined in equation (3.3-77). In the above components of the discretized viscoelastic constitutive equation, the derivative of velocity was given in the format $\acute{u}_x$, which implies derivative of velocity *u* with respect to *x* co-ordinate. The components of the discretized viscoelastic constitutive equation were expressed in the global matrix equation (3.3-1) form. The global matrix form of the viscoelastic constitutive equation in the *xx* component is defined as:

$$[A_{xx}]\{\tau_{pxx}\}=\{F^{xx}\} \tag{3.3-83}$$

and the matrix $[A_{xx}]$ as:

$$A_{xx}[i,j]=\left[\Gamma_{ij}+\Pi_{ij}-2\lambda_1\sum_{k=1}^{4}u'_{x_k}\int_\Omega\Phi_j\Phi_k\Phi_i d\Omega-\alpha\frac{\lambda_1}{\eta_p}\sum_{k=1}^{4}\tau^p_{pxx_k}\int_\Omega\Phi_j\Phi_k\Phi_i d\Omega\right] \tag{3.3-84}$$

and$\{F^{xx}\}$ is same as the right hand side of equation (3.3-76). The global matrix form of the discretized viscoelastic constitutive equation in the *xy* component is defined as:

$$[A_{xy}]\{\tau_{pxy}\}=\{F^{xy}\} \tag{3.3-85}$$

and the matrix $[A_{xy}]$ as:

$$A_{xy}[i,j]=\left[\Gamma_{ij}+\Pi_{ij}-\alpha\frac{\lambda_1}{\eta_p}\sum_{k=1}^{4}\int_{\Omega}\Phi_j\Phi_k\Phi_i d\Omega\left(\tau^{p}_{pxx_k}+\tau^{p}_{pyy_k}\right)-\lambda_1\sum_{k=1}^{4}\int_{\Omega}\Phi_j\Phi_k\Phi_i d\Omega\left(u'_{x_k}+v'_{y_k}\right)\right] \tag{3.3-86}$$

The load vector $\{F^{xy}\}$ is the same as given in the right side *xy* component of the discretized viscoelastic constitutive equation (3.3-78). The global matrix form of the discretized viscoelastic constitutive equation in the *xz* component is defined as:

$$[A_{xz}]\{\tau_{pxz}\}=\{F^{xz}\} \tag{3.3-87}$$

and the matrix $[A_{xx}]$ as:

$$A_{xz}[i,j]=\left[\Gamma_{ij}+\Pi_{ij}-\alpha\frac{\lambda_1}{\eta_p}\sum_{k=1}^{4}\int_{\Omega}\Phi_j\Phi_k\Phi_i d\Omega\left(\tau^{p}_{pxx_k}+\tau^{p}_{pzz_k}\right)-\lambda_1\sum_{k=1}^{4}\int_{\Omega}\Phi_j\Phi_k\Phi_i d\Omega\left(u'_{x_k}+w'_{z_k}\right)\right] \tag{3.3-88}$$

The load vector $\{F^{xz}\}$ is same as the right hand side of equation (3.3-79). The global matrix form of the discretized viscoelastic constitutive equation in the *yy* component is defined as:

$$[A_{yy}]\{\tau_{pyy}\}=\{F^{yy}\} \tag{3.3-89}$$

and the matrix $[A_{yy}]$ as:

$$A_{yy}[i,j]=\left[\Gamma_{ij}+\Pi_{ij}-2\lambda_1\sum_{k=1}^{4}v'_{y_k}\int_\Omega\Phi_j\Phi_k\Phi_i d\Omega-\alpha\frac{\lambda_1}{\eta_p}\sum_{k=1}^{4}\tau^{p}_{pyy_k}\int_\Omega\Phi_j\Phi_k\Phi_i d\Omega\right] \quad (3.3\text{-}90)$$

The load vector $\{F^{yy}\}$ is same as the right hand side of equation (3.3-80). The global matrix form of the discretized viscoelastic constitutive equation in the *yz* component is defined as:

$$[A_{yz}]\{\tau_{pyz}\}=\{F^{yz}\} \quad (3.3\text{-}91)$$

and the matrix $[A_{yz}]$ as:

$$A_{yz}[i,j]=\left[\Gamma_{ij}+\Pi_{ij}-\alpha\frac{\lambda_1}{\eta_p}\sum_{k=1}^{4}\int_\Omega\Phi_j\Phi_k\Phi_i d\Omega\left(\tau^{p}_{pyy_k}+\tau^{p}_{pzz_k}\right)-\lambda_1\sum_{k=1}^{4}\int_\Omega\Phi_j\Phi_k\Phi_i d\Omega\left(v'_{y_k}+w'_{z_k}\right)\right] \quad (3.3\text{-}92)$$

The load vector $\{F^{yz}\}$ is same as the right hand side of the equation (3.3-81). The global matrix form of the discretized viscoelastic constitutive equation in the zz component is defined as:

$$[A_{zz}]\{\tau_{pzz}\}=\{F^{zz}\} \quad (3.3\text{-}93)$$

and the matrix $[A_{zz}]$ as:

$$A_{zz}[i,j]=\left[\Gamma_{ij}+\Pi_{ij}-2\lambda_1\sum_{k=1}^{4}w'_{z_k}\int_\Omega\Phi_j\Phi_k\Phi_i d\Omega-\alpha\frac{\lambda_1}{\eta_p}\sum_{k=1}^{4}\tau^{p}_{pzz_k}\int_\Omega\Phi_j\Phi_k\Phi_i d\Omega\right] \quad (3.3\text{-}94)$$

The load vector $\{F^{zz}\}$ is same as the right hand side of equation (3.3-82). The above matrices and load vectors for all the components of the global discretized viscoelastic constitutive equation were easily evaluated by applying equation (3.3-7) and (3.3-8).

Since the velocity fields are obtained before the viscoelastic constitutive equations are solved, we calculate the derivative of velocity as piecewise linear rather than constant within each element to improve the accuracy. For example, the derivative of velocity u with respect to co-ordinate x at a particular node is defined as:

$$\left(\frac{\partial u}{\partial x}\right)_n=\frac{\sum_{(e)}V^{(e)}\sum_{j=1}^{4}u_j^{(e)}\frac{\partial\Phi_j}{\partial x}}{\sum_{(e)}V^{(e)}} \quad (3.3\text{-}95)$$

where (e) is the elements that are connected to node n, $V^{(e)}$ is the volume of element containing the node n, and Φ is the linear tetrahedral shape function..

Polymeric contributions to the extra-stress tensor are obtained by solving (3.3-83), (3.3-85), (3.3-87), (3.3-89), (3.3-91) and (3.3-93). The boundary conditions for viscoelastic constitutive equation is discussed in chapter five. Since the components of $\boldsymbol{\tau}_p$ are known, the term $\nabla\cdot\boldsymbol{\tau}_p$ for the momentum equation was considered. Simplifying $\nabla\cdot\boldsymbol{\tau}_p$ gives:

$$\nabla\cdot\boldsymbol{\tau}_p=\sum_{i=1}^{3}\boldsymbol{\delta}_i\sum_{j=1}^{3}\frac{\partial\tau_{pji}}{\partial x_j} \quad (3.3\text{-}96)$$

The above equation was discretized using the Galerkin weighted residual. The result of this residual in the *x* co-ordinate is defined as:

$$\nabla \cdot \tau_p(i)_x = \sum_{j=1}^{4} \int_\Omega \Phi_j \Phi_i d\Omega \left(\frac{\partial \tau_{pxx_j}}{\partial x} + \frac{\partial \tau_{pxy_j}}{\partial y} + \frac{\partial \tau_{pxz_j}}{\partial z} \right) \tag{3.3-97}$$

where Φ is the weighting function, which is the same as the linear tetrahedral shape function. Similarly, in the *y* co-ordinate $\nabla \cdot \boldsymbol{\tau}_p$ was discretized to:

$$\nabla \cdot \tau_p(i)_y = \sum_{j=1}^{4} \int_\Omega \Phi_j \Phi_i d\Omega \left(\frac{\partial \tau_{pxy_j}}{\partial x} + \frac{\partial \tau_{pyy_j}}{\partial y} + \frac{\partial \tau_{pyz_j}}{\partial z} \right) \tag{3.3-98}$$

where Φ is the weighting function, which is the same as the linear tetrahedral shape function. Similarly, in the *z* co-ordinate $\nabla \cdot \boldsymbol{\tau}_p$ was discretized to:

$$\nabla \cdot \tau_p(i)_z = \sum_{j=1}^{4} \int_\Omega \Phi_j \Phi_i d\Omega \left(\frac{\partial \tau_{pxz_j}}{\partial x} + \frac{\partial \tau_{pyz_j}}{\partial y} + \frac{\partial \tau_{pzz_j}}{\partial z} \right) \tag{3.3-99}$$

where Φ is the weighting function, which was the same as the linear tetrahedral shape function. Notice that the derivatives of stress terms are calculated as piecewise linear. The derivatives of the stress terms are similar to the derivatives of velocities used in the viscoelastic constitutive equation, which is given in equation (3.3-95). The value of ($\nabla \cdot \boldsymbol{\tau}_p$) in *x*, *y*, and *z* co-ordinate were used in the momentum equations (3.3-26), (3.3-27) and (3.3-28) respectively.

3.4 Section Summary

This chapter outlines the discretization of the single-mode Giesekus and Oldroyd-B constitutive equations using linear tetrahedral shape functions. This discretization was used in a segregated solver solution scheme to predict the flow field. The discretization of governing equations was performed using the Galerkin weighted residual method and linear tetrahedral shape functions. A non-consistent Streamline-Upwind/Petrov-Galerkin (SUPG) method was used to discretize convective terms in the viscoelastic constitutive equations and in the momentum equation. Since pressure was solved independently, the pressure equation was derived from the continuity equation using a velocity-pressure relationship. For accuracy, the derivatives of velocities in the discretized viscoelastic constitutive equations were calculated as piecewise linear rather than a constant within an element. Similarly, the derivatives of components of polymer contribution to stress tensor were calculated as piecewise linear, which was used in the momentum equation.

Since this chapter simplified the governing equations to matrix forms, the next Chapter discusses the overall solution scheme used to obtain velocity, pressure, and stresses in detail.

4. Solution Method

The discretization of governing equations was discussed in Chapter 3. This chapter discusses the solution method used to solve the discretized equations required to obtain the flow field in detail. It primarily discusses the solution methods for the momentum equation for velocity components, pressure equation for pressure, and viscoelastic constitutive equation for stress components at nodes. This chapter also discusses the overall solution scheme and the sequence of governing equation's solution.

4.1 Background and Overview

Finite element approximation has been a very popular tool in numerical simulation of complex equations. This is because of its ability to be applied to almost any numerical problem. In the finite element method, the solution domain or continuum is divided into a number of discrete parts or elements, the behaviours of which are specified by a finite number of parameters.

There are many schemes in finite element approximation methods, such as velocity-pressure scheme, penalty scheme, and segregated scheme. In the velocity-pressure-integrated method the governing equations are solved simultaneously. This method needs a small number of iterations but requires a large amount of memory and computational time.

In the penalty method, pressure is removed from the momentum equation and a penalty parameter is included in the uncoupled solution of the velocity field. Once the velocity is obtained, the Lagrangian multiplier is used to determine the pressure field from the divergence of the velocity solution [Reddy 1984]. The penalty method requires less memory and computational time compared with velocity pressure integrated method, but requires an additional post processing to obtain the pressure field. The penalty method also only approximates the continuity equation.

As computation in three-dimensional space and time requires more memory and computational time, the penalty and velocity-pressure integrated methods are considered to be ineffective. In the segregated solution scheme the basic approach is to first find a solution of flow variables in the entire continuum. This solution is used to determine the next solution field, and so on. This process continues in an iterative way until all the variables are found. Once all the variables are found, the iterative cycle recommences until the solution satisfies the convergence criteria. This method needs much less memory and execution time, satisfying the continuity equation completely. For this reason the Navier-Stokes equations are solved using a segregated finite element algorithm with an equal order interpolation scheme, originally proposed for two-dimension steady state flow by Rice and Schnipke [1986]. In this method velocities and corresponding pressure fields are computed alternately. This is similar to the SIMPLER algorithm [Patankar 1980], using a pressure-velocity coupling widely used in finite volume approximation.

Applying governing equations to each element to express the relationship between the nodal values. In the finite element approximation the node relationships from each element are assembled to produce a set of linear equations, which is again assembled to form an overall system of matrices. The form of these matrices is given as:

$$\begin{bmatrix} a_{11} & a_{12} & \cdot & \cdot & \cdot & a_{1N} \\ a_{21} & a_{22} & \cdot & \cdot & \cdot & a_{2N} \\ \cdot & \cdot & \cdot & \cdot & \cdot & \cdot \\ \cdot & \cdot & \cdot & \cdot & \cdot & \cdot \\ \cdot & \cdot & \cdot & \cdot & \cdot & \cdot \\ a_{N1} & a_{N2} & \cdot & \cdot & \cdot & a_{NN} \end{bmatrix} \begin{Bmatrix} x_1 \\ x_2 \\ \cdot \\ \cdot \\ \cdot \\ x_N \end{Bmatrix} = \begin{Bmatrix} F_1 \\ F_2 \\ \cdot \\ \cdot \\ \cdot \\ F_N \end{Bmatrix} \tag{4.1-1}$$

where a_{ij} are the coefficients, x_i are the nodal value unknowns, and F_i are constants which include effects of applied force and known boundary conditions. The above

matrix structure is the same as the global matrix structure defined in chapter 3, which has the form:

$$[A]\{u\} = \{F\} \tag{4.1-2}$$

where vector u contains the nodal value unknown x_i, matrix A contains coefficient a_{ij}, and the load vector F contains the constant values F_i. The coefficients of the matrix A are calculated from the equations being solved and the geometry of the problem. These coefficients have been derived in the previous chapter for the various governing equations. Similarly the vectors in the load vector are calculated from the equations being solved and the geometry of the problem, and this is done for the various governing equations in Chapter 3. The matrix above is called linear because the matrix A only contains constant coefficients. However, such a matrix system does not imply it only represents linear constitutive equation behaviour. Highly non-linear constitutive equations, such as viscoelastic constitutive equations can also be represented using such a system of equations. In the equation (4.1-1), coefficient a_{ij} can be described as the influence of node i on node j in its solution value, and coefficient a_{ii} describes the influence of node i on itself in its solution value in the linear set of equations. The ith row of the equation (4.1-1) can be considered to solve the ith nodal value. If there are N unknowns i.e. total number of nodes are N, then A is a N X N matrix. Matrix A is generally positive definite, and sparsely populated with non-zero values. Diagonal dominance is ensured by the nature of the finite element matrix assembly for each nodal equation. Contributions to a particular node from other connected or adjacent elements are used in the summation of influence terms. The pivoting node, which will be solved using this equation, is itself present in all adjacent elements. Ergo, following the summation for the equation at a node, the largest term is usually the term for that node itself.

4.2 Matrix Solution

There are generally two kinds of matrix solver, namely direct solver or iterative solver. Direct methods transform the influence matrix A to produce a solution in a predefined number of calculations. In direct methods, computer round off errors can arise because of the repeated transformation of the elements of matrix A. Iterative methods do not transform the matrix A, but rather progressively improve the estimation of the unknown x_i in a finite number of iterations, which is not known in advance. The direct matrix solver methods include amongst others, Gauss-Jordan elimination, and LU-Decomposition [Young *et al.* 1972, Hageman *et al.* 1981]. Iterative solver methods include amongst others, the Bi-Conjugate gradient method [Schewchuk 1994, and Fletcher 1976], Generalised Minimal Residual method (GMRES) [Saad *et al.* 1986, Fortin *et al.* 1992]. Saad and Schultz [1986] first introduced the GMRES method for the resolution of non-symmetric linear systems. This method was first applied to viscoelastic flow problems by Fortin *et al.* [1990]. This method has been extended to the solution of large non-linear systems of equations. One of the advantages of this method was that it allows the resolution of large non-linear systems without computing large Jacobian matrices [Guenette 1995].

The finite element method discretization process produces sparse matrices, which have only a few non-zero terms. Careful selection of an iterative matrix solution method, which takes advantage of the sparse and positive definite system of matrices, allows considerable efficiency in computation and storage requirements. One disadvantage of a direct solution method such as Gauss-Jordan elimination or LU-Decomposition, is that they store all the terms during the matrix transformation, making computational storage expensive. For this reason, in three-dimensional problems, it is inappropriate to use direct solution methods. Generally the iterative methods are more efficient, which preserves the sparse nature of the matrices, and minimises computer round off errors.

There are many numerical techniques that can be used to solve equation (4.1-1). In this work, the Pre-conditioned Conjugate gradient method [Fletcher 1976] has been used to

solve symmetric positive definite systems of equations. For a matrix to be positive and definite means, the matrix is irreducible and diagonal dominant [Young *et al.* 1972]. In mathematical form a matrix to be diagonally dominant implies that for all rows:

$$\left|a_{ii}\right| \geq \sum_{j=1}^{N} \left|a_{ij}\right|_{j \neq i} \tag{4.2-1}$$

and at least one row must have:

$$\left|a_{ii}\right| > \sum_{j=1}^{N} \left|a_{ij}\right|_{j \neq i} \tag{4.2-2}$$

For non-symmetric matrices of equation (4.1-1) the GMRES [Saad *et al.* 1986] method has been used.

The converge criteria for the Pre-conditioned Conjugate gradient method [Fletcher 1976] and Generalised Minimal Residual algorithm (GMRES) [Saad *et al.* 1986] were the same and defined as:

$$\xi = \frac{\left\|Au - F\right\|}{\left\|F\right\|} \tag{4.2-3}$$

Where A is the mass matrix, u is the unknown, F is the load vector and ξ is the error function. It was assumed that the matrix solution converged when the error function ξ was less then 1.0E-06.

4.3 Overall Solution Scheme

Since the resulting mass matrices from the discretization of momentum, pressure, and viscoelastic constitutive equations are large and sparse, special iterative procedures are used instead of direct elimination. The pressure equation is a Poisson-type equation; the resulting matrix is a symmetric positive definite matrix. The Pre-conditioned conjugate gradient method was used to solve this type of matrix. The discretized momentum and viscoelastic constitutive equations generally produce a non-symmetric matrix because of the presence of the convective terms in the equations. The Preconditioned Generalised Minimal Residual algorithm (GMRES) [Saad *et al.* 1986] is used to solve these types of sparse matrices. Diagonal pre-conditioning [Saad *et al.* 1986] was used for both of these systems of equations.

There were two possible ways the viscoelastic constitutive equations can be implemented into the Newtonian calculation. The first is to solve the velocity equation, the pressure equation, and the viscoelastic constitutive equation sequentially in one single iterative loop. The second is to solve the velocity and pressure equation until the Newtonian solution converges. Then using the Newtonian flow field, the viscoelastic constitutive equation is solved, continuing this process alternately until the overall convergence criteria are satisfied. Both methods have been tried. In the first method, for simple shear flow, it was found that the numerical code often did not converge, and took a long time to execute when it did converge. The second method was more stable, and took less time to execute for flows in simple shear. This may be due to the stable Newtonian flow field being used as input to the viscoelastic constitutive equations in second method. Without any further investigation, it was assumed that the second method would give stable results in other flow simulations. This method is explained in detail below.

For Newtonian flow simulation, the discretized momentum equation was solved for the velocity field using previously known or assumed velocity, and pressure. The $(\nabla\cdot\boldsymbol{\tau}_p)$ term in momentum equation (3.2-11) was assumed zero for Newtonian calculations.

First the velocity components *u*, *v*, and *w* were obtained by solving the global matrix form of discretized momentum equations (3.3-30), (3.0-31), and (3.3-32) respectively using known or estimated pressures, and applying appropriate boundary conditions. Once the velocities are known, the velocity components *u*, *v*, and *w* are obtained by solving the discretized momentum equations (3.3-30), (3.0-31), and (3.3-32). Applying the appropriate boundary conditions, the global matrix form of the pressure equation (3.3-56) was solved for the pressure field. Mass continuity was checked after the pressure equation. If the continuity equation was not satisfied the velocities were corrected using equation (3.3-42), (3.3-43), and (3.3-44). Momentum and pressure equations were solved alternatively and in an iterative way until the desired convergence criteria were met. The overall solution scheme schematic for Newtonian flow is given in Figure 4.3-1.

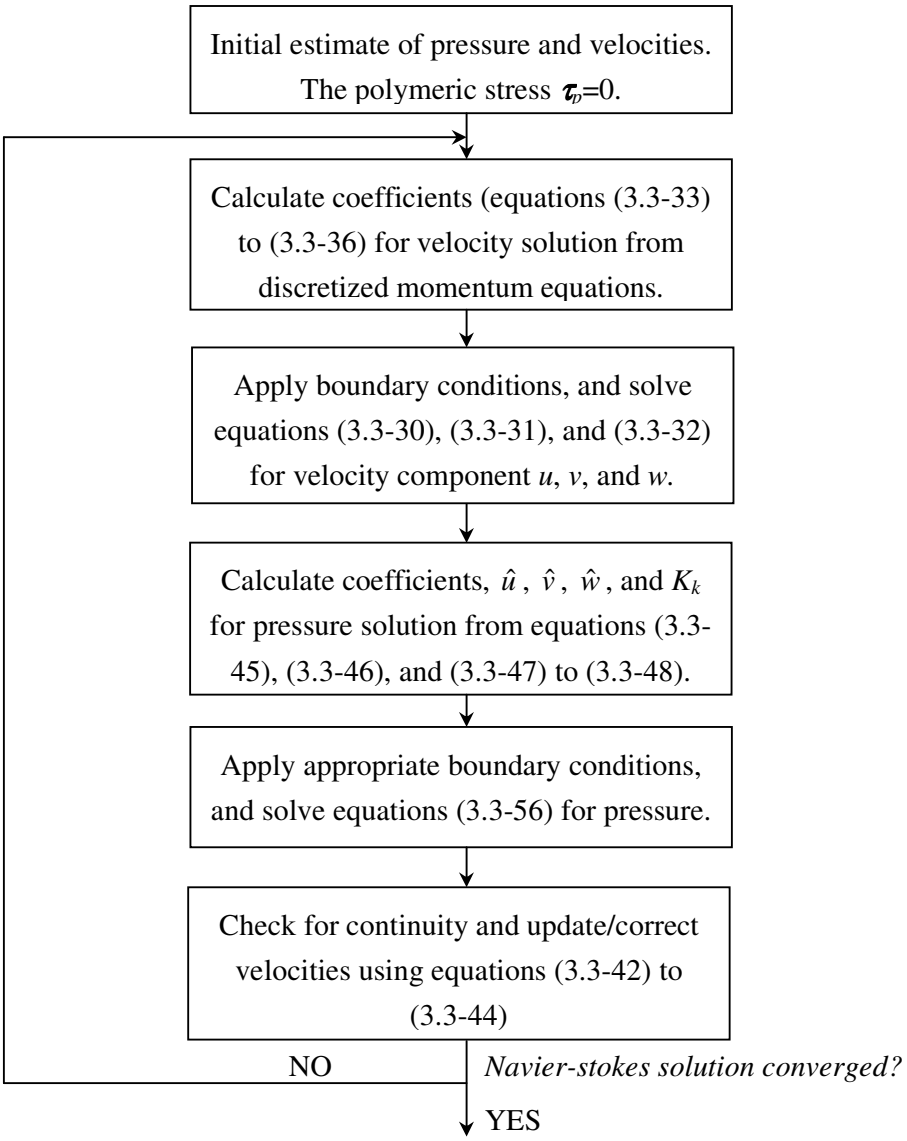

Figure 4.3-1. Solution schematic for Newtonian flow simulation.

Once the velocity components are known for Newtonian flow, the global matrix form of the discretized viscoelastic constitutive equations (3.3-83), (3.3-85), (3.3-87), (3.3-89), (3.3-91), and (3.3-93) were solved sequentially in an iterative way for polymeric contribution to stress components by applying known boundary conditions. The

components of discretized viscoelastic constitutive equations were solved sequentially and in an iterative way, because the load vectors are dependent upon the previous iteration value of other stress components. The schematic for viscoelastic solution only is given in Figure 4.3-2.

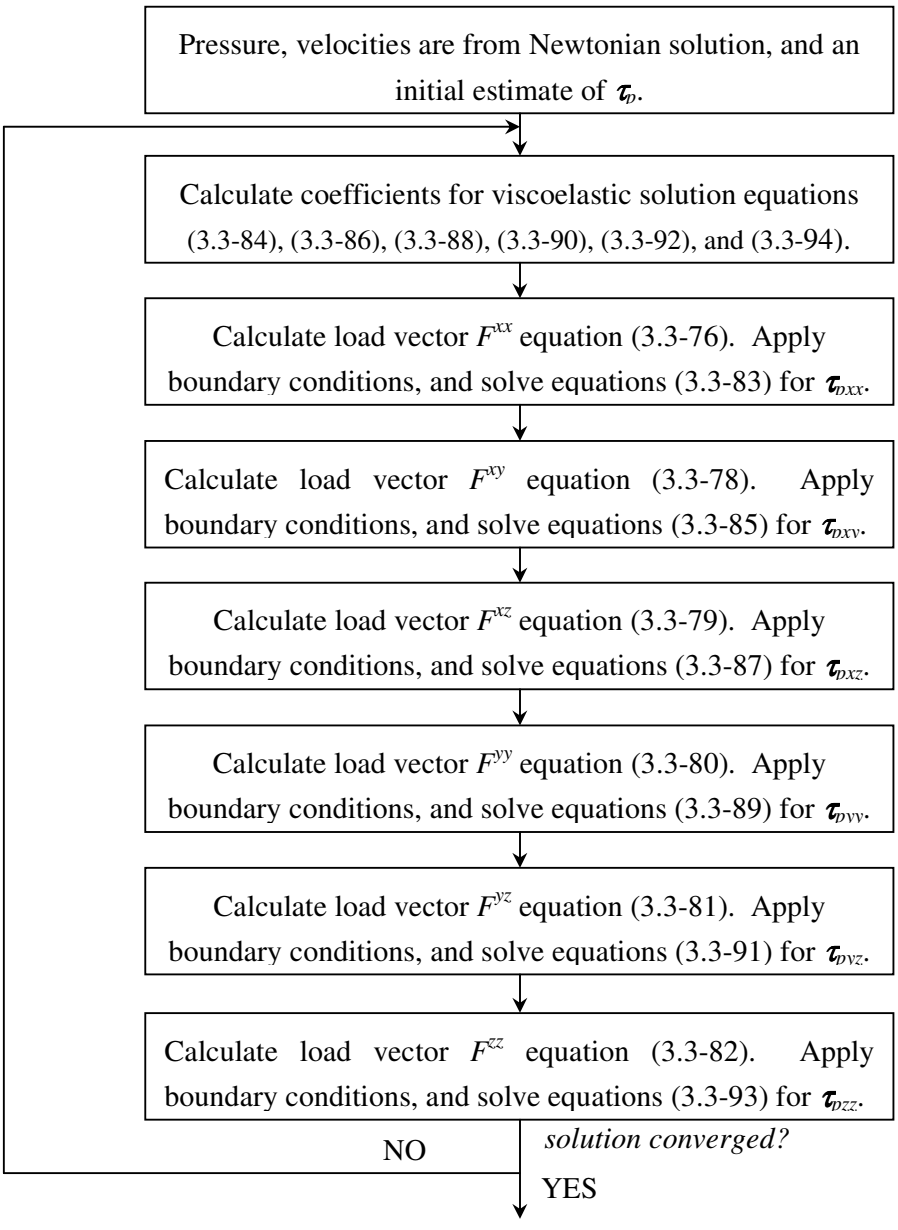

Figure 4.3-2. Solution schematic for Viscoelastic flow simulation.

Note that the momentum equation (3.2-11) has stress terms ($\nabla\cdot\boldsymbol{\tau}_p$) contributed by viscoelasticity. The elastic stress components have to be substituted back into the momentum equation, at least once, before the overall solution convergence criteria is being checked. The overall solution schematic for one time step is given in Figure 4.3-3.

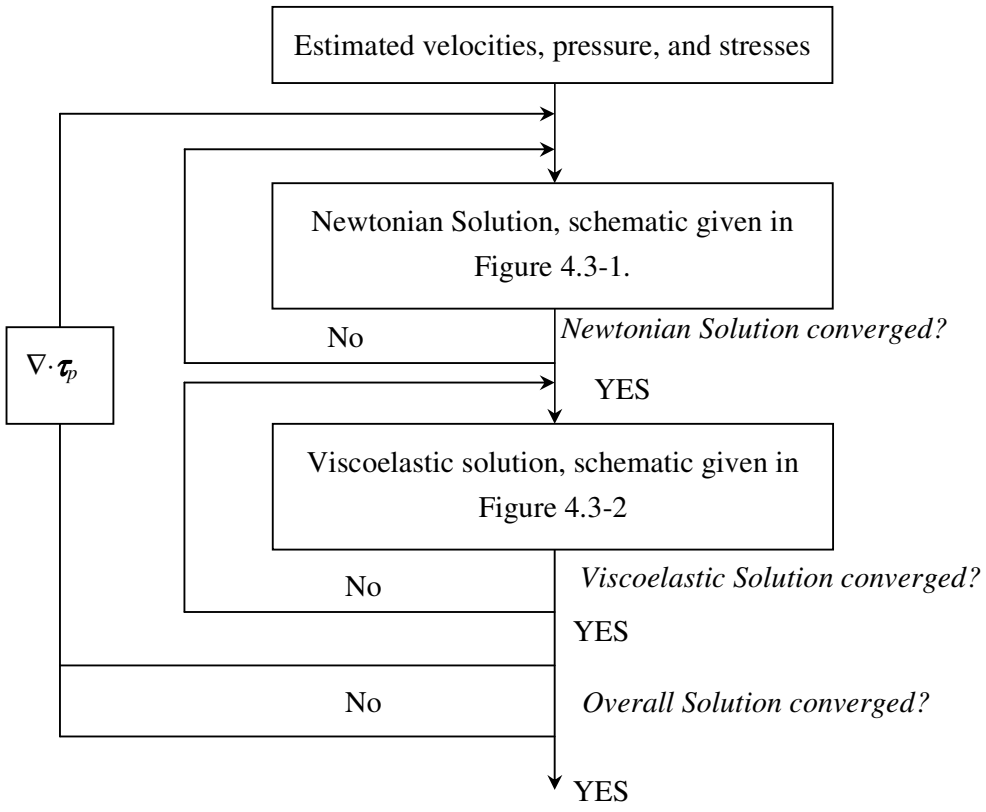

Figure 4.3-3. Overall solution schematic.

The above solutions were obatined by computer programming discretizied governing equations in a combination of FORTRAN-77 and C programming languages. The main subroutine was written in the C language, where memory was dynamically allocated. The other subroutines were written in FORTRAN 77.

4.4 Stability Criteria

Stability criteria for the Newtonian and viscoelastic constitutive equation segregated scheme were the same. For the Newtonian sgeregated scheme (i.e. three velocity component and pressure) the criteria were measured as the summation of the differnece of maximum velocities and pressure value of the current to the previous iteration. For example, the maximum absolute nodal value of velocities and pressure from the current iteration were compared with the previous iteration absolute nodal value and the discrepancy was summed. When the sum of the discrepancy was less than 1.0E-06 it was conceived that the solution is stable. In other words the more segregated iteration would be fruitless and would obtain the same velocity and pressure values. The same criteria were used for the viscoelastic solution and for viscoelasticity. There were six components of strees compared with three velocity and one pressure component in the Newtonian segregated scheme.

4.5 Chapter Summary

A segregated algorithm to solve the viscoelastic flow field has been used. Since the pressure equation is a Poisson-type equation, the resultant system matrix is symmetric, positive-definite, and sparse. Consequently for the pressure equation, the pre-conditioned conjugate gradient method was used to solve pressure. Momentum and viscoelastic constitutive equations contain convective terms and the resultant matrices are non-symmetric and sparse. For momentum and viscoelastic constitutive equations the Generalised Minimal Residual (GMRES) method was used to solve velocity and stress components. Diagonal preconditioning was used for both of these iterative solvers in this research. The advantage of these two types of iterative methods was that they require less computer storage and deliver speedy convergence compared to direct solvers with the large matrices under consideration.

In the overall solution sequence, the Navier-Stokes equations were solved first to obtain convergence of velocities and pressure so that mass and momentum conservation was satisfied. The momentum and pressure equations were solved sequentially, within a segregated loop. Momentum equations were solved sequentially for each component of the velocity, which resulted in an intermediate velocity field. Using these velocities, the pressure equation was solved to obtain new pressure field. A check for mass continuity was done at this stage. If the continuity was not satisfied, velocities were corrected using the velocity correction formulae. This iterative sequence was repeated until a velocity-pressure field that satisfies continuity and momentum conservation within each time step was obtained.

Since the load vectors are dependent on other stress terms in the discretized viscoelastic constitutive equations, the stress components were calculated sequentially and in an iterative way using the velocities from the Newtonian solution. The viscoelastic component calculations continued until all the components satisfied the constitutive equation.

Remembering the fact that momentum equation has viscoelastic contributions, the stresses from the viscoelastic solution were substituted into the momentum equation for recalculation. This sequence continued until the Newtonian and viscoelastic calculation converged. For time dependent flow the whole sequence again was repeated for each time step.

For computer programming implementation, a combination of FORTRAN-77 and C languages was used. The C language was used for dynamic memory allocation. The other subroutines were written in FORTRAN-77.

5. Results and Discussion

This chapter discusses the results of numerical analysis using the solution methods described previously. The first step is to check that our numerical solution works. A logical step for this is to simulate flows in simple geometry, where the analytical flow solutions are known, and compare the numerical flow simulations to the analytical flow solutions.

Numerical flow simulations were conducted in simple shear and planar Poiuseuille flows to check the accuracy of the numerical simulations. Steady state numerical flow simulations were conducted in a benchmark 4:1 contraction [Hassager 1988] geometry. Axisymmetric flow in contraction geometry with rectangular co-ordinate meshing was also simulated, and the numerical results compared with experimental results. Time dependent flow simulations were conducted in a 4:1 benchmark contraction problem.

Section 5.1 discusses simple shear flow. This section also derives the analytical solution for simple shear flow, explains the boundary conditions, and finally presents the results.

The analytical and numerical simulation of a planar Poiseuille flow is discussed in section 5.2. This chapter also includes the boundary conditions and results for this kind of problem.

The numerical simulation of a benchmark 4:1 contraction is given in section 5.3, where the boundary conditions for steady state and time dependent simulation are given. This section also presents result of steady state and time dependent numerical simulations.

5.1 Simple Shear

In simple shear deformation, a fluid deforms continuously under the action of a shearing force, which acts tangentially to the surfaces to be deformed. In this type of flow, material planes slide over one another in one direction. Figure 5.1-1 represents simple shear flow, where the top of the fluid is subjected to a shearing force. In Figure 5.1-1, the velocity of the upper plate is u_{max} and the flow pattern follows linearly with height y.

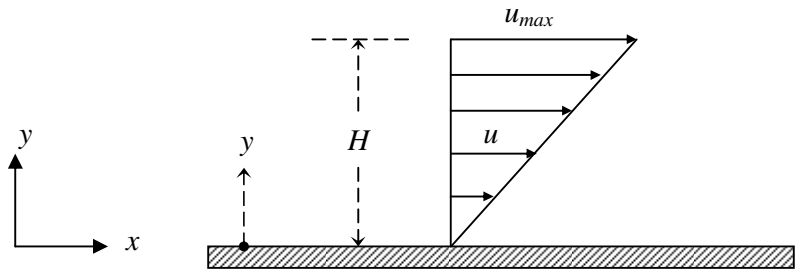

Figure 5.1-1. Simple shear flow.

In the above Figure, u is a function of y only, and H is the total height. The shearing force is applied tangentially to the top surface.

The velocity profile in simple shear flow is defined as:

$$u = \frac{u_{\max}}{H} y \tag{5.1-1}$$

where $u_{\max}$ is the maximum velocity, which was at the upper plate, H is the height of the geometry.

5.1.1 Boundary Conditions

The simple shear flow was modelled as parallel plate flow with upper plate moving at a constant velocity. This is demonstrated in Figure 5.1-2.

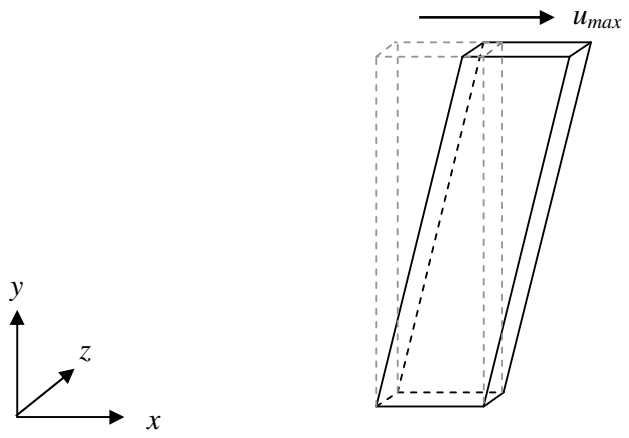

Figure 5.1-2. Flow in Simple Shear Geometry.

The dimension of the object was x = 1.5mm, y = 10mm, and z = 0.5mm.

Since the analytical solution for velocity is given in equation (5.1-1), the analytical solutions for stress components are obtained by simplifying equation (3.3-70) to (3.3-75), with α equals to zero, and no time derivatives.

The polymeric stress contribution in *xx* component was obtained by simplifying equation (3.3-70), to give:

$$\tau_{pxx} = 2\lambda_1 \tau_{pxy} \frac{\partial u}{\partial y} \tag{5.1-2}$$

where λ_1 is relaxation time given in Appendix-1.

The derivative of velocity with respect to *y* is defined as:

$$\frac{\partial u}{\partial y} = \frac{u_{\max}}{H} \tag{5.1-3}$$

Notice that the stress component in *xx* is dependent upon stress in *xy* component. The stress in *xy* component was obtained by simplifying equation (3.3-71), to give:

$$\tau_{pxy} = \eta_p \frac{\partial u}{\partial y} + \tau_{pyy} \frac{\partial u}{\partial y} \tag{5.1-4}$$

where η_p is polymer contribution to zero shear rate viscosity, given in equation (3.2-7). Notice also that the stress in the *xy* component is dependent upon stress in *yy* component.

The stresses in *xz*, *yy*, *yz*, and *zz* components were obtained by simplifying equation (3.3-72) to (3.3-75), to give stresses as zero in those components. Since the *yy* component stress is zero, the *xy* component stress can be obtained from the equation (5.1-4), which yields:

$$\tau_{pxy} = \eta_p \frac{u_{\max}}{H} \tag{5.1-5}$$

Stress in *xx* component was obtained by substituting equation (5.1-5) in equation (5.1-2), to give:

$$\tau_{pxx} = 2\lambda_1 \eta_p \left(\frac{u_{\max}}{H} \right)^2 \tag{5.1-6}$$

The relaxation time λ_1 for simple shear geometry was 0.045 s, η_p was 380.0 Pa.s, and zero-shear rate viscosity was 390.0 Pa.s.

In simple shear flow the velocity boundary conditions for upper plate geometry were, u = 3.0 mm/s, v = 0.0 mm/s, w = 0.0 mm/s. The velocities u, v, and w were the velocity components in x, y, and z direction respectively. The stress boundary conditions for upper boundary conditions were, in xx component τ_{pxx} = 3.078 Pa, and in xy component τ_{pxy} = 114.0 Pa. The stresses in xx, and xy components were obtained by simplifying equation (5.1-6), and (5.1-5) respectively. As mentioned before the values of other stress components were zero.

The velocity boundary conditions for lower plate were zero in all of the three components, and the stress in the lower plate were exactly same as the upper plate.

For pressure boundary conditions, the pressure at inlet and outlet were zero.

5.1.2 Simple Shear Results

Simple shear is a two-dimensional flow. The geometry presented in Figure 5.1-2 was meshed with linear tetrahedral elements. Linear tetrahedral elements with element size of 0.5mm were used for meshing. Although this made the geometry one element thick in the z direction, it did not affect the results. This is because there was no variation of any variables in the z (thickness) direction. We have used FAM® (FEGS Ltd. UK, version 4) to create the mesh. The total numbers of elements was 444, and the total numbers of nodes was 196. Note that this mesh was a very coarse mesh.

Since the analytical results for stress components and velocity are known, this section only compares the computational results of the x velocity, and xx and xy stress components, with analytical results at the outlet.

Figure 5.1-3 compares the analytical and computational results of velocity component in x direction at outlet.

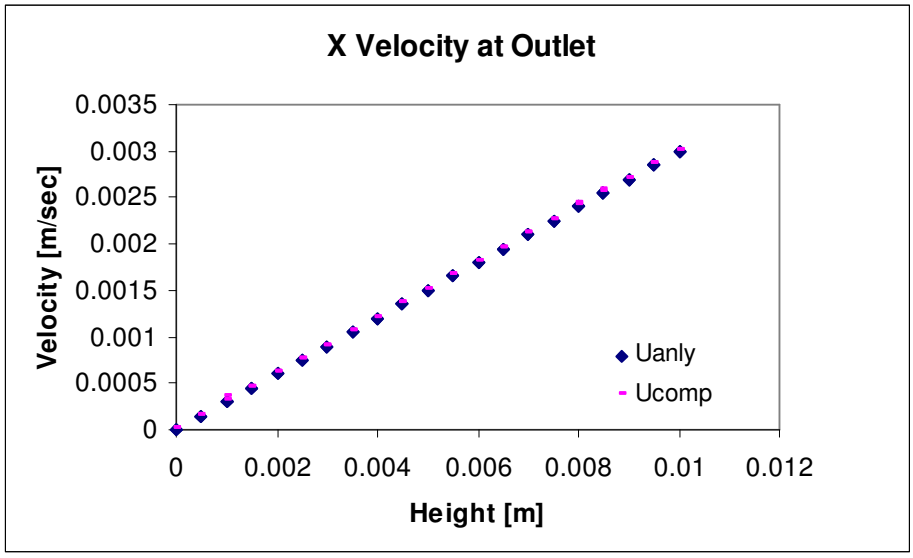

Figure 5.1-3. Computational and analytical x-velocity for simple shear flow at outlet.

Notice that the velocity in x-direction linearly increases with y. The derivative of velocity in x-direction with respect to y is positive and constant, which is the slope of the line in figure 5.1-3. The accuracy of this prediction was satisfactory. The accumlative percentage change of data points was 0.0003.

Figure 5.1-4 compares the analytical and computational results of stress components in xx component τ_{pxx}. Remember the stress component shown in figure 5.1-3 is only polymer contribution to extra stress tensor in xx plane. The total stress in xx plane can

be obtained from equation (3.2-10). Since λ_1, η_p, and derivative of velocity with respect to y is constant, the stress in xx component (5.1-6) is constant. The viscoelastic contributions to the stresses in xx plane were only from relaxation time and η_p (say polymer contribution to zero shear rate viscosity).

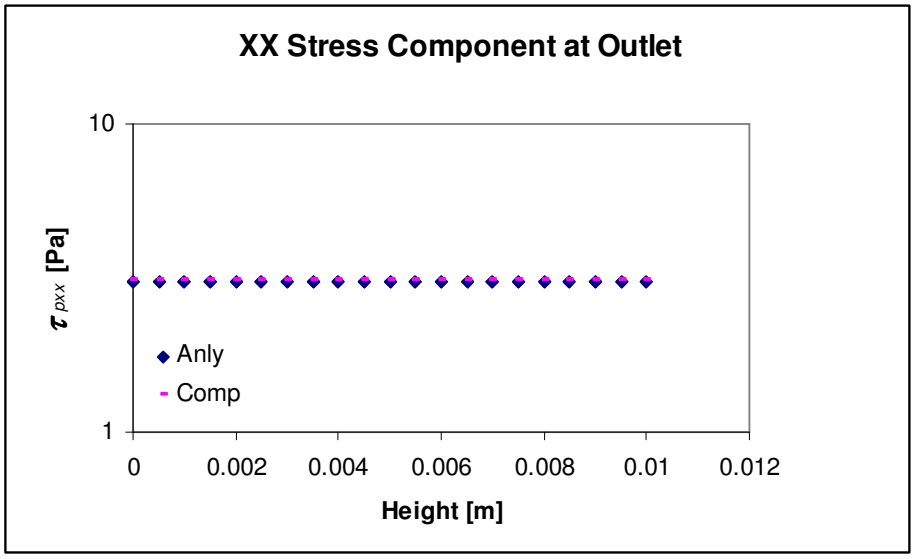

Figure 5.1-4. Computational and analytical xx-scomponent of polymeric stress contribution to extra stress tensor for simple shear flow at outlet.

Figure 5.1-5 compares the analytical and computational results of stress components in xy component τ_{pxy}. The total stress or extra stress tensor in xy plane can be obtained from equation (3.2-10). Since η_p, and derivative of velocity with respect to y was constant the stress in xy component equation (5.1-5) was constant. Previously in equation (3.2-7) the zero shear rate viscosity was decomposed to elastic contribution and solvent contribution. This decomposition was only a mathematical formulation, not a physical phenomenon. Although the xy stress component was dependent on η_p, it is inappropriate to say the τ_{pxy} was affected by viscoelasticity.

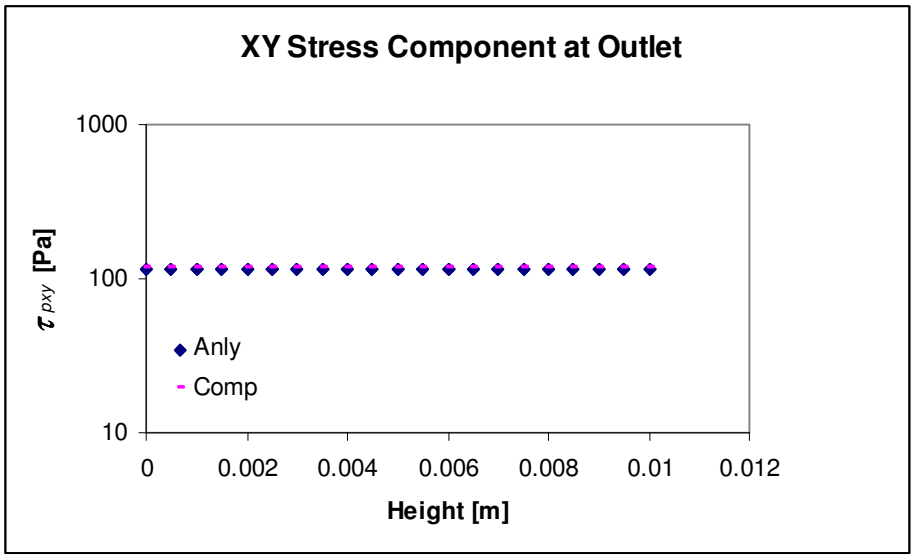

Figure 5.1-5. Computational and analytical *xy*-scomponent of polymeric stress contribution to extra stress tensor for simple shear flow at outlet.

It was shown in Figure 5.1-3, Figure 5.1-4, and Figure 5.1-5 that the numerical and computational results were quite accurate, and considering the coarseness of this mesh the results were excellent. Since simple shear flow was in steady state, and there were no pressure and very little viscoelastic contribution to the flow, it was required to predict flow in another simple geometry to test the accuracy of the numerical code. The next section predicts a flow between parallel plates.

5.2 Planar Poiuseuille Flow

The next test was flow between horizontal parallel plates, otherwise known as planar Poiseuille flow. In planar Poiuseuille flow, the material flows between two fixed plates as shown in Figure 5.2-1. The inlet flow can be of any description. In this research work, we have assumed steady and uniform laminar flow between parallel plates. The velocity profile for steady laminar flow [Douglas 1986] is given as:

$$u = \frac{1}{2\eta_0}\frac{dP}{dx}\left(y^2 - Hy\right) \tag{5.2-1}$$

where P is the pressure, H is the total height, and η_0 is zero shear rate viscosity, which was defined in equation (3.2-7).

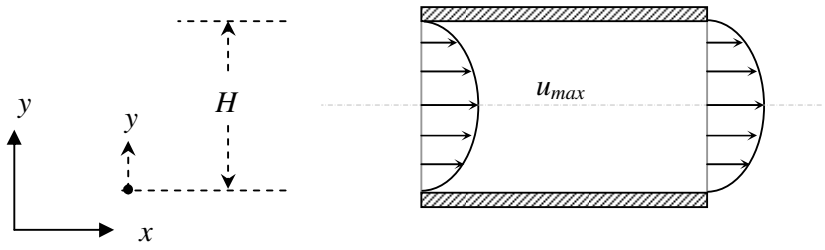

Figure 5.2-1. Steady laminar flow between horizontal Parallel Plate.

Equation (5.2-1) can be further simplified in terms of maximum velocity, to give:

$$u = \frac{4u_{\max}}{H^2}\left(Hy - y^2\right) \tag{5.2-2}$$

where u_{max} is the maximum x direction velocity, which is at the centreline of the parallel plate arrangement.

5.2.1 Boundary conditions

In addition to the numerical boundary conditions mentioned in section 3.3.5, the velocity boundary conditions for planar Poiseuille flow are given in Figure 5.2-2. The dimension of the parallel plate arrangement is x = 1.5mm, y = 10mm, and z = 0.5mm. Inlet was at $x = 0$, $0 \le y \le 10$mm, and $0 \le z \le 0.5$mm. Outlet was at x = 1.5mm, $0 \le y \le 10$mm, and $0 \le z \le 0.5$mm. Symmetries were at $0 \le x \le 1.5$mm, $0 \le y \le 10$mm, and z = 0, & 0.5mm.

Assuming Poiseuille flow at the entrance, the analytical solutions for stress components of $\boldsymbol{\tau}_p$ for Oldroyd-B model were obtained by simplifying equation (3.3-70) to (3.3-75), with α equals to zero, and no time derivatives.

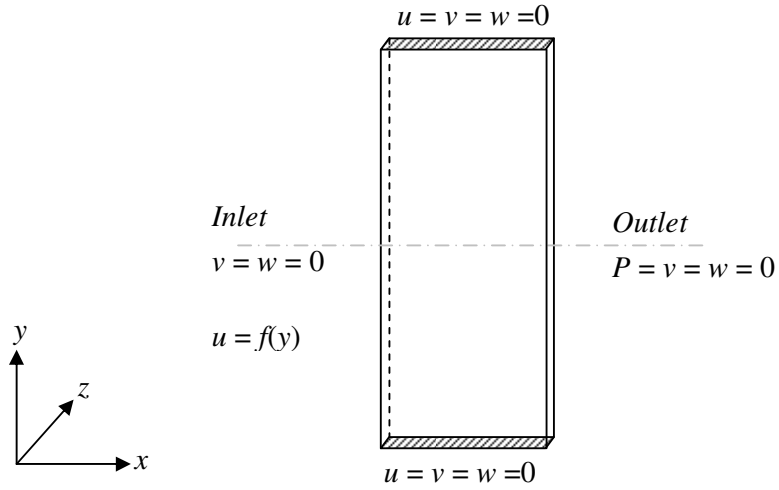

Figure 5.2-2. Velocity boundary conditions for horizontal parallel plate in laminar steady state flow.

The polymeric stress contribution to extra stress tensor in *xx* component was obtained by simplifying equation (3.3-70), to give:

$$\tau_{pxx} = 2\lambda_1 \tau_{pxy} \frac{\partial u}{\partial y} \tag{5.2-3}$$

where λ_1 is relaxation time given in Appendix-1, and the derivative of velocity with respect to *y* is defined as:

$$\frac{\partial u}{\partial y} = \frac{4u_{\max}}{H^2}(H - 2y) \tag{5.2-4}$$

Notice that the stress component in *xx* is dependent upon the *xy* stress component. The *xy* stress component was obtained by simplifying equation (3.3-71), to give:

$$\tau_{pxy} = \eta_p \frac{\partial u}{\partial y} + \tau_{pyy} \frac{\partial u}{\partial y} \tag{5.2-5}$$

where η_p is the polymer contribution to zero shear rate viscosity, given in equation (3.2-7). Notice also that the stress in the *xy* component direction is dependent upon the *yy* stress component.

The *xz*, *yy*, *yz*, and *zz* components of stresses were obtained by simplifying equation (3.3-72) to (3.3-75), which gave stresses as zero in those components. Since the *yy* component of stress is zero, the *xy* component of stress can be obtained from equation (5.2-5), to give:

$$\tau_{pxy} = \frac{4\eta_p u_{\max}}{H^2}(H - 2y) \tag{5.2-6}$$

Stress in *xx* component was obtained by substituting equation (5.2-6) in equation (5.2-3), to give:

$$\tau_{pxx} = \frac{32\lambda_1 \eta_p u_{\max}^2}{H^4}(H - 2y)^2 \tag{5.2-7}$$

The relaxation time λ_1 for planar Poiseuille flow case was 0.005 s, η_p was 189.0 Pa.s, and the zero-shear rate viscosity was 390.0 Pa.s.

The velocity boundary conditions for upper and lower plate were, u = 0.0 mm/s, v = 0.0 mm/s, w = 0.0 mm/s. The velocities u, v, and w were the velocity components in x, y, and z direction respectively.

At the inlet, v and w velocities were zero, and the u velocity was specified at every node at the inlet from equation (5.2-2), with u_{max} = 1.0m/sec. The value of τ_{pxx} was specified at each node at the inlet from equation (5.2-7). The value of τ_{pxy} in each node at the inlet was specified from equation (5.2-6). Other components of stress were zero at the nlet.

For the outlet boundary conditions, pressure was specified as zero at every node in the outlet.

For symmetry boundary conditions (z = 0, and z = 0.05mm) the w velocity was zero. Stresses in xz, yz components were also zero at these locations.

5.2.2 Planar Poiseuille Flow Results

Similar to simple shear flow, planar Pouseuille flow is two-dimensional. The geometry shown in Figure 5.2-2 was meshed with linear tetrahedral elements. We have used the same mesh as in simple shear flow case. The total numbers of elements was 444, and the total numbers of nodes was 196.

In the previous section, we demonstrated that analytical results for stress components in *xz*, *yy*, *yz*, *zz* were zero, and velocity components in the *y*, *z* direction were also zero. Therefore, this section only compares the computed results of *x* velocity, *xx* stress component, and *xy* component with analytical results at the outlet.

Figure 5.2-3 compares the analytical result equation (5.2-2), and computed result of velocity component in *x* direction at outlet.

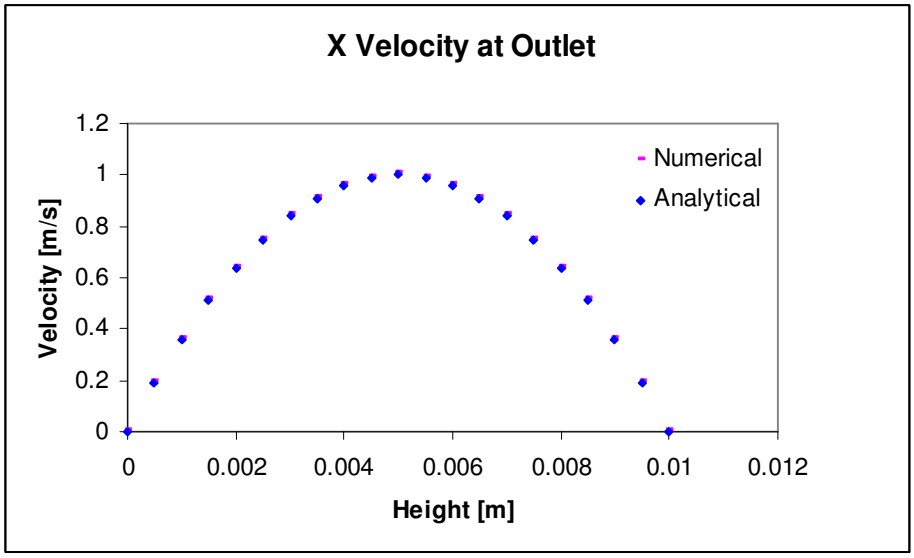

Figure 5.2-3. Computational and analytical *x*-velocity at outlet of horizontal parallel plate arrangement.

From equation (5.2-2), for laminar steady flow between horizontal parallel plates the velocity has a parabolic profile. The accuracy of computed results is quite good. The accumulative precentage change of data points were 0.0015.

Figure 5.2-4 compares the analytical result equation (5.2-7), and computed result of stress components in *xx* component τ_{pxx}. Remember the stress component shown in figure 5.2-4 is only the polymer contribution to extra stress tensor in *xx* plane. The total stress in *xx* plane can be obtained from equation (3.2-10). The viscoelastic contributions to the stresses in *xx* plane were only from relaxation time and polymer contribution to zero shear rate viscosity.

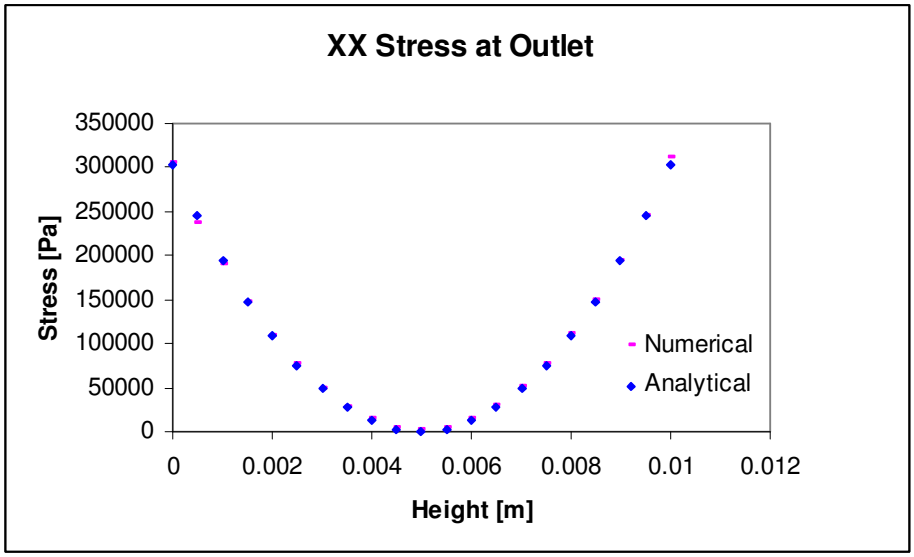

Figure 5.2-4. Computated and analytical *xx* component of polymeric stress contribution to extra stress tensor at the outlet for planar Poiseuille flow.

Figure 5.2-5 compares the analytical result equation (5.2-6), and computational computed results of stress components in *xy* component τ_{pxy}. The total stress in the *xy* plane can be obtained from equation (3.2-10). Previously in equation (3.2-7) the zero shear rate viscosity was decomposed to elastic contribution and solvent contribution. This decomposition was only a mathematical formulation, not a physical phenomenon. Although the stress components dependent on η_p, it is inappropriate to say the τ_{pxy} was affected by viscoelasticity.

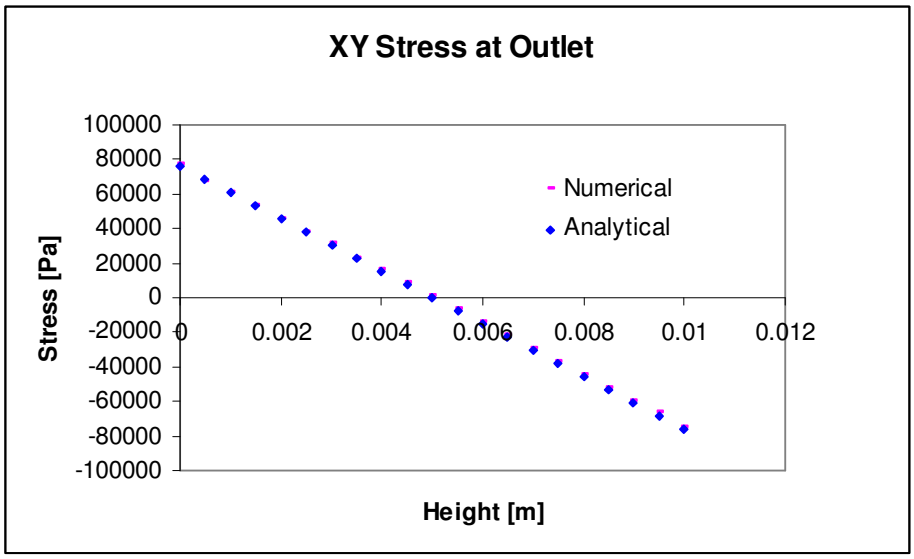

Figure 5.2-5. Computational and analytical *xy* component of polymeric stress contribution to extra stress tensor at the outlet for planar Poiseuille.

From Figure 5.2-3, Figure 5.2-4, and Figure 5.2-5 it is clear, that the results of the numerical simulations were satisfactory. Considering the coarseness of the mesh the

numerical scheme was quite accurate. The accumulative percentage change of data points in figure 5.2-3 to figure 5.2-5 were less than 0.00151.

From numerical simulations of simple shear and planar Poiseuille flow, the results of the numerical schemes were seen to be quite accurate and satisfactory. However, flows in both cases were simple with viscoelastic effects that posed no numerical intractability. To test the numerical scheme further, a logical next step was to simulate flows in a benchmark 4:1 contraction problem. The next section presents boundary conditions and numerical results of 4:1 contraction.

5.3 Four to One Contraction

One of the basic and most important subjects in the study of viscoelastic constitutive equations that has drawn the attention of many researchers is the flow of viscoelastic fluid through contractions [Isayev *et al.* 1985,Loh *et al.* 1996, McKinley *et al.* 1991, and Park *et al.* 1992].

The particular flow problem addressed in this section is a 4:1 planar and axisymmetric contraction, extensively cited in literature. A four to one contraction problem manifests sufficiently complex flow phenomena to render a suitable test case to study both two and three-dimensional situations. These phenomena are the presence of re-entrant corner where the stress become extremely high at higher elasticity resulting in numerical instability and loss of convergence [Debbaut *et al.* 1986]. It is generally agreed that, in view of the singularities at the re-entrant corner, the numerical results might not converge when the finite element mesh is refined [Coates *et al.* 1992, Debae *et al.* 1994, and Yurun *et al.* 1995]. In particular 4:1 contraction is a benchmark problem [Hasager 1988] for the development and testing of numerical simulation algorithms. The 4:1 contraction problem provides a challenge to the numerical algorithms and the constitutive equations, particularly for the highly elastic fluid behaviour. The schematic of a 4:1 contraction is given in Figure 5.3-1.

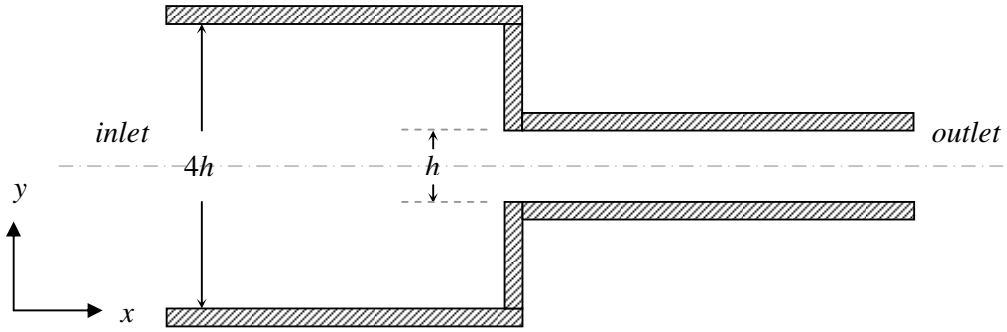

Figure 5.3-1. Schematics diagram of a 4:1 contraction problem.

The 4:1 contraction problem is extensively studied both experimentally and numerically. Most of these experimental studies have used either Boger fluid or aqueous solutions. For example, Evans *et al.* [1986] found that vortex enhancement varies with contraction for Boger fluids and aqueous solutions. For large contraction ratios, re-entrant corner vortex, which was not present in a 4:1 contraction, was shown to have an important influence on the development of vortex enhancement. In a later study, Evans *et al.* [1989] concluded that a lip-vortex mechanism could be responsible for vortex enhancement for any planar-contraction ratio, provided the polymer concentration was chosen carefully or, alternatively the contraction angle was varied. Other literature on experimental studies of 4:1 contraction can be found in the following references [Boger *et al*. 1986, Boger *et al*. 1992, Quinzin *et al.* 1994, White *et al.* 1987, Armstrong *et al.* 1992, and McKinley 1991].

Many numerical simulations of 4:1 contractions have been reported in literature. Carew *et al*. [1993] found that the pressure drop decreased as *Weissenberg* number increased for Oldroyd-B fluid. Yoo *et al.* [1991], and Keiller *et al.* [1993] also reported similar results, where entrance pressure loss decreased with increasing *Weissenberg* number, and increase in entrance pressure loss with increase in *Reynolds* number. Using upper-

convected Maxwell model Coates *et al.* [1990] showed that a Newtonian-like behaviour near the corner allows the numerical simulations to converge at higher *Weissenberg* number. Baaijens [1993] used multi-mode differential models to compare the experimental study by Armstrong *et al.* [1992]. Baaijens [1993] reported satisfactory predictions for the shear stress along the symmetry line, but less satisfactory results for the first normal stress.

Various other research has been reported in the literature on numerical simulations of 4:1 contraction flow [Marchal *et al.* 1986, Sasmal 1995, Sato 1994, and Hulsen 1991].

In spite of the numerous works that have tried to compare theoretical and experimental results, there is still a need for more extensive studies that examine all aspects of the flow at different locations of the contraction geometry. This may help to establish a systematic comparison between experimental observations and numerical calculations for the stress and velocity fields simultaneously [Azaiez 1996].

Section 5.3.1 discusses boundary conditions for a 4:1 planar contraction. To ensure that our numerical algorithm works, section 5.3.2 predicts steady state flows in 4:1 planar contraction, and compares it with the existing results previously cited in literature.

Section 5.3.3 discusses boundary conditions for an axisymmetric 4:1 contraction, while section 5.3.4 compares the numerical prediction against experimental observations for a 4:1 axisymmetric contraction.

5.3.1 Boundary Conditions for Planar Contraction

The schematic of a 4:1 contraction was given in Figure 5.3.1. It is obvious that the geometry is symmetric along the centreline. We have modelled the 4:1 planar contraction geometry using only half of the geometry. In addition to the numerical boundary conditions elucidated in section 3.3.5, the velocity boundary conditions are given in Figure 5.3.2.

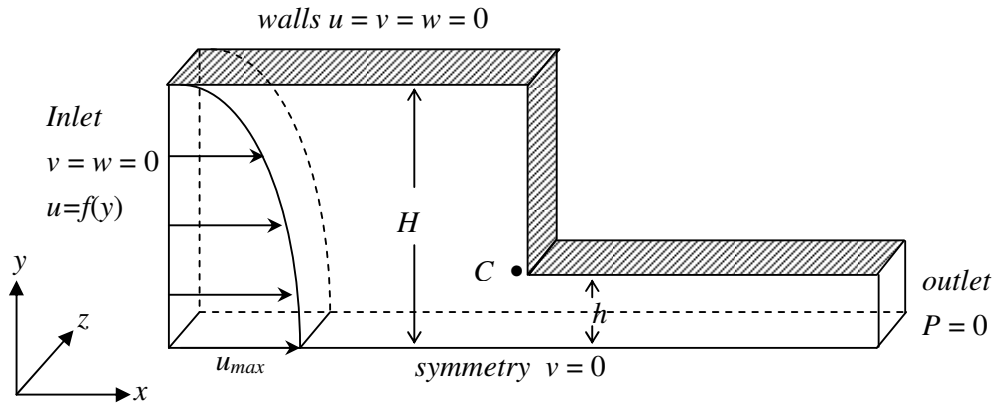

Figure 5.3.2. Velocity boundary conditions for 4:1 planar contraction.

In this figure the dimension of H = 4mm, h = 1mm. The length of the upstream was 15mm, and downstream was 5mm. The geometry has uniform thickness Δz, which was equal to h. The re-entrant corner C was at x = 14.8mm and y = 1.2mm.

The inlet was treated as a parallel plate flow. The velocity profile for the inlet condition was steady laminar flow. The velocity profile was obtained by simplifying (5.2-1) with *y* at the centre. The velocity in *x*-direction was defined as:

$$u = \frac{u_{\max}}{H^2}\left(H^2 - y^2\right) \tag{5.3-1}$$

5.3.1.1 Steady Sate Boundary Condition

Assuming Poiseuille flow at the entrance, the analytical solutions for stress components of $\boldsymbol{\tau}_p$ for Oldroyd-B model were obtained by simplifying equation (3.3-70) to (3.3-75), with α equals to zero, and no time derivatives. Similar to parallel plate case earlier, the stress components in *xz*, *yy*, *yz*, and *zz* components were zero. The stress in *xx* component was given as:

$$\tau_{pxx} = 2\lambda_1 \tau_{pxy} \frac{\partial u}{\partial y} \tag{5.3-2}$$

where λ_1 is the relaxation time, and the derivative of velocity with respect to *y* is defined as:

$$\frac{\partial u}{\partial y} = \frac{-2yu_{\max}}{H^2} \tag{5.3-3}$$

Notice that the stress component in *xx* is dependent upon stress in *xy* component. The stress in *xy* component was obtained by simplifying equation (3.3-71), to give:

$$\tau_{pxy} = \eta_p \frac{\partial u}{\partial y} + \tau_{pyy} \frac{\partial u}{\partial y} \tag{5.3-4}$$

where η_p is the polymer contribution to zero shear rate viscosity, given in equation (3.2-7). Notice also that the stress in *xy* component is dependent upon stress in *yy* component.

Since the *yy* component stress is zero, the *xy* component of stress can be obtained from equation (5.3-4) by substituting equation (5.3-3), to give:

$$\tau_{pxy} = \frac{-2y\eta_p u_{\max}}{H^2} \tag{5.3-5}$$

Stress in *xx* component was obtained by substituting equation (5.3-3) and (5.3-5) in equation (5.3-2), to give:

$$\tau_{pxx} = 8\lambda_1\eta_p\left(\frac{yu_{\max}}{H^2}\right)^2 \tag{5.3-6}$$

For the Oldroyd-B fluid the relaxation time λ_1 for 4:1 contraction geometry was 0.002 s, η_p was 77.0 Pa.s, and the ration between retardation and relaxation time ($\lambda_2/\lambda_1=\eta_s/\eta_0$) was 1/9.

No-slip boundary conditions for the walls were applied. The velocity at walls were u = 0.0 m/s, v = 0.0 m/s, w = 0.0 m/s. The velocity u, v, and w were the velocity components in x, y, and z direction respectively.

At the inlet, v and w velocities were zero, and the u velocity was specified at every node at the inlet from equation (5.3-1), with u_{max} = 0.15m/s. The value of τ_{pxx} was specified at each node at the inlet from equation (5.3-6). The value of τ_{pxy} in each node at the

inlet was specified from equation (5.3-5). Other stress components of stress were zero at the inlet.

For outlet boundary conditions, pressure was specified to be zero at every node at the outlet. The velocity in *y* and *z* directions was zero at the outlet.

For symmetry boundary condition at $y = 0$, velocity normal to that plane was zero, which means $v = 0$. Stress in *xy*, and *yz* component were zero.

For symmetry boundary conditions in *z*-axis ($z = 0$, and $z = 1$mm) the *w* velocity was zero. Stresses in *xz*, *yz* component were zero at these symmetry positions.

5.3.1.2 Time Dependent Boundary Conditions

The transient boundary condition for Oldroyd-B model was obtained by solving equations (3.3-70) to (3.3-75), with α equals to zero, and with time derivatives. The Equations (3.3-70) to (3.3-75) was written in the form of a first order linear differential equation [Kreyszig 1993] as:

$$y' + p(x)y = r(x) \tag{5.3-7}$$

The solution to the above equation was:

$$y(x) = e^{-h}\left[\int e^{h} r dx + c\right] \tag{5.3-8}$$

where *h* was defined as:

$$h = \int p(x)dx \tag{5.3-9}$$

Since the stress components in *xz*, *yy*, *yz*, and *zz* for Oldroyd-B model are zero for a planar contraction, the stress component in *xx* direction was obtained by applying

equations (5.3-7) to (5.3-9) to the equation (3.3-70). The stress in *xx* component was then defined as:

$$\tau_{pxx} = 2\lambda_1\left(\tau_{pxy}\frac{\partial u}{\partial y}\right)\Big|_{t=n} + 2\lambda_1 e^{-t/\lambda_1}\left[\left(\tau_{pxy}\frac{\partial u}{\partial y}\right)\Big|_{t=0} - \left(\tau_{pxy}\frac{\partial u}{\partial y}\right)\Big|_{t=n}\right] \quad (5.3\text{-}10)$$

where subscript ($_{t=0}$) means the value at time $t = 0$, and the subscript ($_{t=n}$) means the current time $t = n$ value.

Similarly the stress component in the *xy* direction was obtained by applying equations (5.3-7) to (5.3-9) to the equation (3.3-71) to give:

$$\tau_{pxy} = \eta_p \frac{\partial u}{\partial y}\Big|_{t=n} + e^{-t/\lambda_1}\left[\eta_p \frac{\partial u}{\partial y}\Big|_{t=0} - \eta_p \frac{\partial u}{\partial y}\Big|_{t=n}\right] \quad (5.3\text{-}11)$$

For the transient boundary condition equation (5.3-10) and (5.3-11) were applied to the inlet of the contraction geometry instead of equation (5.3-5) and (5.3-6). Other boundary conditions were the same as the steady state boundary conditions mentioned before.

5.3.2 Planar Contraction Results

The geometry shown in Figure 5.3-2 was meshed with linear tetrahedral elements. The element size was chosen so that the geometry was 4 elements thick in the *z* direction. This was done to have more internal nodes. The total numbers of elements was 20157, and the total numbers of nodes was 4620.

In the previous section, we demonstrated that analytical results for stress components for *xz*, *yy*, *yz*, *zz* were zero at the inlet, and velocity component in *y*, *z* direction were also zero at the inlet. However the stresses and velocities in those components for the overall geometry may not be zero. There are no deterministic analytical solutions

available for a 4:1 contraction to be compared with computational results. Therefore this section compares the computed results and *xx*, *xy*, *yy*, and *zz* stress component with the published numerical results. This section also presents pressure and velocity distributions in the *x*, *y* directions. Furthermore, this section presents entrance pressure loss for an Oldroyd-B fluid in a 4:1 planar contraction and a time dependent *xx* component stress plot at re-entrant corner using polypropylene melt.

Figure 5.3-3 presents the stress pattern in *xx* components. The stress contours are similar to the stress contours obtained by Baaijens [1993] using similar fluid in multi-mode differential models.

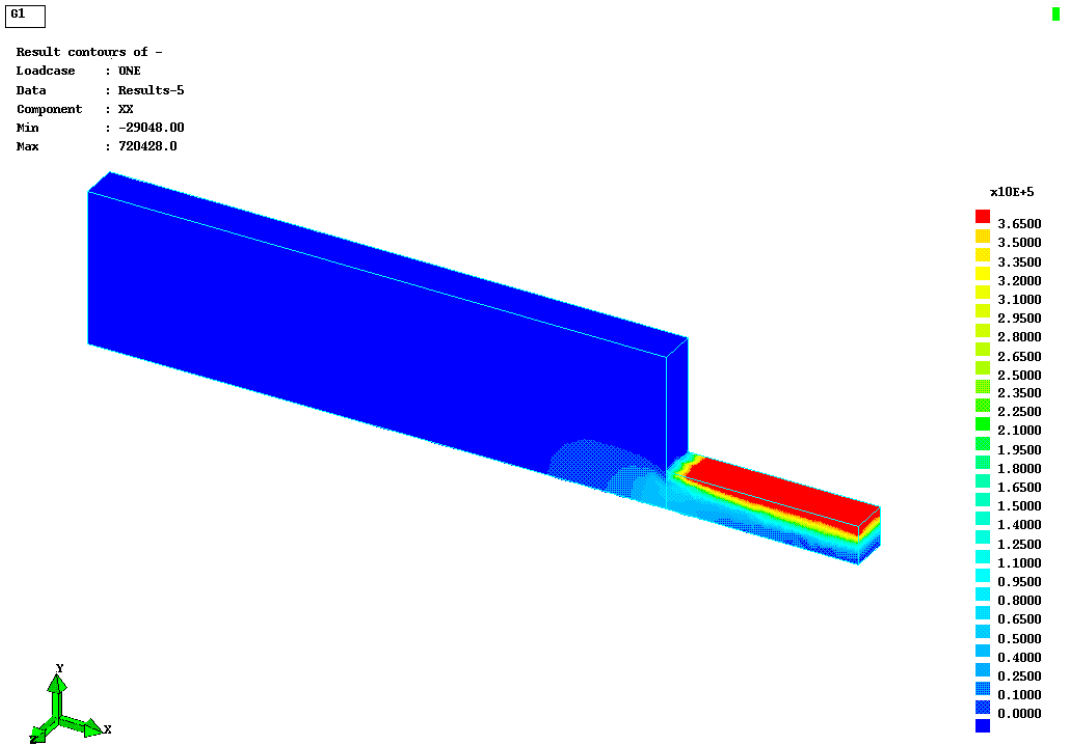

Figure 5.3-3. Stress contours for *xx* components in 4:1 planar contraction.

Figure 5.3-4 presents the stress pattern in *xy* components. The stress contours are similar to the stress contours obtained by Baaijens [1993] using similar fluid in multi-mode differential models

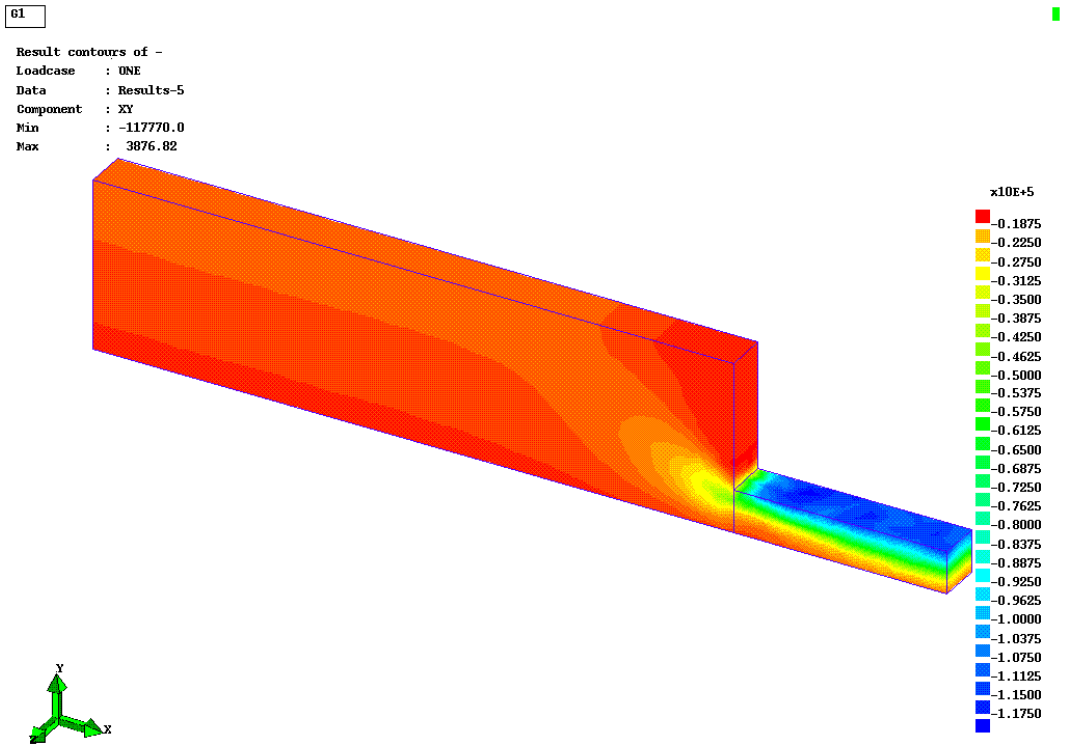

Figure 5.3-4. Stress contours for *xy* components in 4:1 planar contraction.

Figure 5.3-5 presents the stress pattern in *yy* components. The stress contours in *yy* component are similar to the stress contours in *yy* component obtained by Baaijens [1993] using similar fluid in multi-mode differential models

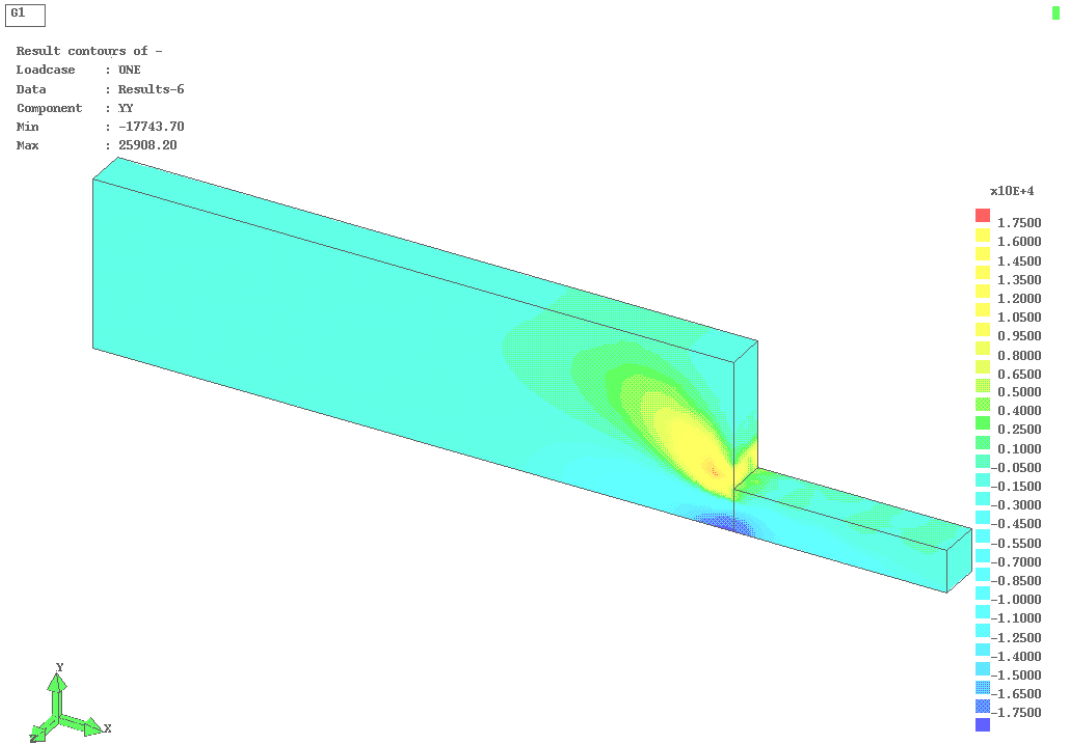

Figure 5.3-5. Stress contours for *yy* components in 4:1 planar contraction.

The velocity contours are given in Figure 5.3-6. Since we have assumed steady Poiseuille flow boundary conditions at the inlet, the outlet velocity pattern is assumed to be similar to the inlet pattern. In this case the velocity pattern at the inlet and outlet was parabolic. The maximum velocity at the outlet can be analytically calculated. We did this by balancing the mass at the inlet and the outlet. Since the velocity components in y and z direction were zero at the inlet, the flow rate at the inlet was defined as:

$$Q = \int_0^H udzdy \tag{5.3-12}$$

where Q is the flow rate. Since the 4:1 contraction has uniform thickness, the dz term in the above equation was treated as constant. Substituting (5.3-1) and simplifying the flow rate Q was defined as:

$$Q = \frac{2u_{\max_i} H}{3} \tag{5.3-13}$$

where H is the height of inlet/upstream section, and $u_{\max\ i}$ is the maximum velocity at inlet. Similarly, the flow rate at the outlet was given as:

$$Q = \frac{2u_{\max_o} h}{3} \tag{5.3-14}$$

where $u_{\max\ o}$ is the maximum velocity at the outlet, and h is the height of the outlet or downstream. Comparing equation (5.3-13) and (5.3-14), and using the fact that $H = 4h$ in a 4:1 contraction the maximum velocity at the outlet is 4 times than that of maximum velocity at the inlet. Since the maximum velocity at inlet was 0.15 m/s, the maximum outlet velocity in x-direction should be close to 0.6 m/s. The maximum velocity at the outlet was 0.61 m/s, which was at the symmetry plane in the y direction.

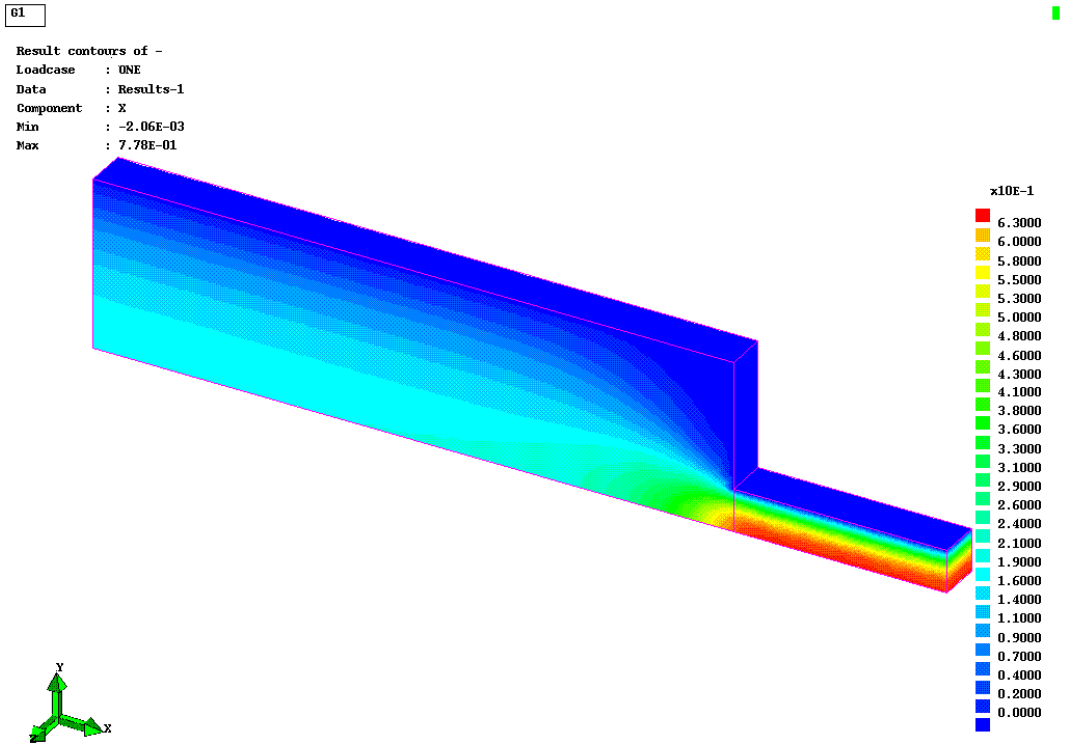

Figure 5.3-6. Velocity contours for *x* direction in 4:1 planar contraction.

Since we are unable to analytically calculate the velocity in *y* direction, the contours of velocity distribution in *y* direction are given in Figure 5.3-7.

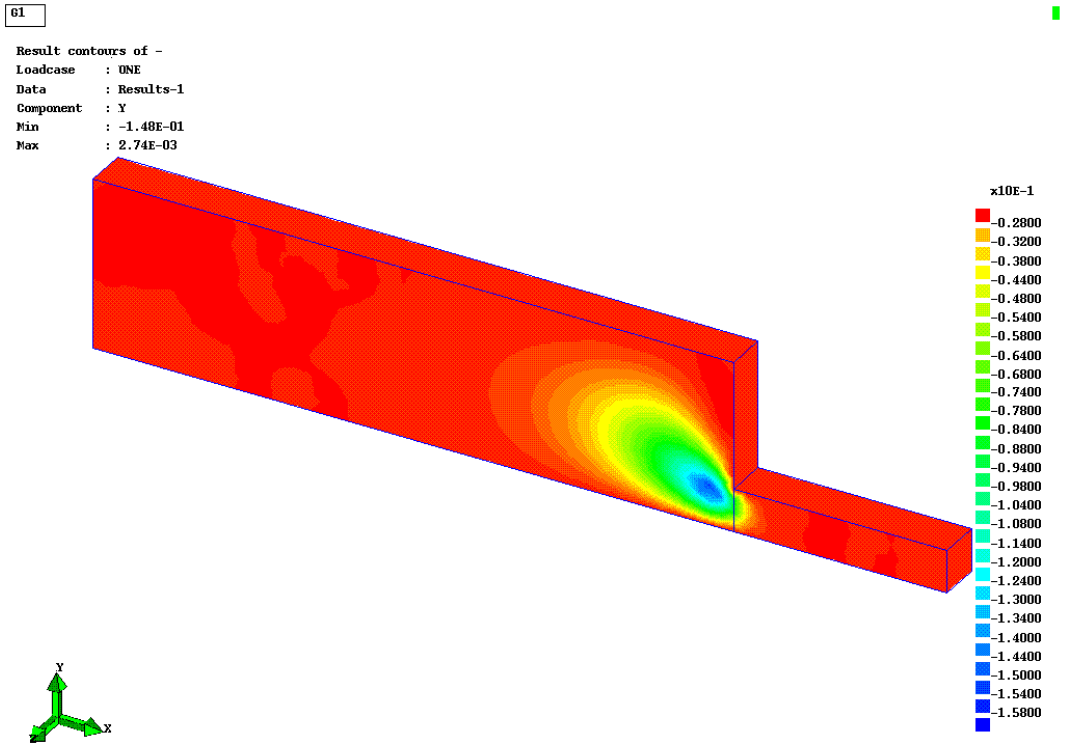

Figure 5.3-7. Velocity contours for *y* direction in 4:1 planar contraction.

The pressure contours are given in Figure 5.3-8. From the contour it is clear that the flow was fully developed at inlet and outlet, this was expected for steady flow in 4:1 planar contraction.

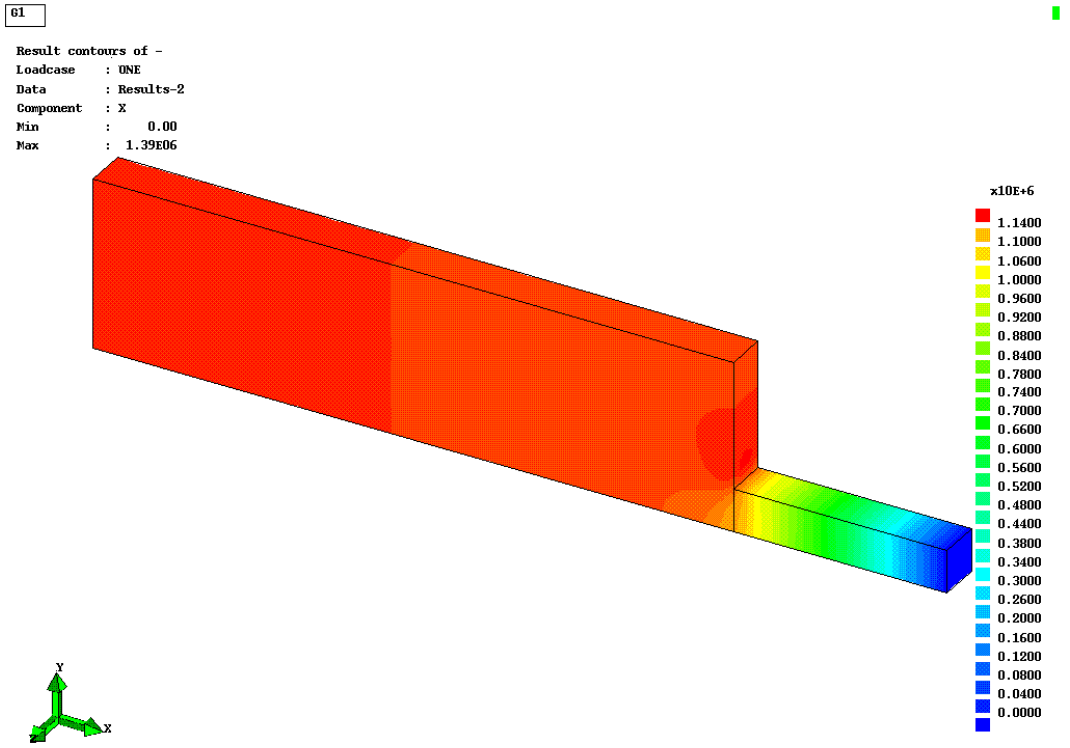

Figure 5.3-8. Pressure contours in 4:1 planar contraction.

The entrance pressure loss in 4:1 contraction is given in Figure 5.3-9. Ideally, the pressure drop in the upstream section and the pressure drop in the downstream section should equal to the total pressure drop between inlet and outlet. However, this is not generally true because in the contraction region or re-entrant corner, the polymer is forced to flow from a large cross-sectional area into a smaller cross-sectional area. Therefore, the material must extend as it flows into the smaller section while at the same time undergoing shearing forces. These additional stresses associated with the flow into the smaller cross-sectional area results in an additional pressure drop called a 'contraction pressure loss' or 'entrance pressure loss'. For the large contractions that typically occur at gates and nozzles in injection moulding processes, the contraction pressure losses can become relatively large at high flow rates. Therefore, realistic

prediction of contraction pressure loss has practical relevance to commercial manufacturing process. So the contraction pressure loss was calculated by calculating pressure drops in the downstream and upstream sections alone, and subtracting it from the total pressure difference between inlet and outlet. The entrance pressure loss is defined as:

$$\Delta P_{ent} = \Delta P - \left(\Delta P_U + \Delta P_D\right) \tag{5.3-15}$$

where ΔP_{ent} is entrance pressure loss, ΔP is the total pressure drop between inlet and outlet, ΔP_{U} is the pressure drop in the upstream section and ΔP_D is the pressure drop in the downstream section. The upstream pressure drop is given by:

$$\Delta P_U = \frac{-3\eta_0 Q}{H^3}\Delta X_U \tag{5.3-16}$$

where ΔX_U is the length of upstream section, Q is the flow rate, and η_0 is the zero shear rate viscosity defined in equation (3.2-7). Similarly, the pressure drop in the down stream section is given by:

$$\Delta P_D = \frac{-3\eta_0 Q}{h^3}\Delta X_D \tag{5.3-17}$$

where ΔX_D is the length of upstream section.

In Figure 5.3-9, we have plotted entrance pressure loss of an Oldroyd-B fluid against *Weissenberg* number. In this case the *Weissenberg* number is defined as the product of the relaxation time and downstream wall shear rate. In mathematical form, this is given by:

$$We = \lambda_1 \dot{\gamma}_w \tag{5.3-18}$$

In Figure 5.3-9, the entrance pressure loss is shown to decrease with increasing *Weissenberg* number. These results agree with the result published by Yoo and Na [1991], Keiller [1993], and Carew *et al.* [1993] for Oldroyd-B fluid in 4:1 planar contraction.

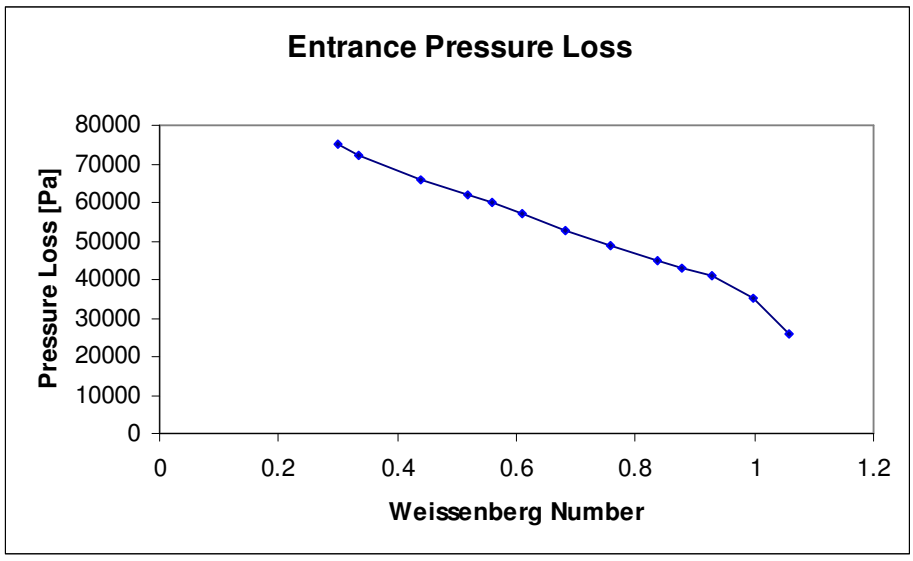

Figure 5.3-9. Entrance pressure loss for Oldroyd-B fluid in 4:1 planar contraction.

Figure 5.3-10 shows the *xx* stress component versus time at the re-entrant corner *C* shown in Figure 5.3-2. In this simulation we have assumed that at time $t = 0$ everything was zero. In this simulation we have used polypropylene melt data with η_p = 8750 Pa.s, λ_1 = 0.1s, and flow rate Q = 7.52E-06 m^3/s.

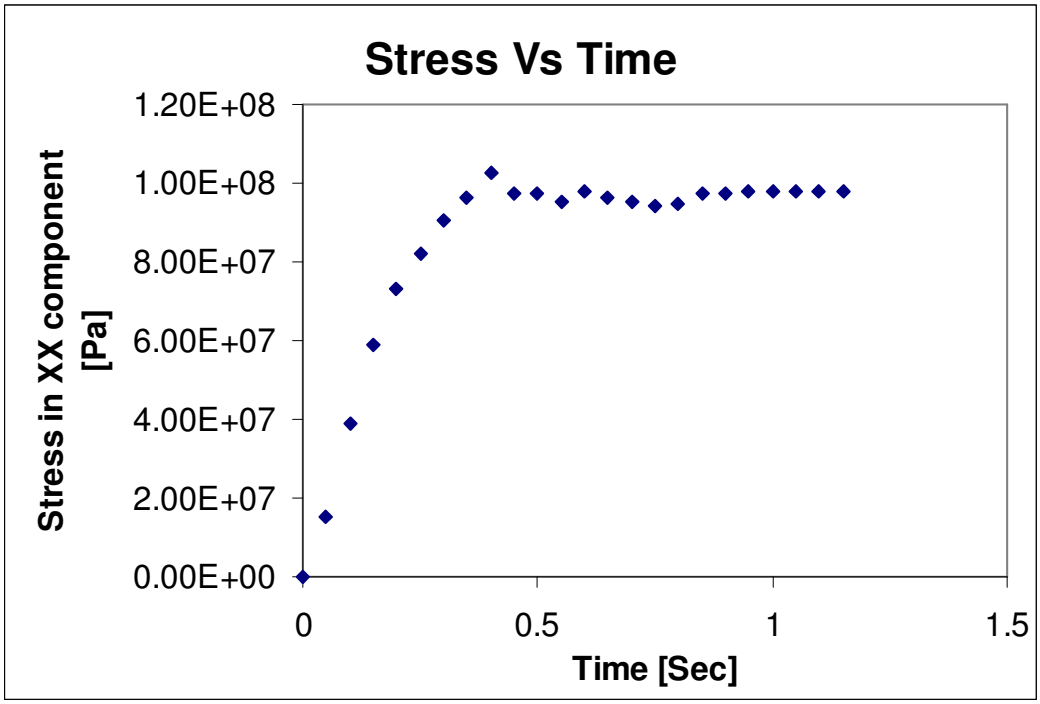

Figure 5.3-10. The *xx* stress component vs time at re-entrant corner in planar contraction.

Notice that the material takes 0.9 seconds to reach steady state. As expected the stress increases as the process begins and reaches a maximum before settling down to a steady state result. The maximum stress in *xx* direction in planar contraction was 103.0 MPa and when the stress settled to steady state the value was 97.0 MPa.

Since numerical accuracy and results for steady-sate prediction were satisfactory, the next section compares numerical computations with experimental results of an axisymmetric 4:1 contraction.

5.3.3 Boundary Conditions for Axisymmetric Contraction

The schematic of a 4:1 contraction was given in Figure 5.3.10. It was obvious that the geometry is symmetric along the centreline. The 4:1 axisymmetric contraction

geometry has been modelled by only considering one quarter of the full geometry because the geometry is symmetrical along the *y* and *z*-axes. In addition to the numerical boundary conditions elucidated in section 3.3.5, the velocity boundary conditions are given in Figure 5.3.10.

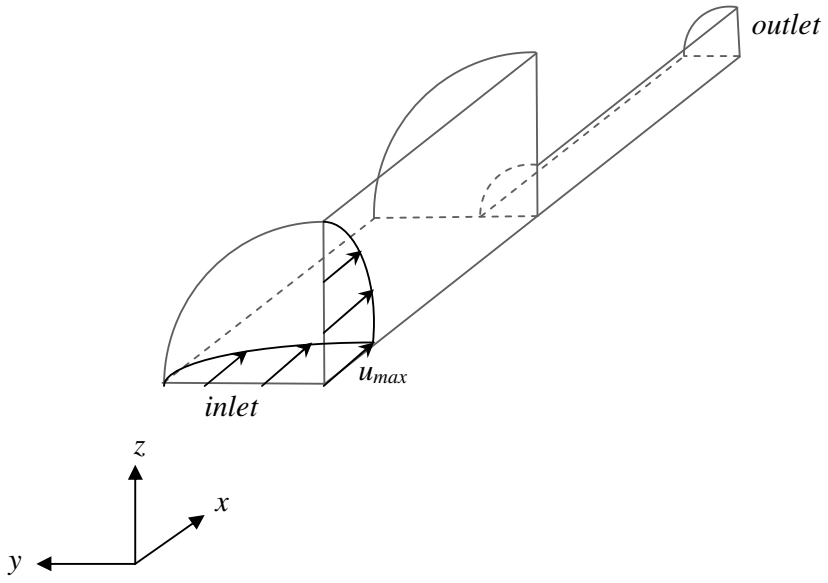

Figure 5.3-10. Velocity boundary conditions for axisymmetric 4:1 contraction.

In Figure 5.3-10, the symmetry planes are *xy*, and *xz*. The length of the upstream section was 20mm, and downstream was 25mm. The upstream radius R = 7mm, and the downstream radius was 1.75mm.

Analogously to the planar contraction the inlet was treated as steady laminar flow in a tube. The velocity profile for steady laminar flow in a tube [Douglas 1986] is given as:

$$u = \frac{R^2 - r^2}{R^2} u_{\max} \tag{5.3-19}$$

where u_{max} is the maximum velocity in the x-direction at the inlet, which was on the symmetry planes, and r^2 is the radius variable. The radius variable is defined as:

$$r^2 = y^2 + z^2 \tag{5.3-20}$$

5.3.3.1 Steady State Boundary Conditions

Assuming Poiseuille flow at the entrance, the analytical solutions for stress components of $\boldsymbol{\tau}_p$ for Oldroyd-B model were obtained by simplifying equation (3.3-70) to (3.3-75), with α equals to zero, and no time derivatives. The stress components in yy, yz, and zz components were zero. The stress in xx components for Oldroyd-B model are given as:

$$\tau_{pxx} = 2\lambda_1 \left(\tau_{pxy} \frac{\partial u}{\partial y} + \tau_{pxz} \frac{\partial u}{\partial z} \right) \tag{5.3-21}$$

where λ_1 is relaxation time given in Appendix-1, and the derivative of velocity with respect to y is defined as:

$$\frac{\partial u}{\partial y} = \frac{-2yu_{\max}}{R^2} \tag{5.3-22}$$

Similarly, the derivative of velocity with respect to z is defined as:

$$\frac{\partial u}{\partial z} = \frac{-2zu_{\max}}{R^2} \tag{5.3-23}$$

Notice that the stress component in *xx* is dependent upon stress in *xy*, and *xz* components. The stress in *xy* component was obtained by simplifying equation (3.3-71), to give:

$$\tau_{pxy} = \eta_p \frac{\partial u}{\partial y} + \lambda_1 \tau_{pyy} \frac{\partial u}{\partial y} + \lambda_1 \tau_{pyz} \frac{\partial u}{\partial z} \tag{5.3-24}$$

where η_p is the polymer contribution to zero shear rate viscosity, given in equation (3.2-7). Notice that the stress in *xy* component is dependent upon stresses in *yy*, and *zz* components.

Since *yy,* and *yz* component stresses are zero, the *xy* component stress can be obtained from the equation (5.3-24) by substituting equation (5.3-22), to yield:

$$\tau_{pxy} = \frac{-2y\eta_p u_{\max}}{R^2} \tag{5.3-25}$$

The stress in *xz* component was obtained by simplifying equation (3.3-72), to give:

$$\tau_{pxz} = \eta_p \frac{\partial u}{\partial z} + \lambda_1 \tau_{pzz} \frac{\partial u}{\partial z} + \lambda_1 \tau_{pyz} \frac{\partial u}{\partial y} \tag{5.3-26}$$

where η_p is the polymer contribution to zero shear rate viscosity, given in equation (3.2-7). Notice also that the stress in *xy* component is dependent upon stresses in *yz* and *zz* components.

Since *yz* and *zz* component stresses are zero, the *xz* component of stress can be obtained from the equation (5.3-26) by substituting equation (5.3-23), to give:

$$\tau_{pxz} = \frac{-2z\eta_p u_{\max}}{R^2} \tag{5.3-27}$$

Stress in *xx* component was obtained by substituting equation (5.3-22), (5.3-25), (5.3-23), and (5.3-27) in equation (5.3-21), to give:

$$\tau_{pxx} = 8\lambda_1\eta_p\left(\frac{u_{\max}}{R^2}\right)^2\left(y^2 + z^2\right) \tag{5.3-28}$$

The no-slip boundary conditions for the walls were applied. The velocity at walls were, u = 0.0 m/s, v = 0.0 m/s, w = 0.0 m/s. The velocity u, v, and w were the velocity components in x, y, and z direction respectively.

At the inlet, both the v velocity and w velocity were zero, and the u velocity was specified at every node at the inlet from equation (5.3-19), with u_{max} = 0.15m/s. The value of τ_{pxx} was specified at each node in the inlet from equation (5.3-28). The value of τ_{pxy} in each node at the inlet was specified from equation (5.3-25). The value of τ_{pxz} in each node at the inlet was specified from equation (5.3-27). Other stress components of stress were zero at the inlet.

For the outlet boundary conditions, pressure was specified at every node at the outlet to be zero. The velocity in the y and z directions was zero at the outlet.

For symmetry boundary conditions along the *xz* plane, velocity normal to that plane was zero, which means *v* equals to zero. Stresses in *xy* and *yz* components were zero at this symmetry position.

For symmetry boundary conditions along the *xy* plane, the *w* velocity was zero. Stresses in *xz*, *yz* components were zero at this symmetry position.

5.3.3.2 Time Dependent Boundary Condition

The transient boundary condition for the axi-symmetric contraction geometry with Oldroyd-B model was obtained in the same way as for the planar contraction.

The stress components in *yy*, *yz*, and *zz* for Oldroyd-B model were zero for axisymmetric contraction. The stress component in *xz* direction were non zero. Since the *xz* component stress was not zero, the stress component in *xx* direction had *xz* component contributions. The stress in *xx* component was defined as:

$$\begin{aligned}\tau_{pxx} = 2\lambda_1\left(\tau_{pxy}\frac{\partial u}{\partial y}+\tau_{pxz}\frac{\partial u}{\partial z}\right)\Big|_{t=n} + \\ 2\lambda_1 e^{-t/\lambda_1}\left[\left(\tau_{pxy}\frac{\partial u}{\partial y}+\tau_{pxz}\frac{\partial u}{\partial z}\right)\Big|_{t=0} - \left(\tau_{pxy}\frac{\partial u}{\partial y}+\tau_{pxz}\frac{\partial u}{\partial z}\right)\Big|_{t=n}\right]\end{aligned} \tag{5.3-29}$$

Similarly the stress component in the *xy* direction was obtained by applying equations (5.3-7) to (5.3-9) to the equation (3.3-71) to give:

$$\tau_{pxy} = \eta_p \frac{\partial u}{\partial y}\Big|_{t=n} + e^{-t/\lambda_1}\left[\eta_p \frac{\partial u}{\partial y}\Big|_{t=0} - \eta_p \frac{\partial u}{\partial y}\Big|_{t=n}\right] \tag{5.3-30}$$

Similarly the stress component in the *xz* direction was obtained by applying equations (5.3-7) to (5.3-9) to the equation (3.3-72) to give:

$$\tau_{pxz} = \eta_p \left.\frac{\partial u}{\partial z}\right|_{t=n} + e^{-t/\lambda_1}\left[\eta_p \left.\frac{\partial u}{\partial z}\right|_{t=0} - \eta_p \left.\frac{\partial u}{\partial z}\right|_{t=n}\right] \tag{5.3-31}$$

For transient boundary conditions, equation (5.3-29) and (5.3-31) were applied to the inlet of the contraction geometry. Other boundary conditions were the same as the steady state boundary conditions described previously.

5.3.4 Axisymmetric Contraction Results

The geometry shown in Figure 5.3-10 was meshed with linear tetrahedral elements using IDEAS® [SDRC®, USA] software. The element size was chosen so that the geometry was 3 elements thick in z direction in the downstream section. This was done to have more internal nodes. The total numbers of elements was 39508, and the total numbers of nodes was 8041. The mesh for this geometry is shown in Figure 5.3-11.

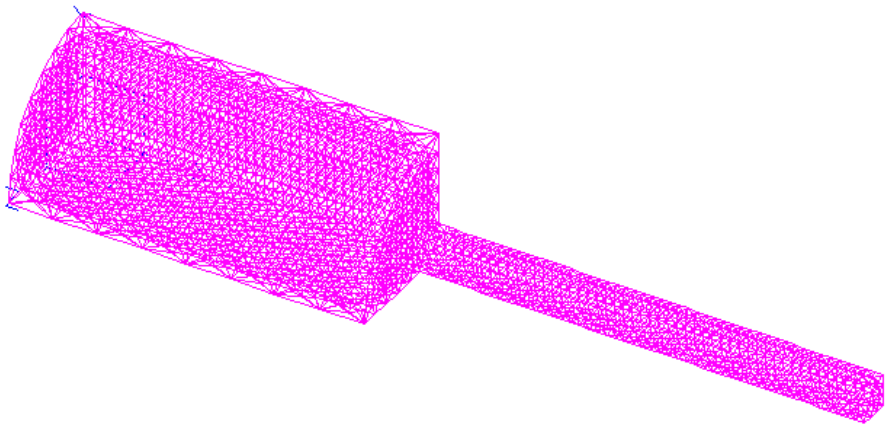

Figure 5.3-11. Axisymmetric 4:1 contraction mesh.

The pressure drop/difference between inlet and outlet was computed and compared with experimental data. To obtain experimental data a fifteen tonne injection-moulding machine, an axisymmetric 4:1 contraction geometry, and Polypropylene material was used. Polypropylene material was used because it was characterised for viscoelastic parameters previously. Polypropylene melt at 240^{o}C was extruded through the axisymmetric contraction geometry at various flow rates, and the pressure drops corresponding to the flow rates were recorded. The length of the upstream region of the axisymmetric 4:1 contraction geometry was 40mm, and the radius was 7mm. For the downstream section, the length was 25mm and the radius was 1.75mm. Notice that the modelled geometry had 20mm upstream length (Figure 5.3-10/11). Since the diameter of upstream tube was so much larger than the downstream radius, we assumed that the pressure drop between the actual inlet in the experimental die and half way through the upstream region was negligible. One of the benefits of modelling only half of the upstream section is that it reduces the number of nodes by about half. A plot of experimental and computed pressure drops against shear rates in the downstream capillary is shown in Figure 5.3-12.

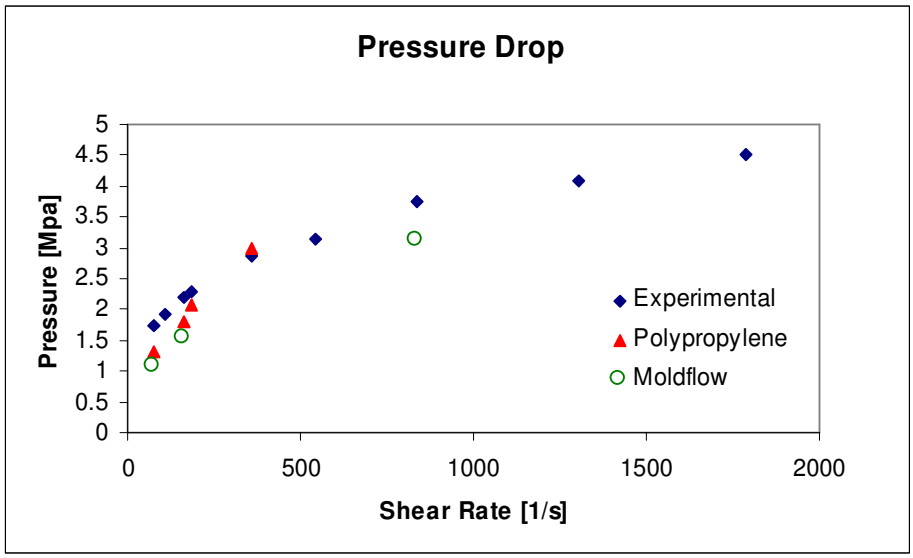

Figure 5.3-12. Comparison of experimental and computational pressure drop in 4:1 axisymmetric contraction.

In the plot above the legends correspond to the following:

- Experimental – measured pressure drop for a polypropylene melt extrusion
- Polypropylene - single-mode Oldroyd-B model with polypropylene material data given in Appendix-1
- MoldFlow - Moldflow® [Moldflow Intl. Ltd., Australia] software prediction (purely viscous flow)

The data for the plot above is given in Appendix-2 in tabular format.

For Polypropylene, predictions at a shear rate of 357 s^{-1} could be made. This corresponded to a *Weissenberg* number of 5.44. For more values of shear rate or *Weissenberg* number the numerical algorithm would not converge.

From the computational reuslts shown in Figure 5.3-12, the viscoelastic model, for all its shortcommings does a better job in general of predicting pressure drop than a purely viscous fluid simulation. Also notice that at low shear rate region (first two points of the graph) the values of viscoelastic prediction is better than viscous flow prediction. However, the viscoelastic prediction is close to viscous flow prediction. The reason for this is that in one mode viscoelastic model (section 2.4 data fitting graph) the the viscosity is constant in low shear rate/frequency region. So the prediction in the low shear rate region is similar to viscous flow prediction. The third and fourth point has better prediction because the single mode dada fitted very well in this shear rate/frequency region. The single mode viscoelastic constitutive equation fits only a narrow region of frequencies, say approximately 150-450 rad for the plots given in section 2.4.

Figure 5.3-13 is a plot of *xx* stress component versus time at the re-entrant corner, which is located at x = 39.85mm, y = 1.23mm, z = 1.23mm as shown in Figure 5.3-10. In this simulation we have assumed that at time t = 0 everything is zero. In this simulation we have used polypropylene melt data with η_p = 8750Pa.s, λ_1 = 0.1s, and flow rate Q = 7.52E-06 m^3/s.

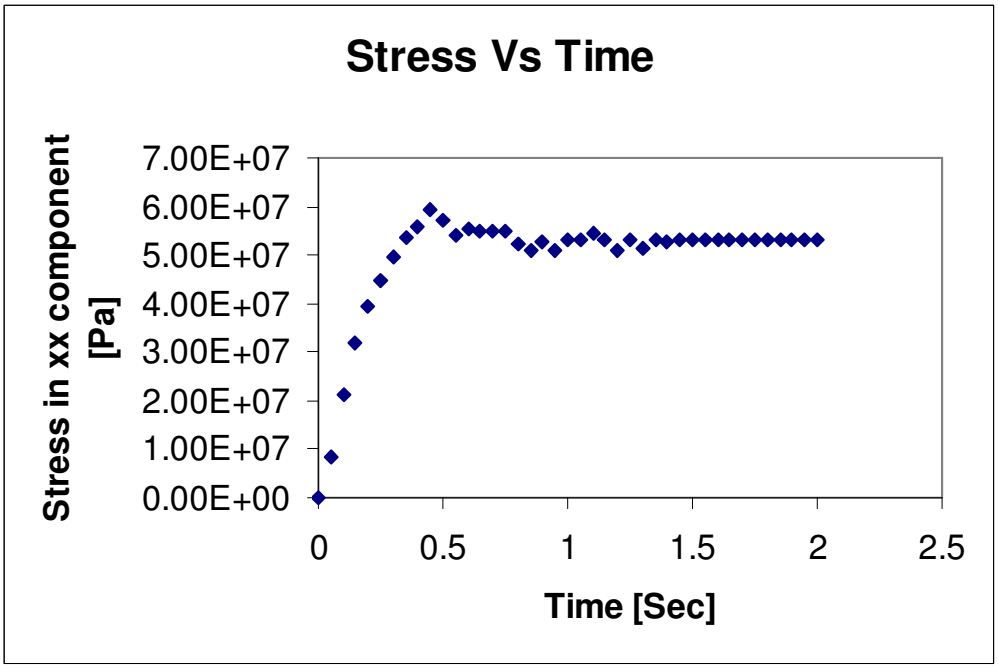

Figure 5.3-13. The *xx* stress component versus time at re-entrant corner in axi-symmetric contraction.

Notice that the material takes 1.5 seconds to reach steady state. As expected the stress increases as the process begins and reaches a maximum before settling down to a steady state result. Under the same conditions in a planar contraction it took 0.9 seconds to reach steady state. The maximum stress in the *xx* direction in the axi-symmetric contraction was 60.0 MPa and when the stress settled to steady state the value is 53.0 MPa.

5.4 Chapter Summary

The numerical simulation of simple shear flow and planar Poiseuille flow demonstrated that the numerical algorithm was quite accurate and considering the coarse mesh, the results of the prediction were satisfactory.

In a planar 4:1 contraction, the flow at the inlet was assumed to be fully developed Poiseuille flow. The prediction of polymeric stress contributions to the extra stress tensor components in *xx*, *xy*, *yy* directions, was similar to previously published results using similar fluid and geometry. The prediction of pressure indicates that the flows were fully developed at inlet and outlet regions. The entrance-pressure loss decreases with increasing *Weissenberg* number, which was expected of Oldroyd-B fluid.

In the comparison of experimental and computed pressure drop in axisymmetric 4:1 contraction, predictions have only been possible in the low shear rate regions.

The *xx* component of stress seems to take longer to settle down to steady state in axi-symmetric contraction than in planar contraction flows.

6. Conclusion and Recommendations

After the review of viscoelastic constitutive equations, differential type viscoelastic constitutive equations were selected. Considering that the more modes, the more computationally expensive the simulations, it was decided to simulate single-mode viscoelastic constitutive equations. Polypropylene melt was characterised to obtain material and equation parameters for viscoelastic constitutive equations. The finite element method with SUPG was applied to discretize the single-mode viscoelastic constitutive equations. An equal order velocity-pressure formulation along with EVSS was used to provide the relationships between velocity, pressure, and polymer contribution to the extra stress tensor. After testing the accuracy of the numerical algorithms in simple shear and parallel plate flow, flow simulation in a 4:1 planar and axisymmetric contraction was conducted and the results were presented in Chapter 5. The results of the single-mode viscoelastic constitutive equation simulation were satisfactory and quite accurate.

The conclusions to our research are given in Section 6.1. The recommendations for future work are given in Section 6.2.

6.1 Research Conclusions

After reviewing the characteristics of a wide range of viscoelastic constitutive equations, it was concluded that there are no viscoelastic constitutive equations which are well suited for predicting complex flows in arbitrary geometries as seen in injection moulding processes. Each viscoelastic constitutive equation is only capable of predicting a particular simple flow. After due consideration, including those of Larson, the Giesekus and Oldroyd-B models were chosen for investigation. Although the selections were considered to be made upon the basis of the best available facts, the selections of constitutive equations still depends on personal choice and preference.

The material data for viscoelastic constitutive equations was obtained from experiments. Material and equation parameters for differential type viscoelastic constitutive equations was obtained by fitting only steady state rate sweep experimental data. However, to predict a variety of flows realistically, it was logical to characterise polymer material rhelogically in as many flows as possible. The procedures followed to obtain material and equation parameters were as follows:

- Data fitting of the viscoelastic constitutive equations to stress-relaxation experiments at various temperatures.
- Data fitting of the viscoelastic constitutive equations to dynamic frequency-sweep experiments at various temperatures.
- Data fitting of the viscoelastic constitutive equations to steady rate sweep experiments at various temperatures.

The relaxation times for differential type viscoelastic constitutive equations were obtained from the stress relaxation experiments (linear viscoelastic experiment). The retardation times were obtained from the dynamic frequency sweep (oscillatory shear flow) experiments. The mobility factors were obtained from the steady state rate sweep experiments. It was found that realistic characterisation of polymer material was near impossible using single-mode differential type viscoelastic constitutive equations. However it was possible to characterise the material if the flow range (i.e. temperature and shear rate or frequency) of interest was known. The data fitting of 3-mode and 9-mode viscoelastic constitutive equations were adequate. Comparing the three-mode and nine-mode viscoelastic constitutive equation data fitting, it was found that the 3-mode model was nearly as good as the 9-mode in many instances, however overall nine-mode model fitted data more accurately than three or one mode model. Generally the more modes, the more computationally expensive are the simulations. In multi-mode simulation, the number of unknowns in a problem will increase almost linearly with the number of modes. This material characterisation procedure could also be applied to obtain equation and material parameters for integral type viscoelastic constitutive

equations. However, certain integral type viscoelastic constitutive equations may present difficulties in determining the potential function.

In numerical methods employed, the governing equations were discretized using Galerkin's weighted-residual and finite element method. We have extended Rice and Schnipke's equal-order velocity-pressure formulation originally proposed for Newtonian steady flow in two-dimension to viscoelastic flow in three dimensions. The linkage between Newtonian and viscoelastic model was created by the EVSS formulation for the extra stress tensor. There were two possible ways viscoelasticity could be implemented into the Newtonian calculation; these are described as follows:

1) The first was to solve the velocity equation, the pressure equation and the viscoelastic constitutive equation sequentially in one single iterative loop.
2) The second was to solve the velocity equation and the pressure equation until Newtonian solution converged, then use the Newtonian flow field solution to solve the viscoelastic constitutive equation, and continue this process alternately until the overall convergence criteria were satisfied.

Both methods were attempted. In the first method, for simple shear flow, it was found that the numerical code did not often converge, and took longer if it did. The second method was more stable, and took less time for flows in simple shear.

It was found that the accuracy of the derivatives of velocities was improved by calculating them as piecewise linear rather than constants within elements. Similarly, the derivatives of components of polymer contribution to stress tensor were calculated as piecewise linear, which was used in the momentum equation.

The extension of the numerical method of Rice and Schnipke to 3D and with the incorporation of viscoelastic constitutive equations was found to be very powerful. The accuracy of viscoelastic computations was demonstrated by comparing solutions with

analytical and other numerical results published in literature on similar flow fields and the agreement was excellent. The numerical simulation of simple shear flow and planar Poiseuille flow demonstrated that the numerical algorithm was quite accurate and considering the coarseness of the mesh, the results of the prediction were satisfactory. In planar 4:1 contraction, the prediction of the polymeric stress contribution to the extra stress tensor components in *xx*, *xy*, *yy* were similar to previously published results in similar fluid and geometry. The entrance-pressure loss decreases with increasing *Weissenberg* number, which was expected of Oldroyd-B fluid.

In the comparison of experimental and computational pressure drop for polypropylene melt in axisymmetric 4:1 contraction, good agreement has been shown in the low shear rate regions. The reason for this might be that the parameters for single-mode viscoelastic constitutive equations were obtained from data fitting in the low shear rate region.

In time dependent behaviour it was observed that the stress field, indeed all the flow variables, evolved over a characteristic time span after a disturbance was introduced. Although in both examined geometries the re-entrant corner point was almost identical, in the planar contraction the stress took less time to settle down to steady state than in the axi-symmetric contraction. Also in the planar contraction the maximum stress and the steady state stress was more than the axisymmetric contraction. This discrepancy is may be due to the inadequate boundary conditions in planar contraction. For example the stress in *xz* direction was ignored in planar contraction. However, further investigation is needed to know more about this discrepancy.

6.2 Recommendation For Future Improvements

The numerical analysis should be extended towards flows in complex geometry, which will be a more rigorous test for the numerical scheme.

It was concluded that the multi-mode viscoelastic constitutive equations characterise polymer material well. The numerical techniques developed in this work should be improved and extended to implement multi-mode viscoelastic constitutive equations economically.

Since complex flows involve a mixture of shear and elongation flows, the characterisation of polymer material should be extended to include elongation flows. Most polymer processes involve high shear rates. The material characterisation was in relatively low shear rates/frequencies compared with most polymer-processing techniques. In the previous section it was demonstrated/concluded that the single-mode viscoelastic constitutive equation only predicts the flow at a particular shear rate or in a narrow shear rate region. So for flow prediction in wider range of shear rates/frequencies the role of multi-mode model should be investigated.

The time dependent results showed difference in stresses in planar and axi-symmetric contraction. Further investigation is necessary to fully understand this issue.

Since most polymers are viscoelastic in nature, it is logical to use viscoelastic constitutive equations to predict realistic flow behaviours in polymer processing techniques. The final goal of this on-going research is to predict realistic flow behaviour in polymer processing using viscoelastic constitutive equations. For this purpose, empirical or semi-empirical constitutive equations that describe commercial polymers well should be investigated further. This may lead to an *ad hoc* constitutive equation for polymer processing techniques.

7. References

Acierno, D., Lamanta, F. P., Marrucci, G. & Titomanlio, G. (1976). "A non-linear viscoelastic model with structure-dependent relaxation times. I. Basic formulation." *Journal of Non-Newtonian Fluid Mechanics*, 1.

Armstrong, R. C., Brown, R. A., Quinzani, L. M., McKinley, G. H., and Bryars, J. (1992). "Measurement of velocity and stress fields in complex polymer flows. Moldanaers, P., and Keunnings, R. eds. *Theoretical and applied Rheology, Proc. Xith Int. Congress Rheol*., Brussels, 27-32.

Aziez, J., Guénette, R., and Aït-Kadi, A. (1996). "Numerical simulation of viscoelastic flows through a planar contraction." *Journal of Non-Newtonian Fluid Mechanics*, 62, 253-277.

Baaigens, F. P. T. and Douven L. F. A (1990). "Calculation of Flow Residual Stresses in Injection Moulded Products." *Integration of Theory and Applications in Applied Mechanics*, (Editors- J.F Dijksman and F.T.M Nieuwstadt) 73-90.

Baaigens, F. P. T. (1993). "Numerical analysis of start-up planar and axisymmetric contraction flows using multi-mode differential constitutive model." *Journal of Non-Newtonian Fluid Mechanics*, 48, 147-180.

Baaijens, F. P. T. (1993). "Numerical analysis of start-up planar and axisymmetric contraction flows using multi-mode differential constitutive model." *Journal of Non-Newtonian Fluid Mechanics*, 48, 147-180.

Baaijens, H. (1994). "Evaluation of constitutive equations for polymer melts and solutions in complex flows." *PhD Thesis,* Eindhoven University of Technology.

Baird, D.G. (1988). "Working group on interplay between experiments and numerical solution." *Journal of Non-Newtonian Fluid Mechanics*, 29, 6-8.

Bernstein, B. (1969). "Small Shearing Oscillations Superposed on Large Steady Shear of the BKZ Fluid." *International Journal of Nonlinear Mechanics*, 4, 183-200.

Bird, R. B., Armstrong, R. C., and Hassager, O. (1987). *Dynamics of Polymeric Liquids.* John Wiley & Sons, New York.

Boger, D. V., Crochet, M. J. & Keiller, R. A. (1992). "On viscoelastic flows through abrupt contractions." *Journal of Non-Newtonian Fluid Mechanics*, 44, 267-279.

Boger, D. V., Hur, D. U., and Binnington, R.J. (1986). "Further observations of elastic effects in tubular entry flow." *Journal of Non-Newtonian Fluid Mechanics,* 20, 31-49.

Brooks, A. N., and Hughes, T. J. R. (1982). "Streamline upwinding/Petrov-Galerkin formulations for convection dominated flows with particular emphasis on the incompressible Navier-Stokes equations." C*omputer methods in applied mechanics and engineering,* 32, 192-259.

Brown, R.A., & McKinley, G.H. (1994). "Report on the VIIIth international workshop on numerical methods in viscoelastic flows." *Journal of Non-Newtonian Fluid Mechanics*, 52, 407-413.

Burnett, D. S. (1987). *Finite element analysis from concept to applications.* Addison-Wesley publishing company, Reading, Massachusetts.

Bushko, W. C., and Stokes, V. K. (1996). "Solidfication of Thermoviscoelastic Melts. Part 3: Effects of Mold Surface Temperature Difference on Warpage and Residual Stresses" *Polymer Engineering and Science,* Vol. 36, 3, 322-335.

Carew, E. O. A., Townsend, P., and Webster, M. F. (1993). "A Taylor-Petrov-Galerkin algorithm for viscoelastic flow." *Journal of Non-Newtonian Fluid Mechanics*, 50, 253-287.

Coates, P. J., Armstrong, R. C., and Brown, R.A. (1992). "Calculation of steady-state viscoelastic flows through axisymmetric contractions with the EEME formulation." *Journal of Non-Newtonian Fluid Mechanics*, 42, 141-188.

Couniot, A., Dheur, L., Hansen, O. & Dupert, F. "A finite method for simulating injection molding of thermoplastics." *Private Communication.*

Coyle, D.J., Blake, J.W. & Macosko, C.W. (1987). "The kinematics of fountain flow in mold filling." *AIChE Jrnl*., 33.

Crochet, M. J., Debbaut, B., and Van Schaftingen, J. J. (1985). *Fourth Workshop on Numerical Methods in Non-Newtonian Flow,* Belgium.

Crochet, M.J. (1986). "Recent developments in the numerical simulation of viscoelastic flow." *NUMIFORM*, Gothenburg.

Currie, P.K. (1982) "Constitutive equations for polymer melts predicted by the Doi-Edwards and Curtis-Bird kinetic theory models." *Journal of Non-Newtonian Fluid Mechanics*, 11.

Debae, F., Legat, V., & Crochet, M.J. (1994). "Practical evaluation of four mixed finite element methods for viscoelastic flow." *Journal of Rheology*, 38, 421-442.

Debbaut, B., and Crochet, M. J. (1986). "Further results on the flow of a viscoelastic fluid through an abrupt contraction." *Journal of Non-Newtonian Fluid Mechanics,* 20, 173-185.

Douglas, J. F., Gasiorek, J. M., and Swaffield, J. A. (1986). *Fluid Mechanics.* Longman Scientific & Technical, Essex, England.

Eggen, S., and Hinrichsen, E. L. (1996). "Swell and distortion of High-Density Polyethylene Extruded Through Capillary dies" *Polymer Engineering and Science,* Vol. 36, 3, 410-424.

Evans, R. E., and Walters, K. (1986). "Flow characteristics associated with abrupt changes in geometry in the case of highly elastic liquids." *Journal of Non-Newtonian Fluid Mechanics,* 20, 11-29.

Evans, R. E., and Walters, K. (1986). "Further remarks on the lip-vortex mechanism of vortex enhancement in planar-contraction flows." *Journal of Non-Newtonian Fluid Mechanics,* 32, 95-105.

Feigl, K., and Öttinger, H. C. (1994). "The floe of a LDPE melt through an axisymmetric contraction: A numerical study and comparison to experimental results." *Journal of Rheology,* 38, 847-874.

Fletcher, T. (1976). *Conjugate gradient methods for indefinite systems. Lecture notes in Mathematics.* Springer-Verlag, Berlin.

Fortin, A., Zine, A., & Agassant, J.F. (1992). "Computing viscoelastic fluid flow problems at low cost." *Journal of Non-Newtonian Fluid Mechanics*, 45, 209-229.

Fortin, M., & Esselaoui, D. (1987). "A finite element procedure for viscoelastic flows." *Intl. Jr. Num. Methods,* 7, 1035-1052.

Fortin, M., and Fortin, A. (1989). "A new approach for the FEM simulation of viscoelastic flows." *Journal of Non-Newtonian Fluid Mechanics*, 32, 295-310.

Giesekus, H. (1982) "A simple constitutive equation for polymer fluids based on the concept of deformation-dependent tensorial mobility." *Journal of Non-Newtonian Fluid Mechanics*, 11, 69-109.

Giesekus, H. (1983) "Stressing Behaviour in Simple Shear Flow as Predicted by a New Constitutive model for polymer fluids." *Journal of Non-Newtonian Fluid Mechanics*, 12, 367-374.

Giesekus, H. (1982) "A unified Approach to a Variety of Constitutive Models for Polymer Fluids Based on the Concept of Configuration-Dependent Molecular Mobility." *Rheologica Acta*, 21, 366-375.

Guénette, R. & Fortin, M. (1995). "A new mixed finite element method for computing viscoelastic flows." *Journal of Non-Newtonian Fluid Mechanics*, 60, 27-52.

Hadj, M.E. & Tanguy, P.A. (1990). "A finite element procedure coupled with the method of characteristics for simulation of viscoelastic fluid flow." *Journal of Non-Newtonian Fluid Mechanics*, 36, 333-349.

Hageman, L. A., and Young, D. M. (1981). *Applied Iterative Methods.* Academic Press, San Diego.

Hassager, O. (1988). "Working group on numerical techniques." *Journal of Non-Newtonian Fluid Mechanics*, 29, 2-5.

Hulsen, M.A., & Zanden, J.V. (1991). "Numerical simulation of contraction flow using a multi mode Giesekus model." *Journal of Non-Newtonian Fluid Mechanics*, 38, 183-221.

Isayev, A.I., & Upadhyay, R.K. (1985). "Two dimensional viscoelastic flows: experimentation and modeling." *Journal of Non-Newtonian Fluid Mechanics*, 19, 135-160.

Johnson, M. W. Jr, and Segalman, D. (1977). "A Model for Viscoelastic Fluid Behaviour Which Allows Non-AFfine Deformation." *Journal of Non-Newtonian Fluid Mechanics*, 2, 255-270.

Johnson, M. W. Jr, and Segalman, D. (1977). "Description of Non-Affine Motions of Dilute Polymer solutions by the Porous Molecule Model" *Journal of Non-Newtonian Fluid Mechanics*, 9, 33-56.

Kearsley, E. A. and Zapas, L. J. (1976). "Experimental Tests of Some Integral Rheological Relations." *Trans. Soc. Rheology*, 20, 623-637

Keiller, R. A. (1993). "Entry-flow calculations for the Oldroyd-B and FENE equations." *Journal of Non-Newtonian Fluid Mechanics*, 46, 143-178.

Keunings, R. (1986). "On the high Weissenberg number problem." *Journal of Non-Newtonian Fluid Mechanics,* 20, 209-226.

King, R.C., Apelian, M.R., Armstrong, R.C., & Brown, R.A. (1988). "Numerical stable finite element techniques foe viscoelastic calculations in smooth and singular geometries." *Journal of Non-Newtonian Fluid Mechanics*, 29, 147-216.

Larson, R.G. (1984). "A Consitutive Equation for Polymer Melts Based on Partially Extending Strand Convection." *Journal of Rheology*, 28, 545-571.

Larson, G. (1988a). *Constitutive Equations for Polymer Melts and Solutions.* Butterworth Publishers, Stoneham, Massachusetts.

Larson, R.G. (1988b). "Working group on constitutive equations and modeling." *Journal of Non-Newtonian Fluid Mechanics*, 29, 5-6.

Laso, M., & Öttinger, H.C. (1993). "Calculation of viscoelastic flow using molecular models: the CONNFFESSIT approach." *Journal of Non-Newtonian Fluid Mechanics*, 47, 1-20.

Leonov, A.I., Lipkina, E. H., Pashkin, E. D. and Prokunin, A. N. (1976). "Theoretical and Experimental Investigation of Shearing in Elastic Polymer Liquids." *Rheologica Acta*, 15, 411-426.

Leonov, A.I. (1992). "Analysis of simple constitutive equations for viscoelastic liquids." *Journal of Non-Newtonian Fluid Mechanics*, 42, 323-350.

Loh, K.W.L., Teoh, S.H., & Tay, A.A.O. (1996). "Computer simulation of viscoelastic flow at the entry region." *Ploy. Eng. and Sci.*, 36, 368-377.

Lou, X.-L., & Tanner, R. I. (1986). "A streamline element scheme for solving viscoelastic flow problems. Part I. Differential constitutive equations." *Journal of Non-Newtonian Fluid Mechanics*, 21, 179-199.

Lou, X.-L., & Tanner, R. I. (1988). "Finite element simulation of long and short circular die extrusion experiments using integral models." *International Journal for Numerical Methods in Engineering,* 25, 9-22.

Lou, X.-L., and Tanner, R. I. (1989). "A decoupled finite element streamline-upwind scheme for viscoelastic flow problems." *Journal of Non-Newtonian Fluid Mechanics*, 31, 143-162.

Lunsman, W.J., Genieser, L., Armstrong, R.C., & Brown, R.A. (1993). "Finite element analysis of steady viscoelastic flow around a sphere in a tube: calculations with

constant viscosity models." *Journal of Non-Newtonian Fluid Mechanics*, 48, 63-99.

Macosko, C. W. (1994). *Rheology Principles, Measurement, and Applications.* VCH Publishers, New York.

Maders, H., Vergnes, B., Demay, Y., & Agassant, J.F. (1992). "Steady flow of a White-Metzner fluid in a 2-D abrupt contraction: computation and experiments." *Journal of Non-Newtonian Fluid Mechanics*, 45, 63-80.

Marchal, J. M., and Crochet, M. J. (1986). "Hermitian finite element for calculating viscoelastic flow." *Journal of Non-Newtonian Fluid Mechanics*, 20, 187-207.

Marchal, J.M., & Crochet, M.J. (1987). "A new finite element for calculating viscoelastic flow." *Journal of Non-Newtonian Fluid Mechanics*, 26, 77-114.

McKinley, G.H., Raiford, W.P., Brown, R.A., & Armstrong, R.C. (1991). "Nonlinear dynamics of viscoelastic flow in axisymmetric abrupt contractions." *Journal of. Fluid Mechanics*, 223, 411-456.

Oldroyd, J.G. (1961). *Rheologica Acta*, 1, 337-344.

Olsson, F. (1994). "A solver for time dependent viscoelastic fluid flows." *Journal of Non-Newtonian Fluid Mechanics*, 51, 309-340.

Papanastasiou, A.C., Scriven, L.E. & Macosko, C.W. (1983). "An Integral Constitutive Equation for Mixed Flows: Viscoelastic Characterization." *Journal of Rheology*, 27, 387-410.

Papanastasiou, A.C., Scriven, L.E. & Macosko, C.W. (1987). "A finite element method for liquid with memory." *Journal of Non-Newtonian Fluid Mechanics*, 22.

Papathanasiou, T. D., & Kamal, M. R., (1993). "Filling of a Complex-Shaped Mold With a Viscoelastic Polymer. Part I: The Mathematical Model." *Polymer Engineering and Science,* 33, 400-409.

Park, H.J. & Mitsoulis, E. (1992). "Numerical simulation of circular entry flows of fluid M1 using an integral constitutive equation." *Journal of Non-Newtonian Fluid Mechanics*, 42, 301-314.

Patankar, S. V. (1980). *Numerical heat transfer and fluid flow.* Hemisphere publishing co.

Phan-Thien, N. (1978). "A nonlinear network viscoelastic model." *Journal of Rheology*, 22, 259-283.

Phan-Thien, N., & Tanner, R. I. (1977). "A new constitutive equation derived from network theory." *Journal of Non-Newtonian Fluid Mechanics*, 2, 353-365.

Phillips, M. C., (1977a). "The Prediction of Time-Dependent Non-Linear Stresses inViscoelastic Materials. I. Selection of Constitutive Equation and Strain Measure." *Journal of Non-Newtonian Fluid Mechanics*, 2, 109-121.

Phillips, M. C., (1977b). "The Prediction of Time-Dependent Non-Linear Stresses inViscoelastic Materials. II. Prediction of Shear and Uniaxial Elongation Behaviour." *Journal of Non-Newtonian Fluid Mechanics*, 2, 123-137.

Phillips, M. C., (1977c). "The Prediction of Time-Dependent Non-Linear Stresses inViscoelastic Materials. III. Meomory-Function Non-Linearity." *Journal of Non-Newtonian Fluid Mechanics*, 2, 139-149.

Quinzani, L. M., Armstrong, R. C., and Brown, R. A. (1994). "Birefringence and Laser-Doppler Velocimetry (LDV) Studies of Viscoelastic Flow Through Plannar Contraction." *Journal of Non-Newtonian Fluid Mechanics*, 52, 1-36.

Rajgopalan, D., Armstrong, R.C, & Brown, R.A. (1990). "Finite element methods for calculation of steady, viscoelastic flow using constitutive equations with Newtonian viscosity." *Journal of Non-Newtonian Fluid Mechanics*, 36, 159-192.

Rajgopalan, D., Phillips, R.j., Armstrong, R.C, Brown, R.A., & Bose, A. (1992). "The influence of viscoelasticity on the existence of steady solutions in two dimensional rimming flow." *Journal of Fluid Mechanics,* 235, 611-642.

Rajupalem, V., Talwar, K. K., and Friedl (1997). "Three Dimensional Mould Filling Using a Segregated Finite Element Scheme." *World Congress on Manufacturing Technology,* Cairns.

Rao, R.R., Finlayson, B.A. (1992). "Viscoelastic flow simulation using cubic stress finite elements." *Journal of Non-Newtonian Fluid Mechanics*, 43, 61-82.

Rasmussen, H.K. & Hassager, O. (1993). "Simulation of transient viscoelastic flow." *Journal of Non-Newtonian Fluid Mechanics*, 46, 289-305.

Rasmussen, H.K. & Hassager, O. (1995). "Simulation of transient viscoelastic flow with second order time integration." *Journal of Non-Newtonian Fluid Mechanics*, 56, 65-84.

Reddy, J. N. (1984). *An introduction to the Finite Element Method.* McGraw Hill, New York.

Rice, J. G., and Schnipke, R. J. (1986). "An equal-order velocity-pressure formulation that does not exhibit spurious pressure modes." *Computer Methods in Applied Mechanics and Engineering,* 58, 135-149.

Rivlin, R. S., and Sawyers, K. N. (1971). "Non Linear Continuum Mechanics of Viscoelastic Fluids." *Annual Review of Fluid Mechanics*, 3, 117-146.

Saad, Y., and Schultz, M. H. (1986). "GMRES: a generalized minimal residual algorithm." *SIAM J. Sci. Stat. Comput.,* 7, 856-869.

Sasmal, G. P. (1995). "A finite volume approach for calculation of viscoelastic flow through an abrupt axisymmetric contraction." *Journal of Non-Newtonian Fluid Mechanics*, 56, 15-47.

Sato, T. & Richardson, S.M. (1994). "Explicit numerical simulation of time dependent viscoelastic flow problems by a finite element/finite volume method." *Journal of Non-Newtonian Fluid Mechanics*, 51, 249-275.

Shakib, F., Hughes, T.J. R., and Johan Z. (1989). "A multi-element group preconditioned GMRES algorithm for non-symmetric systems arising in Finite Element Analysis." *Computer Methods in Applied Mechanics and Engineering,* 75, 415-456.

Shewchuk, J. R. (1994). "An introduction to the Conjugate Gradient Method without the agonizing pain." *Private Communication.*

Szady, M. Z., Salmon, T. R., Liu, A. W., Bornside, D. E., Armstrong, R. C. & Brown, R. A. (1995). "A new mixed finite element method for viscoelastic flows governed by differential constitutive equations." *Journal of Non-Newtonian Fluid Mechanics*, 59, 215–243.

Talwar, K.K. and Khomami, B. (1995). "Flow of viscoelastic fluids past periodic square arrays of cylinders. Inertial and shear thinning viscosity and elasticity effects." *Journal of Non-Newtonian Fluid Mechanics*, 57, 177-202.

Wagner, M. H. (1979). "Network Theory of Polymer Melts." *Rheological Acta*., 18, 33-50.

Wesson, R.D., Papanastasiou, A.C. & Wilkes, J.O. (1989). "Problems in modeling viscoelastic flows with integral constitutive equations. Constitutive prediction and numerical instability." *Journal of Rheology*., 33, 1047-1057.

White, J. L. and Metzner A. B. (1963). *Journal of Applied Polymer Science"*, 7, 1867-1889.

White, S. A., Gotsis, A. D., and Baird, D. G. (1987). "Review of The Entry Flow Problem: Experimental and Numerical." *Journal of Non-Newtonian Fluid Mechanics*, 24, 121-160.

Yasuda, K., Armstrong, R. C., and Cohen, R. E. (1981). "Shear Flow Properties of Concentrated Solutions of Linear and Star Branched Polystyrenes." *Rheologica Acta*, 20, 163-178.

Yoo, J. Y., and Na, Y. (1991). "A numerical study of the planar contraction flow of a viscoelastic fluid using SIMPLER algorithm." *Journal of Non-Newtonian Fluid Mechanics*, 39, 89-106.

Young, D. M., and Gregory, R.T. (1972). *A Survey of Numerical Mathematics.* Dover Publications Inc. New York.

Yurun, F., and Crochet, M. J. (1995). "High-order finite element methods for steady viscoelastic flows." *Journal of Non-Newtonian Fluid Mechanics,* 57, 283-311.

Zapas, L. J. and Phillips, J. C. (1981). "Nonlinear Behavior of Polystyrene Solutions as a Function of Concentration." *Journal of rheology*, 25, 405-420.

Zienkiewicz, O. C. (1979). *The Finite element Method.* Tata McGraw-Hill Publishing Company, New Delhi.

Zheng, R. (1991). "Boundary Element Method for Some Problems in Fluid Mechanics and Rheology." *PhD Thesis,* University of Sydney.

Appendix-1

The relaxation times (λ_1), the retardation times (λ_2), and the mobility factors (α) for the polypropylene used in this work, were the same at each temperature in the range of 180°C to 240°C. However the zero shear rate viscosity (η_0), was different at each temperature.

The relaxation times for 1-mode, 3-mode and 9-mode are shown in Table-1.

Mode No.	1-Mode	3-Mode	9-Mode
1	9.0E-03	0.0054	0.006
2		0.0714	0.0284
3		2.3	0.053787
4			0.10185
5			0.19287
6			0.36523
7			0.69161
8			1.3097
9			2.48

Table-1. Relaxation times for Polypropylene melt in Oldroyd-B/Giesekus model.

The retardation times for 1-mode, 3-mode and 9-mode are shown in Table-2.

Mode No.	1-Mode	3-Mode	9-Mode
1	8.30E-04	6.69E-08	1.92E-08
2		8.81E-07	9.1E-08
3		2.84E-05	1.72E-07
4			3.26E-07
5			6.18E-07
6			1.17E-06
7			2.22E-06
8			4.2E-06
9			7.94E-06

Table-2. Retardation times for Polypropylene melt in Oldroyd-B/Giesekus model.

The mobility factors for 1-mode, 3-mode and 9-mode are shown in Table-3.

Mode No.	1-Mode	3-Mode	9-Mode
1	0.001	0.0001	0.057916
2		0.001	0.01
3		0.365429	0.364434
4			0.102029
5			0.01
6			0.49
7			0.01
8			0.01
9			0.49

Table-3. The Mobility Factors of Oldroyd-B/Giesekus model for Polypropylene melt.

The zero shear rate viscosity varies with temperature. The zero shear-rate viscosity of polypropylene melt for the 9-mode Oldroyd/Giesekus model in the temperature range 180°C to 240°C is given in Table-4.

Mode No.	**180°C**	**200°C**	**220°C**	**240°C**
	η_0	η_0	η_0	η_0
1	628.7539	581.2039	472.884	388.0113
2	15.34582	21.77517	11.26311	12.97756
3	1.067883	1.077751	1.042708	631.3179
4	2182.695	2245.713	1001.949	0.000001
5	1253.273	131.8733	1117.316	602.8496
6	648.2861	578.8344	0.00001	382.7775
7	435.6918	1603.538	17.67798	267.8928
8	1.051558	1.053399	1.038538	1.052558
9	6879.835	4859.931	2506.729	1061.821

Table-4. The zero shear-rate viscosity of Polypropylene melts for 9-mode Oldroyd-B/Giesekus model.

The zero shear-rate viscosity of polypropylene melt for the 3-mode Oldroyd/Giesekus model in the temperature range of 180°C to 240°C is given in Table-5.

Mode No.	**180°C**	**200°C**	**220°C**	**240°C**
η_0	η_0	η_0	η_0	η_0
1	519.9649	501.9775	395.0822	372.0456
2	2631.567	2358.959	1501.515	1210.626
3	8894.468	7164.063	3233.303	1766.028

Table-5. The zero shear-rate viscosity of Polypropylene melts for 3-mode Oldroyd-B/Giesekus model.

The zero shear-rate viscosity of polypropylene melt for the 1-mode Oldroyd/Giesekus model in the temperature range of 180°C to 240°C is given in Table-6.

Mode No.	**180°C**	**200°C**	**220°C**	**240°C**
	η_0	η_0	η_0	η_0
1	950	850	650	540

Table-6. The zero shear-rate viscosity of Polypropylene melts for 1-mode Oldroyd-B/Giesekus model.

The solvent contribution to viscosity (η_s) was calculated from the relaxation and retardation time relationship (Equation 3.2-21). Since our simulations of differential type constitutive equations were in single mode, we have calculated the solvent viscosity for single-mode differential type constitutive equations. The solvent-

contribution to viscosity of polypropylene melt for the single-mode Oldroyd-B/Giesekus model in the temperature range 180°C to 240°C is given in Table-7.

Mode No.	**180°C**	**200°C**	**220°C**	**240°C**
	η_s	η_s	η_s	η_s
1	88	78	60	50

Table-7. The solvent-contribution to viscosity of Polypropylene melts for 1-mode Oldroyd-B/Giesekus model.

Appendix-2

The total pressure drop values for Experiment, Oldroyd-B model and Moldflow® software with Polypropylene melts as shown in Figure 5.3-12 are given in Table below.

Flow Rate [cm^3/sec]	Shear rate [1/s]	Experiment ∇P [Mpa]	Polypropylene /Oldroyd-B Model ∇P [Mpa]	Moldflow® ∇P [Mpa]
0.326	77.4486	1.73	1.3	1.06
0.45	106.9076	1.93		
0.686	162.9747	2.18	1.81	1.52
0.785	186.4943	2.28	2.06	
1.506	357.784	2.86	3	
2.287	543.3281	3.14		
3.515	835.067	3.74		3.11
5.492	1304.748	4.08		
7.521	1786.782	4.51		

List of Publications From This Research

Ray, S. R., Siores, E., and Friedl, C. (1999). "A Three dimensional simulation strategy for of viscoelastic constitutive equation." *15th International Conference on Production Research*, Limerick, Ireland.

Ray, S. R., Talwar, K. K., and Friedl, C. (1998). "Three dimensional simulation of viscoelastic constitutive equations using a segregated finite element scheme." *Engineering Mathematics and Applications International Conference,* Adelaide, Australia.

Ray, S. R., Talwar, K. K., Friedl, C., and Thompson W. (1997). "Incorporation of viscoelastic constitutive equations in the injection moulding process." *World Congress on Manufacturing Technology,* Cairns.